University of Stavanger

Faculty of Science and Technology

MASTER'S THESIS

Study program: MSc in Petroleum Engineering Specialization: Well Engineering	Spring semester, 2016 Open
Writer: Martin Tveiterå	*Martin Tveiterå* _____ (Writer's signature)
Faculty supervisor: Dan Sui External supervisor(s): N/A	
Title of thesis: Investigation of temperature- and pressure effects on drilling fluid properties and related downhole torque and drag calculations	
Credits (ECTS): 30	
Keywords: Drilling fluid properties Simulation of downhole conditions Temperature- and pressure modelling Density- and viscosity modelling Buoyancy factor Torque and drag force	Pages: 84 +enclosure: 32 Stavanger, June, 2016

Investigation of temperature- and pressure effects on drilling fluid properties and related downhole torque and drag calculations

by
Martin Tveiterå

Thesis
Presented to the Faculty of Science and Technology
The University of Stavanger

The University of Stavanger
June 2016

Acknowledgements

I would like to express a great gratitude to my supervisor, Dan Sui, for her great guidance and help through the work on this thesis. Her dedication and support all through my work with this thesis is highly appreciated. It has been a great pleasure working under her supervision.

Abstract

Investigation of temperature- and pressure effects on drilling fluid properties and related downhole torque and drag calculations

Martin Tveiterå, Master of Science in Petroleum Engineering
The University of Stavanger, 2016

Supervisor: Dan Sui

Increasing temperature and pressure with depth, affects the properties of drilling fluid. The effect of temperature and pressure on the density and viscosity of drilling fluid is of great importance. This is because, among several reasons, it affects the calculation of downhole pressure and the buoyancy factor for the well. Correct pressure estimation, could pose a great concern regarding well integrity. The buoyancy factor would affect the effective weight of the drillstring, which again would be a property of calculation of torque and drag force in a well.

In the work of evaluating the downhole temperature and pressure, modelling is important. In this thesis, models to do so, is investigated. Simulation of downhole conditions have been carried out. Sensitivity analysis, regarding the most critical parameters of the temperature, is performed. The effect of different sized pipes and equipment's on the temperature and pressure will be investigated. If the result of changed size of a pipe is higher or lower temperature and/or pressure, this would again affect the density and viscosity of drilling fluid.

Torque and drag force is, as mentioned, connected to the calculation of the buoyancy factor. Torque and drag control is an important aspect of well design. In order to be able to drill as far as desired, drag force and torque loss needs to be properly handled. In the evaluation of torque and drag force, it is differentiated between straight inclined wellbore and curved wellbore. Conditions for determining whether the wellbore is either straight inclined or curved, will be implemented in the torque and drag force calculations. In addition, the effect of combined motion on the torque and drag force, will be investigated. Findings regarding the combined motion, indicates that torque and drag force is affected by combined motion. Regarding the drag force, it is observed, that generally, the drag force is lower for the cases with constant buoyancy factor throughout the well, than for the cases with varying buoyancy factor with depth. For the torque, it was observed, that generally, the torque for cases including lowering, hoisting and static conditions of the drillstring, the torque in the well is lowered when a constant buoyancy factor is applied.

Table of Contents

List of Figures

List of tables

Nomenclature

f	Fanning friction factor	Dimensionless number
ε	Roughness	ft
ΔT	Temperature difference across the surface	°C
A_a	Area annulus	m²
A_d	Area drillpipe	m²
U_a	Velocity annulus	m/s
U_d	Velocity drillpipe	m/s
D_a	Diameter annulus	m
D_d	Diameter drillpipe	m
F	Drag force	N
T	Torque	Nm
β	Buoyancy factor	Dimensionless number
ρ_o	Density outside	kg/m³
ρ_i	Density inside	kg/m³
A_i	Area inside	m²
A_o	Area outside	m²
ρ_{pipe}	Density pipe	kg/m³
L_{pipe}	Pipe length	m
w	Pipe weight	N/m
α	Inclination of the wellbore	°
μ_{fric}	Friction coefficient	Dimensionless number
r	Radius of pipe	m
D	Depth	m
θ	Absolute change in direction	°
ψ	Angle between axial and tangential velocity	°
V_h	Axial velocity	m/s
V_r	Tangential pipe speed	m/s
N_r	Rotary pipe speed	rpm or s⁻¹
I	Inclination	°
Azi	Azimuth	°
A	Area	m²
Re	Reynolds number	Dimensionless number
P	Pressure	Pa

LIST OF ABBREVIATIONS

Symbol:	Definition:	Unit:
BHA	Bottomhole assembly	
RPM	Revolutions per minute	rpm or s⁻¹
TVD	True vertical depth	m
MD	Measured depth	m
OD	Outer diameter	m
ID	Inner diameter	m
HPHT	High pressure, high temperature	
BHP	Bottomhole pressure	Pa
s.g.	Specific gravity	s.g
DLS-filter	Dogleg severity filter	
DLS	Dogleg severity	°/m

DL	Dogleg	°
MWD	Measurements while drilling	
WBM	Water-based mud	
OBM	Oil-based mud	
HSE	Health, safety and environment	
ECD	Equivalent circulating density	
ESD	Equivalent static density	
LCM	Lost circulation material	

Chapter 1: Introduction and problem statement

During drilling of a petroleum well, as drilling progress deeper, the temperature and the pressure in the well increases. This increase in temperature and pressure, affects the properties of drilling fluid in the well. This thesis will focus on the effect of downhole conditions, namely temperature and pressure, on drilling fluid. The effect of ignoring these downhole effects on drilling fluid, will be investigated. These changes in the drilling fluid, include density and viscosity variations as a function of temperature and pressure. These changes of the properties of drilling fluid, will again affect properties like the pressure and buoyancy factor in the well. These two properties are important for several reasons. Correct pressure estimation could for example pose a great concern regarding well integrity. The buoyancy factor would affect the effective weight of the drillstring, which again is a property of calculation of torque and drag force in a well. This is something that will be investigated in this thesis.

In the work of this thesis, models to estimate the temperature in the drilling mud, will be investigated. The main use of the temperature model is the predicting of downhole temperature. This is in order to more precisely estimate the density and viscosity behavior of drilling fluid in the well. This is, among other reasons, in order to be able to predict the buoyancy factor, and thereby to be able to calculate torque and drag force more accurate than if assuming constant buoyancy factor throughout the whole well. The temperature model will also be used in more precise calculation of the downhole well pressure. The advantages by the temperature model include possibility to calculate the temperature for the entire well, and also study the effect of the different parameters.

The effect of different sized pipes and equipment's in the well, on the temperature and pressure will be investigated. Results indicates that if the size of either pipes or equipment's in the well is changed, this will either lower or increase the temperature, depending whether the size is increased or decreased. This temperature change, would again affect the density and viscosity of the drilling fluid.

The temperature behavior will be used in models to more accurate predict the fluid viscosity and density. The behavior of the drilling fluid, is also a function of the pressure in the well, so in addition to the temperature model, models to predict the pressure in the well will be investigated. All these different models will aid in the accuracy of predicting the density and viscosity of drilling fluid.

One of the properties, which is affected by the behavior of drilling fluid, is torque and drag force. It is desirable to keep the torque losses and drag at a minimum to be able to drill as far as required. As it will be looked into, especially the torque loss is considerable as the inclination of the well increases, i.e. in horizontal wells the torque loss could be a major limiting factor to as how far it is possible to drill. In a successful well completion, torque and drag force control is of great importance. In the evaluation of torque and drag force, an important criteria is whether the wellbore is straight inclined or curved. An aspect of determining torque and drag force would then be to determine whether the wellbore is considered straight inclined or curved. This is something that will be investigated in this thesis. Another aspect that will be looked into is the effect of combined motion on torque and drag force.

A large part of the work carried out in this thesis, involves simulation of several performance states of drilling fluid. Simulation is an operation that is trying to imitate a real-world process or system over time. To carry out the simulation processes, a program called MATLAB is used. MATLAB is a program for numerical computation and data visualization. It is a fairly simple, but yet a powerful simulation tool. For the models developed in MATALB, they are made in such a way that they calculates the different properties, e.g. temperature, in different segments with depth. I.e. if there is a 3000 meters deep well, and it is desirable to measure the temperature for each pipe stand (30 m), the well would have to be divided into 100 segments. The models in MATLAB, is easily updated depending on how many segments that is required. It is of great advantage to divide the well into several segments in order to more precisely calculate the intended variable.

With theory and models in place, finally a case study will be presented. A case study with its intention to provide relevant examples and confirm theory and statements that have been made in earlier parts of the thesis.

Chapter 2: Background

2.1: DRILLING FLUID

In this thesis, the behavior of drilling fluid during downhole conditions is investigated. Before this behavior is studied, some background about drilling fluid will be presented.

Drilling fluid or so-called drilling mud is very important for a petroleum well. It is typically distinguish between water-based mud (WBM) and oil-based mud (OBM). It is important that the mud keep its desired properties not just only topside, but also downhole when the mud is exposed to different pressures and temperatures. As mentioned, changing pressures and temperatures will change the density and viscosity of the mud.

2.2: FUNCTIONAL REQUIREMENTS OF DRILLING FLUID

Normally for drilling fluid, it is distinguish between oil-based drilling fluid and water-based drilling fluid. These two types of fluid have different properties that affects the downhole performance. The drilling fluid have several important functions as:[1]

- **Provide hydrostatic pressure:** If the hydrostatic pressure is too low, formation fluids could enter the well and a potential kick situation could arise. The definition of kick is influx of formation fluid into the well. Formation fluid could be oil, gas or water. It occurs in situations where the pressure in the well is lower than the formation pressure. For many operations in a well, the fluid column serve as a primary barrier. The hydrostatic pressure is given by the equation:

$$P = \rho g h \qquad\qquad (\,2\text{-}1\,)$$

    Where P is hydrostatic pressure, ρ the drilling fluid density, g is the gravitational acceleration constant and h is the height of the fluid column in the well.

- **Hole cleaning:** Drilling fluid serve to transport drilled formation rock out of the well. If the well is not properly cleaned, cuttings will accumulate and can lead to pack-off of the drillstring. During pack-off, the ability to circulate is reduced or lost, and if a pack-off situation is not properly handled, the pipe could become stuck.[2] If the pipe becomes stuck, a worst-case situation could be a sidetrack of the well. This is very expensive, and is highly preferred avoided. There will also be a large increase in pump pressure, with the potential for fracturing of the formation, which again can lead to mud loss.[3] According to Fjelde[4], cutting transport is a function of several parameters like: flow rate, rotation of the drillpipe, rate of penetration, size of the drilled particles, inclination of the well, size of the well diameter, mud weight and rheology of the fluid. For this thesis, the focus is on parameters like mud weight and fluid rheology. The effect of different mud weights on cuttings transport is connected to the buoyancy factor. If a high density of drilling fluid, this will increase the buoyancy in the well, i.e. reduce the effective weight of the cuttings, and this will be good for cuttings transport. For the fluid rheology, according to Fjelde, the viscosity effect on cuttings transport can be both positive and negative. It could be positive with high viscosity fluid during a vertical well and laminar conditions. It could be positive with low viscosity of the mud for horizontal well and turbulent flow. This is because the settled cutting beds is more easily disturbed.

- **Cool the drill bit:** During drilling, the drill bit is crushed against the formation rock. This creates friction that again creates large amount of heat. This heat can lead to problems for e.g. equipment's in the bottomhole assembly. Drilling fluid is used to cool the bit during drilling for this purpose.
- **Buoyancy:** The drilling fluid, as previously mentioned, affects the buoyancy in the well and thereby the effective weight of the drillstring. A lighter or heavier drilling string would affect the torque and drag force. This effect will be studied thoroughly later.
- **Lubrication:** Drilling fluid, especially oil-based and synthetic-based drilling fluids, adds lubrication to the well. Good lubrication is positive for low torque and drag.
- **Add wellbore stability:** In open-hole sections in the well, drilling fluid is important to keep the borehole stable.
- **Energy transfer:** Hydraulic power is transmitted to the bit to make it rotate and able to drill. To make it rotate, fluid is circulated.

2.3: WATER-BASED MUD

There are two major types of drilling fluids. Water-based mud is one of these types. It is one of the types of drilling fluid that is most used in the world. It normally consist of water or saltwater and bentonite.[5] Actually, water alone could be used as drilling fluid, but in most cases additives is required to give the drilling fluid desired properties. These properties could include density, viscosity etc. Drilling fluid should for example have some degree of viscosity in order to suspend the rock cuttings. By increasing the viscosity, the lifting capacity of the mud is improved. This allows for transporting cuttings from the bottom- to the top of the well. By adding clay or polymers to the water-based mud, higher viscosity can be achieved. Later a viscosity experiment will be presented. In the experiment, different additives were tested, in order to investigate their effect on the viscosity of the mud. Clay is said to be the cheapest and most common additive used to increase the viscosity of water-based mud.[6]

When to decide which mud to use in a well, there are several considerations to make. Some advantages and disadvantages regarding water-based mud could be mentioned:[7]

Advantage:

- Less expensive than oil-based mud
- More environmental friendly than oil-based mud
- A potential kick will more easily be detected in water-based mud compared to oil-based mud
- Less concerns regarding health, safety and environment (HSE)

Disadvantage:

- Less lubrication than for oil-based mud
- Water-based mud could lead to a phenomenon called swelling of clay. This can make the drillstring stuck
- Higher chance to get differential stuck because of thicker mudcake. A mudcake is deposits on a permeable formation when drilling fluid is pressed against the formation. Since the formation is permeable the filtrate/liquid in the mud passes through the formation, but the larger particles in the mud do not passes and builds up a so-called mudcake. The mudcake can make the pipe stuck.[8]

For water-based mud, there are some general considerations regarding high pressure, high temperature (HPHT) wells:[9]

- A potential kick is easier to detect in water-based mud compared to oil-based mud. In oil-based mud, the kick can be undetected.
- A potential kick will migrate upwards in the well, even though the well is shut-in.
- Concerns regarding casing design, because maximum casing shoe and choke pressures will be large compared to oil-based mud.
- A potential kick is expected at an earlier stage at surface than for oil-based mud.

2.4: OIL-BASED MUD

The second type of the major types of drilling fluids is oil-based mud. *Oil-based mud is an invert-emulsion mud whose continuous phase is oil.*[10] The oil base can be made of different substances like diesel, crude oil etc. Oil-based mud is favorable to avoid problems with swelling clay, therefore in cases where it is expected that swelling clay can be a problem, oil-based mud should be used. During high temperature conditions, oil-based mud could be favorable, because the high temperature could dehydrate water-based mud.

When to decide which mud to use in a well, there are several considerations to make. Some advantages and disadvantages regarding oil-based mud could be mentioned: [11]

Advantage:

- Typical more compatible with the reservoir
- Better lubrication than for oil-based mud. Because of better lubrication, oil-based mud could be good for horizontal wells
- Less chance to get differential stuck because of a mudcake, than for water-based mud. This is because the mudcake is thinner than for water-based mud
- Less problem with swelling clay compared to water-based mud

Disadvantage:

- More environmental damaging than for water-based mud. More strict procedures for handling and disposing the mud compared to water-based mud
- More expensive than water-based mud
- More concerns regarding HSE
- Kick can hide in the mud during HPHT conditions, which makes it more difficult to detect a potential kick.

For oil-based mud and HPHT wells, there are some generally considerations.[12]

- During high pressures a potential kick will dissolve in the oil-based mud
- Kick can be undetected
- Requires fast action during an event, because of large expansion
- Gas kick is expected later at top of the well, than for water-based mud

The type of drilling fluid one should use in a HPHT well, depend on several factors. For oil-based mud, they are said to be stable at high temperature in terms of rheology. According to Adamson et al.[13], most oil-based muds are stable up to 230 °C in 16-hour lab-tests. One disadvantage for oil-based mud during HPHT conditions, is that a gas kick could dissolve in the oil-based fluid, this would make detection of the kick a challenge.

3

Chapter 3: Temperature model

3.1: INTRODUCTION TO THE TEMPERATURE MODEL

As drilling advance deeper in the well, drilling fluid will experience increased pressure and temperature. The increased pressure and temperature will affect the density of the drilling mud. Higher pressure increase the drilling fluid density, while higher temperature decrease the drilling fluid density. This is because the drilling fluids are compressed by pressure, and hence the density increase. When drilling fluids are heated it expands, and hence lower density.[14] Therefore, in order to predict the correct density of drilling fluid used in a well, knowledge about density behavior is essential. In this section of the thesis, the effect of temperature on drilling fluid density will be focused upon. Later, the effect of pressure on drilling fluid will be studied. In the work of evaluating the temperature effect, a temperature model will be investigated.

3.2: BACKGROUND OF THE TEMPERATURE MODEL

To know how the temperature in drilling fluid develops, is important for estimation of the bottomhole pressure and interpretation of well kicks.[15] The temperature of the circulating fluid is a function of several properties like depth of the well, inlet drilling fluid temperature, formation thermal conductivity, geothermal gradient, surface earth temperature etc. These properties, along with others, will be studied in the further investigation of the temperature model. Modern equipment's give the possibility to perform direct temperature measurements at a given depth and time for the drilling operations, but without a temperature model to model the heat transfer, temperature cannot be predicted for arbitrary performance states.[16] A temperature model is useful because with such a model it is possible to calculate the temperature for the entire well and also study the effect of the different parameters.

For HPHT wells, the effects of temperature on drilling fluid is higher. Therefore, especially in such wells, it is important with accurate temperature models in order to predict the temperature correctly. HPHT wells is defined as wells where the shut-in pressure exceeds 690 bar (10 000 psi), and where the static bottomhole temperature is above 150 °C.[17]

In a petroleum well, drilling fluid is circulated. According to Kårstad[18], a non-linear heating of the mud system can be observed. This can be explained by when drilling fluid is being circulated in the well, the lower part of the well is often cooled. It can then be observed transfer of heat to the upper part of the well because the drilling fluid at the bottom of the well is heated and transported upwards. Figure 3-1 illustrates this concept with circulation of drilling fluid in a well.

When considering drilling fluid temperature in a well, both temperature in the drillpipe fluid and the annular fluid should be considered. In the well, it will be observed heat flow from the annulus to the drillpipe. When the temperature of the drilling fluid is lower than the temperature of the formation, heat from the formation will be distributed to the borehole. Opposite, if the temperature in the borehole fluid is higher than the formation, heat will be transported to the formation. This situation could be the case in the upper part of the borehole. As the figure below, of the borehole, describes, there will be heat transfer from the formation to the annulus and from the annulus to the drillpipe. The cold drilling fluid inside the drillpipe will be heated up in contact with the pipe that is heated by the annular

fluid. When the drilling fluid travels down the drillpipe, it finally reaches the drill bit at the bottom of the well and enter the annulus. From this point, the drilling fluid flows up the annulus and to the top of the well. The fluid travelling from the bottom of the well to the top of the well in the annulus, can be called return fluid. This return fluid, experience heat transfer from both the annulus and the outside of the drillpipe.[19] The return fluid could be heated directly from the formation. If there is casing(s) and/or cement in the hole, the fluid will be heated through the casing and/or cement. As it is possible to see from the figure below, the lower part of the annulus will be cooled from the cold drilling fluid pumped down the drillpipe. From the figure, it is also possible to see that the upper part of the annulus will be heated from the warmer fluid that is flowing up the annulus from the bottom of the well.
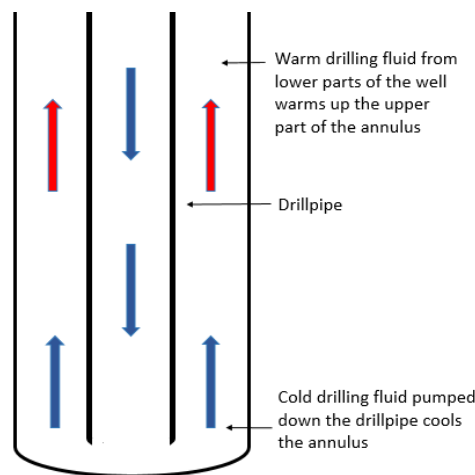
Figure 3-1: Illustration of the fluid circulation in the well

There are different operational modes for circulating drilling fluids; forward circulation and reverse circulation. During forward circulation, the fluid flows down inside the drillpipe and back up in the annulus. For reversed circulation, the drilling fluid flows down the annulus and back up the drillpipe. The focus in this thesis will be on forward circulation, but it could be mentioned that for reversed circulation it is expected higher temperature loss from the well than for forward circulation.[20] This has to do with the fact that during reverse circulation, the drilling fluid is exposed to the large diameter wellbore, instead of a small diameter drillpipe, as in forward circulation.[21] The heat loss during reverse circulation will also be less than for forward circulation, because the fluid is transported upward through the smaller diameter drillpipe, instead of the lager diameter annulus as in forward circulation.

A temperature model is useful because with such a model it is possible to calculate the temperature for the entire well and study the effect of the different parameters. Some of these parameters are not possible to manipulate. Examples of such parameters could be properties of the rock and geothermal gradient. However, some of the other parameters are not constant and is possible to change, for example flowrate, inlet-temperature. To have knowledge about how these properties affects the temperature could therefore be of great interest. Later, a sensitivity analysis will be performed. This is done in order to evaluate which of the parameters in the temperature model that affects the drilling fluid temperature in the greatest amount.

The figure below shows an illustration of the wellbore. It can be observed that the heat enters the drillpipe through convection, i.e. heat is transported into the system by circulation of the drilling fluid. It can also be observed that heat is transported from the annulus to the drillpipe through conduction, i.e. heat transfer through the pipe itself caused by temperature differences between the inside and outside of the pipe. The figure illustrates what has been mentioned earlier, with heat flow from the formation to the annulus, and heat flow from the annulus to the drillpipe.
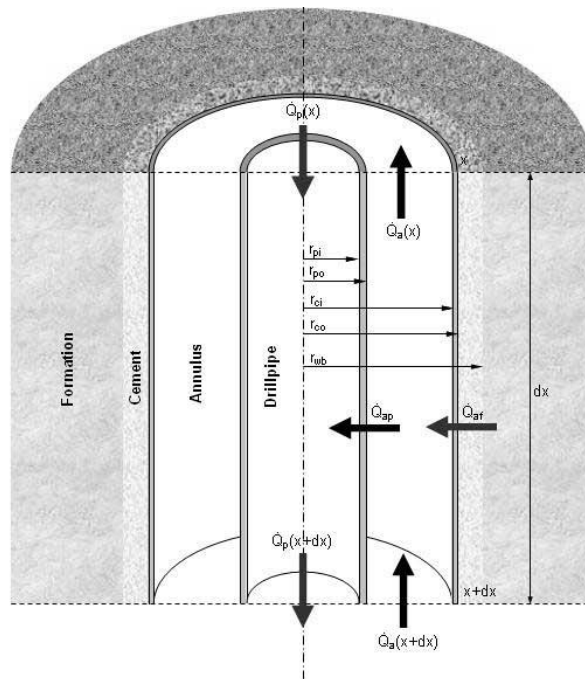
Figure 3-2: Illustration of the wellbore[22]

Different parameters to consider for temperature of drilling fluid are mentioned by Apak.[23] He mentions five important parameters to consider:

1) Frictional energy losses caused by frictional contact between the rotating drillpipe by either casing or the borehole.
2) Viscous energy losses of the drilling fluid
3) Energy loss of the cuttings
4) Frictional energy losses from the drill bit
5) Heat flow from the formation

Heat flow from the formation is considered to be the dominant parameter. Heat flow from the formation is the parameter that will be considered during the work in this thesis.

The figure below shows a plot of the fluid temperature inside the drillpipe, and in the annulus when fluid is circulated. An interesting observation is that the temperature is not at its highest at the bottom of the well. This has to do with, what it is previously mentioned, that the fluid continues to heat when it flows back up the annulus. It continues to heat because it is heated from the formation.

6
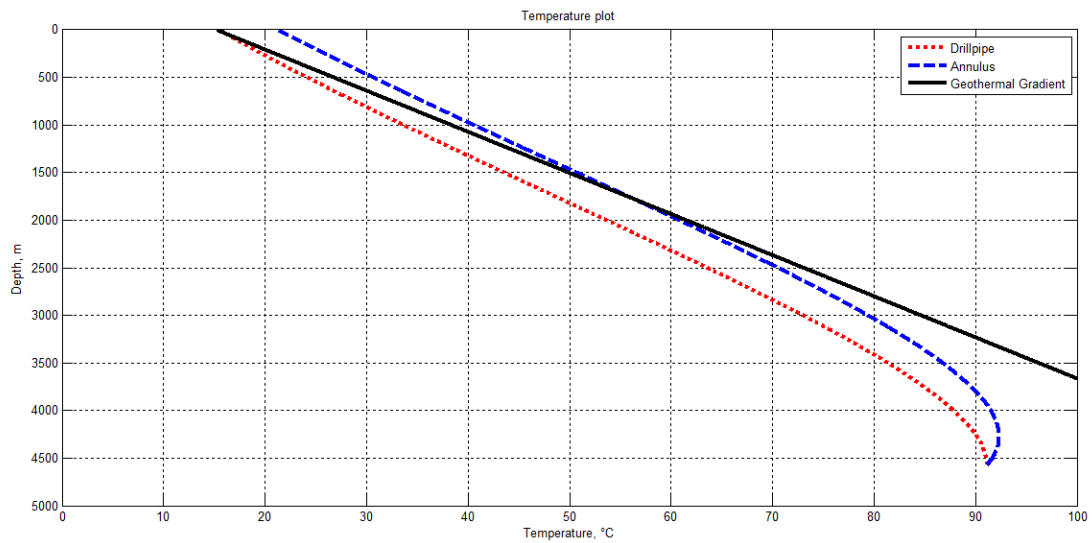
Figure 3-3: Temperature in annulus and drillpipe

The situations mentioned above is during circulation, i.e. dynamic conditions. If the circulation is very low, it is possible to observe that the temperature approaches the geothermal gradient. If investigating a case where the circulation rate was original 0,0133 $\frac{m^3}{s}$, and is now set to 0,00004 $\frac{m^3}{s}$. The case with original circulation rate can be seen in the figure 3-3 above. The situation with new circulation rate, 0,00004 $\frac{m^3}{s}$, can be seen in the figure 3-4 below. From the figure below, it appears like the temperature profile for the annulus has "disappeared", but a zoomed view reveals that the temperature profile for the annulus is overlapped by the geothermal gradient for most depths. A zoomed view is included in figure 3-5 to illustrate this. The fluid temperature in the drillpipe and the annulus will approach the geothermal gradient of the formation because there is no mud that is flowing, and therefore the mud is static and will be highly affected by the formation temperature. As for the previous case mentioned above, where circulation take place (dynamic conditions) there will be transport of the drilling fluid and the temperature profile for the mud in the drillpipe and the annulus will be different from the geothermal gradient.

7
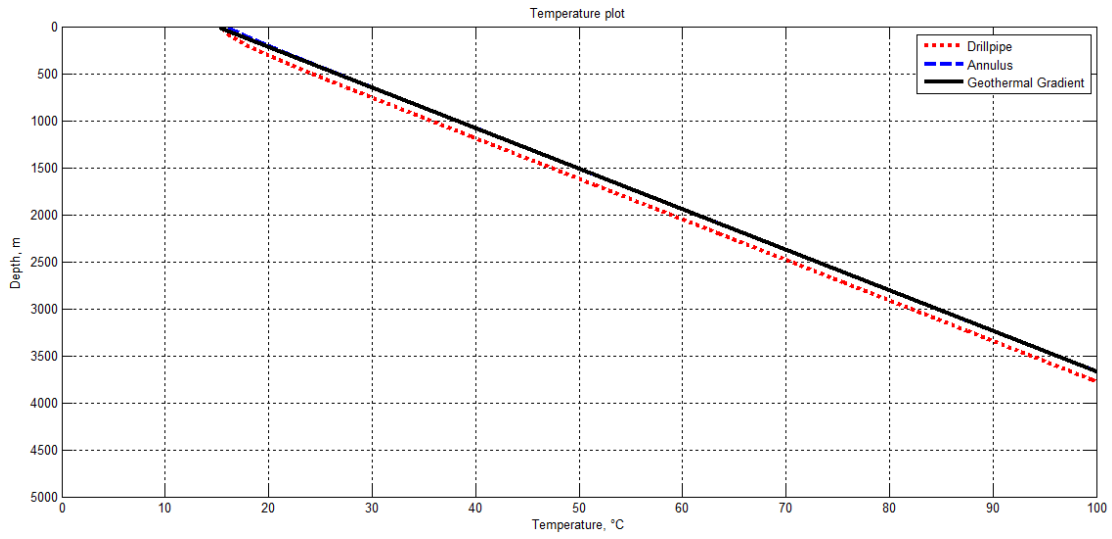
Figure 3-4: Temperature profile during low circulation rate
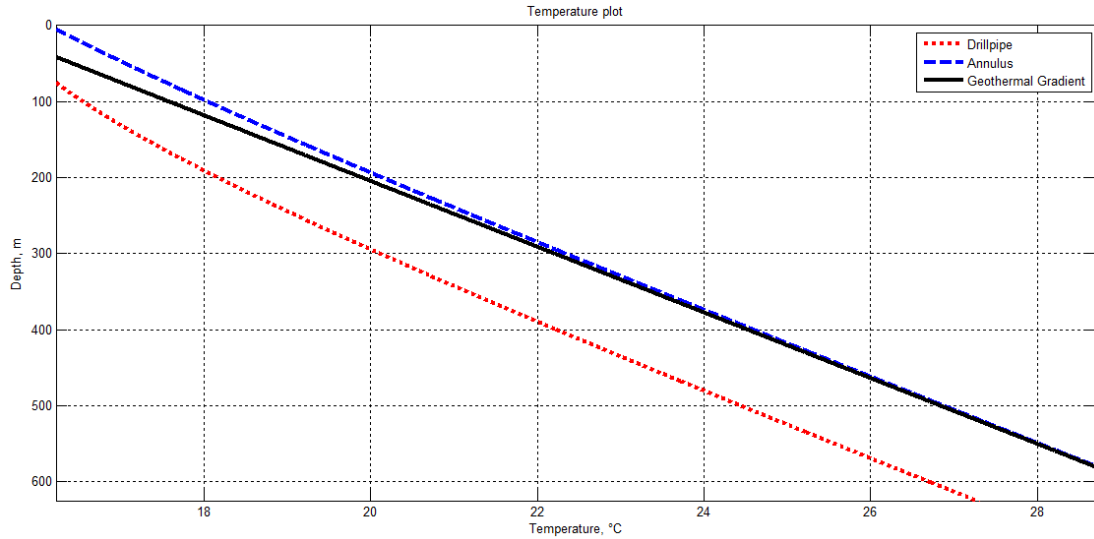
Figure 3-5: A zoomed view of the temperature profile during low circulation rate conditions

3.3: TEMPERATURE MODEL

In this section, the temperature model is presented. The aim of the temperature model is to investigate temperature profiles during drilling. Different models for investigation of temperatures exist. The temperature model, presented in this thesis, is based on the work of Kårstad and Aadnøy.[24] Their model can be used to estimate the temperature distribution while drilling for forward- and reverse circulation. The focus here will be on temperature model for forward circulation.

According to Kårstad and Aadnøy, the expression for the annular fluid temperature (T_a) and the tubing fluid temperature (T_t) profiles is given as:

$$T_t(z,t) = \alpha e^{\lambda_1 z} + \beta e^{\lambda_2 z} + g_G z - B g_G + T_s \qquad (3\text{-}1)$$

$$T_a(z,t) = (1 + \lambda_1 B)\alpha e^{\lambda_1 z} + (1 + \lambda_2 B)\beta e^{\lambda_2 z} + g_G z + T_s \qquad (3\text{-}2)$$

8

Where the different parameters, in the equations for T_t and T_a, can be found be the expressions below:

$$\lambda_1 = \frac{1}{2A}\left(1 - \sqrt{1 + \frac{4A}{B}}\right) \tag{3-3}$$

$$\lambda_2 = \frac{1}{2A}\left(1 + \sqrt{1 + \frac{4A}{B}}\right) \tag{3-4}$$

$$A = \frac{\omega C_{fl}}{2\pi r_\omega U_a}\left(1 + \frac{r_\omega U_a f(t_D)}{k_e}\right) \tag{3-5}$$

$$B = \frac{\omega C_{fl}}{2\pi r_t U_t} \tag{3-6}$$

$$\alpha = -\frac{(T_i + Bg_G - T_s)\lambda_2 e^{\lambda_2 D} + g_G}{\lambda_1 e^{\lambda_1 D} - \lambda_2 e^{\lambda_2 D}} \tag{3-7}$$

$$\beta = \frac{(T_i + Bg_G - T_s)\lambda_1 e^{\lambda_1 D} + g_G}{\lambda_1 e^{\lambda_1 D} - \lambda_2 e^{\lambda_2 D}} \tag{3-8}$$

$$f(t_D) = \left(1.1281\sqrt{t_D}\right) * \left(1 - 0{,}3\sqrt{t_D}\right), if\ 10^{-10} \leq t_D \leq 1{,}5 \tag{3-9}$$

$$f(t_D) = (0{,}4063 + 0{,}5 ln t_D * \left(1 + \frac{0{,}6}{t_D}\right), if\ t_D > 1{,}5 \tag{3-10}$$

$$t_D = \frac{\alpha_h t}{r_w^2} * 3600 \tag{3-11}$$

$$\alpha_h = \frac{k_e}{\rho_e c_e} \tag{3-12}$$

The parameters used in the above expressions, and a description of the parameters with its given units, is given in the nomenclature list.

Most of the parameters included in the expressions for $T_t(z, t)$ and $T_a(z, t)$ can be measured or calculated, except for the overall heat transfer coefficients of the annulus and tubing. Overall heat transfer coefficients is used to calculate the total heat transfer in the well, and it is dependent on the fluid and the properties of the fluid in the annulus and inside the tubing. The overall heat transfer coefficient for the tubing can be given as:[25]

$$\frac{1}{U_t} = \frac{1}{h_t} + \frac{r_{ti}}{k_t} Ln\left(\frac{r_{to}}{r_{ti}}\right) + \frac{r_{ti}}{r_{to}}\frac{1}{h_a} \tag{3-13}$$

Several unknowns needs to be calculated in order to find the overall heat transfer coefficient. The coefficient of heat transfer in the tubing (h_t) and coefficient of heat transfer in annulus (h_a) needs to be calculated. According to several authors,[26,27] h_t can be found using the work of McAdams. It is determined by:

$$h_t = 0{,}023\frac{k}{2r_t}\left(N_{REp}\right)^{0{,}8}(N_{Pr})^{0{,}4} \tag{3-14}$$

Two more unknowns needs to be found; the Prandtl number (N_{Pr}) and the Rayleigh number (N_{REp}). The Prandtl number is a dimensionless number and it is defined as the ration of momentum diffusivity to thermal diffusivity. It is defined as:[28]

$$N_{Pr} = \frac{C_{fl}\mu}{k}$$
(3-15)

Where C_{fl} is the specific heat capacity of the fluid, μ the dynamic viscosity of the fluid and k is the thermal conductivity. Thermal conductivity is the capability of a material to conduct electricity.[29] In other words, the conductivity is the opposite of resistivity. It is given with the SI unit watts per meter kelvin ($\frac{W}{mK}$). If the value of thermal conductivity increases, it implies that the materials capability to conduct electricity increases. Therefore, for an isolation material, as an example, it would be preferred to have a low value of the thermal conductivity. The Rayleigh number (N_{REp}) is a dimensionless number that is used to calculate the natural convection.[30] The magnitude of the Rayleigh number for a fluid is an indication whether if the heat transfer is mainly due to conduction or convection. The Rayleigh number is defined as the Prandtl number (N_{Pr}) multiplited with the Grashof number (Gr), which approximates the buoyancy to viscous force that is acting on a fluid.[31] The Rayleigh number is defined as:

$$N_{REp} = GrN_{Pr}$$
(3-16)
$$Gr = \frac{g\beta\rho^2 L^3 \Delta T}{\mu^2}$$
(3-17)

3.4: APPLICATION OF THE TEMPERATURE MODEL

A temperature model is useful and have several benefits. One of these benefits includes the ability to predict downhole fluid temperature changes. Something that is an important aspect of designing a well.

Kårstad mentions several applications for why the there is a need to temperature modelling:[32]

- To be able to determine both the equivalent circulating density (ECD) and the equivalent static density (ESD)
- Composition of drilling mud and annular fluid
- Designing downhole equipment. Could involve design of drill bit, logging tools etc.
- Correlation between different wells
- During cement operations
- Pressure, volume and temperature (PVT) analyses
- Determination of fluid density and viscosity

In this thesis, the main use of the temperature model will be on the last mentioned application above, i.e. determination of fluid density and viscosity. The temperature model can be used in prediction of downhole fluid temperature to be able to more precisely estimate the density behavior of the drilling fluid in a well. This is in order to be able to predict the buoyancy factor and thereby to be able to calculate torque and drag more accurate than if assuming a constant buoyancy factor throughout the whole well.

The temperature model, will also be used during viscosity calculations, something that will be looked into later.

3.5: SENSITIVITY ANALYSIS OF PARAMETERS AFFECTING DOWNHOLE TEMPERATURES

In order to investigate which parameters that have the largest influence on the annular fluid temperature and the tubing fluid temperature profiles, a sensitivity analysis is performed. It is important to know which of the parameters that affect the temperature profiles in order to control the temperature of the drilling fluid. To perform the sensitivity analysis, the temperature model presented above, is implemented in the numerical computing tool, previously presented, called MATLAB.

Some of the parameters in the model is possible to change and some are not, when concerning "real-life" conditions. With the word "change", it refers to a variable that is possible to manipulate in real life conditions. As an example, the geothermal gradient of the formation is not possible to change. However, in this analysis, the sensitivity of the different parameters is tested, regardless if they can be changed or not. Regardless if the parameter can be changed or not, it is valuable to know the sensitivity of such a parameter. An example of a parameter that is possible to manipulate could be circulation rate. It is possible to circulate more and it is possible to circulate less if desirable.

For the sensitivity analysis, the different variables are varied by 50%, e.g. the circulation rate at $0,01325 \frac{m^3}{s}$ is varied between $0,00625 \frac{m^3}{s}$ and $0,0199 \frac{m^3}{s}$. All the variables are varied by 50% to get a good view of the relative sensitivity of the variables.

In order to test the sensitivity of the different parameters, a base case is defined. This base case will be compared to different cases where one of the parameters are changed in order to see how it affects the annular fluid temperature and the tubing fluid temperature profiles. The base case is defined in the table below.

Table 3-1: Base case well parameters

Parameter:	Value:
Well depth	4572 m
Tubing inner diameter	0,16193 m
Tubing outer diameter	0,168275 m
Wellbore diameter	0,219075 m
Temperature surface	15,3 °C
Inlet temperature	15,5 °C
Geothermal gradient	0,0231 °C/m
Circulation time	44 hours
Viscosity of fluids	0.04547 PaS
Earth density	2643 kg/m^3
Conductivity of tubing	34,6 W/mK
Conductivity of earth	2,25 (W/mK)
Mass flow rate if fluid	0,01325 m^3/S
Heat capacity of fluid (Drilling fluid specific heat)	1674,7 J/kgC
Heat capacity of earth (Formation specific heat)	837,4 J/kgC

Thermal conductivity drilling fluid	1,73 W/mK
Drilling fluid density	1198,3 kg/m³

For all the different variables, mentioned in table 3-1 above, the temperature is plotted for 50% increase and decrease in the respective variables. Due to the large extent of these plots, only some selected plots is presented. The complete presentation of the plots can be found in Appendix A. By using the temperature model, along with the defined base case, the different variables are varied with 50%. Below, a table with the sensitivity of the different variables is included. It illustrates how much the fluid temperature increase or decrease when the variable is increased with 50% and when the variable is decreased with 50%.

Table 3-2: Sensitivity of the temperature model parameters

Variable:	Variable increased:	Variable decreased:
Circulation rate	Temp. decreased with 7 °C	Temp. increased with 10 °C
Circulation time	Temp. decreased with 2 °C	Temp. increased with 2 °C
Drilling fluid density	Temp. decreased with 6 °C.	Temp. increased with 9 °C
Drilling fluid viscosity	Temp. decreased with 2 °C	Temp. increased with 5 °C
Geothermal gradient	Temp. increased with 40 °C	Temp. decreased with 40 °C
Inlet temperature	Temp. slope increased	Temp. slope decreased
Conductivity of tubing	Temp. increased with 0,0702 °C	Temp. decreased with 0,2099 °C.
Heat capacity of fluid	Temp. decreased with 9 °C	Temp. increased with 11 °C
Earth density	Temp. increased with 1,1577 °C	Temp. decreased with 1,9155 °C
Tubing inner diameter	Temp. increased with 8 °C	Temp. decreased with 11°C
Tubing outer diameter	Temp. decreased with 4,7 °C	Temp. increased with 14,3 °C
Wellbore diameter	Temp. decreased with 6,1 °C	Temp. increased with 5,7 °C
Temperature surface	Temp. increased with 15,7 °C	Temp. decreased with 15,7 °C
Conductivity of earth	Temp. increased with 3,3 °C	Temp. decreased with 6,6 °C
Heat capacity of earth	Temp. increased with 1,2 °C	Temp. decreased with 1,9 °C
Thermal conductivity drilling fluid	Temp. increased with 3,8 °C	Temp. decreased with 7,6 °C

From table 3-2 above, it is possible to observe that the fluid temperature in both the drillpipe and the annulus is sensitive to changes in different parameters. It can be observed that the bottomhole fluid temperature is most sensitive to variables like the circulation rate, drilling fluid density, tubing inner and outer diameter, geothermal gradient and heat capacity of the fluid, when varying the given variable by 50%. Table 3-2 above shows the different temperature increase and decrease for the different variables. It is observed that the geothermal gradient is the variable that affects the fluid temperature in the largest amount. However, for the geothermal gradient and other variables like the earth density, heat capacity of earth and conductivity of earth, they are not possible to change, in the

meaning that they are constant and cannot be manipulated, as which is possible for the other variables. Nevertheless, it is still useful to have information about how these constant variables affects the fluid temperature.

For the dimensions, regarding the tubing inner and outer diameter and the wellbore diameter, it can be observed that the fluid temperature is affected by changes in their dimensions. For the wellbore diameter, the bottomhole fluid temperature increases with 5,7 °C when the wellbore diameter is decreased with 50%. When the wellbore diameter is increased with 50%, the bottomhole fluid temperature decrease 6,1 °C. For the outer diameter of the tubing, the fluid temperature decreases with increasing outer diameter and the fluid temperature increases for decreasing outer diameter. For the inner diameter of the tubing, the opposite is the case. For increasing inner diameter, the fluid temperature increases and for decreasing inner diameter, the temperature decreases. To illustrate the effect of the inside- and outside diameter of the tubing and wellbore on the fluid temperature, plots illustrating these cases have been included. The two plots to the left below illustrates the base case, and the two top plots to the right illustrates the temperature for 50% decrease in the inner diameter of the tubing, and the bottom plot illustrates the temperature for 50% decrease in the wellbore diameter.
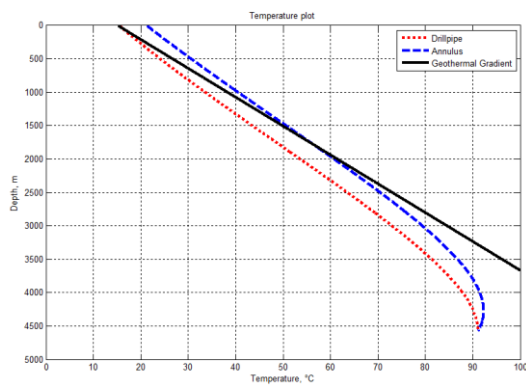
Base case
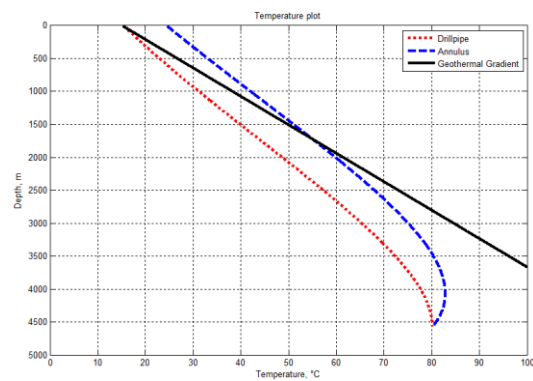
Decrease in inner pipe diameter
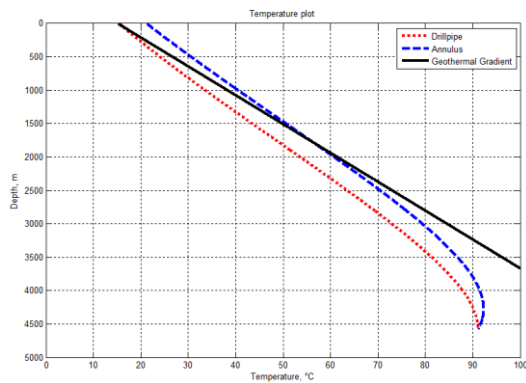
Base case
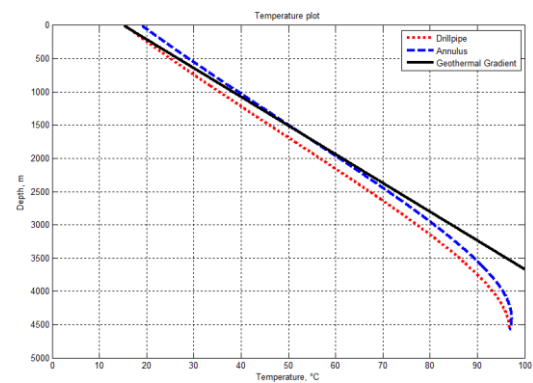
Decrease in wellbore diameter

13

In this thesis, particular focus is on the density and viscosity of drilling fluid. If the temperature is studied, first for the fluid density, it can be observed that for 50% increase in the drilling fluid density, the bottomhole temperature decreases with 6 °C. For 50% decrease in the drilling fluid density, the bottomhole fluid temperature increases with 9 °C. The plots below illustrates this. The plots to the left represent the base case. The two top plots to the right illustrates the increase in the drilling fluid density and the bottom plot illustrates the decrease in the fluid density.
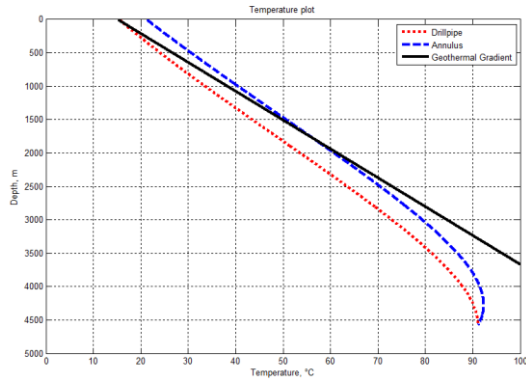
Base case
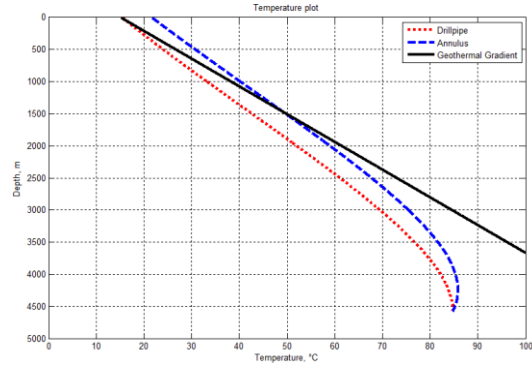
Increase in density
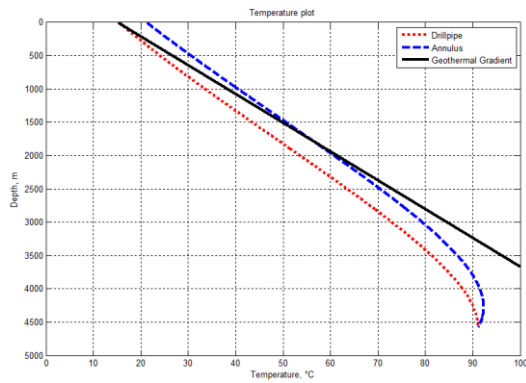
Base case
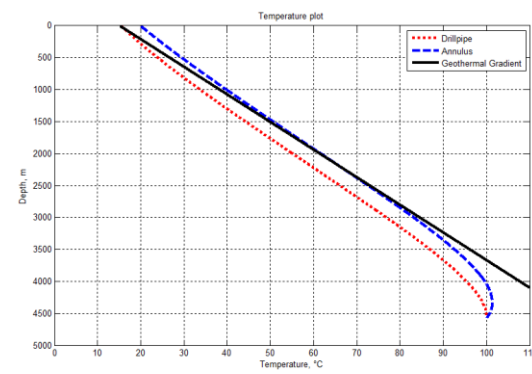
Decrease in density

If the drilling fluid viscosity is studied, it can be observed that for 50% increase in the fluid viscosity, the bottomhole fluid temperature decreases with 2 °C. For 50% decrease in the fluid viscosity, the bottomhole fluid temperature increases with 5 °C. The plots below illustrates this. The two plots to the left represent the base case. The top plot to the right illustrates the increase in the drilling fluid viscosity and the bottom plot illustrates the decrease in the fluid viscosity.

Base case

Increase in viscosity

Base case

Decrease in viscosity
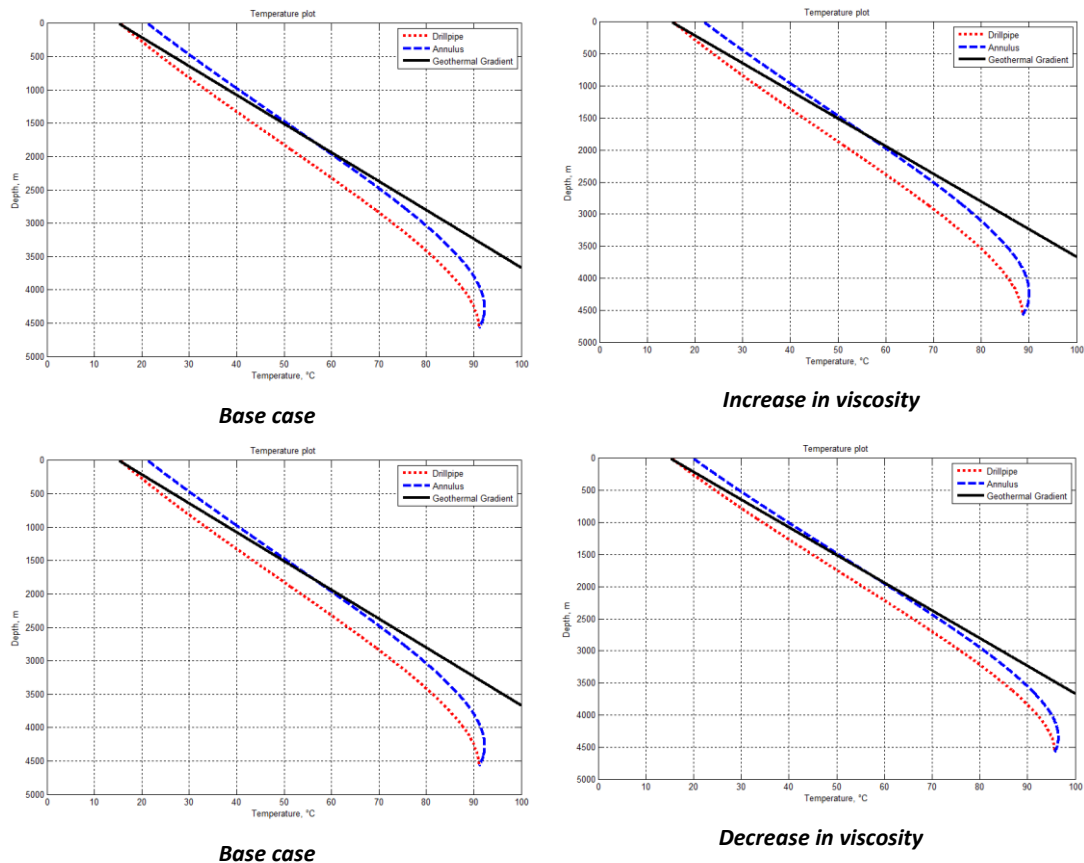
It can be noticed, that the bottomhole fluid temperature, according to these findings above for density and viscosity, are most sensitive to changes in the density.

Some other comments regarding the different parameters could be mentioned:

- Inlet temperature: For 50% increase and decrease in the inlet temperature, the bottomhole fluid temperature is constant. The initial temperature of the plots varies with the inlet temperature, and since the bottomhole fluid temperature is constant, the slope of the plotted temperature in the well varies when the inlet temperature is varied. For increased inlet temperature, the slope of the plots is "moved" to the right, in other words the temperature is increased. For decreased inlet temperature the slope of the plots is "moved" to the left, the temperature is decreased.
- Conductivity of tubing: For 50% increase in the conductivity, the bottomhole temperature is not affected in any meaningful way, i.e. the temperature is increased by 0,0702 °C. For 50% decrease in the conductivity, the bottomhole temperature is decreased by 0,2099 °C. An interesting observation, is that for very high and low

15

values (unrealistic), the temperature is almost not affected by increased conductivity and highly effected by decreased conductivity. For e.g. 0.03459 ($\frac{W}{mK}$) (low value), the temperature is only increased by 0,211 °C. For e.g. 34591.54 ($\frac{W}{mK}$) (high value), the temperature is decreased with 55 °C.

Chapter 4: Evaluation of drilling fluid properties

4.1: DRILLING FLUID PROPERTIES

The above presented temperature model allow for the fluid temperature downhole to be calculated. This is important knowledge since the temperature affects the drilling fluid properties. In this section, the effect of temperature and pressure on drilling fluid properties, like density and viscosity, will be investigated. Models for density and viscosity calculation will be presented.

4.2: BACKGROUND OF THE DENSITY MODEL

Drilling fluid density is affected by temperature and pressure. Increasing pressure increases drilling fluid density, while increasing temperature decreases drilling fluid density. This is because drilling fluids are compressed by pressure, and thereby leading to an increase in the fluid density. When drilling fluids is heated it expands, and thereby leading to a decrease in fluid density. The figure below illustrates this. From the figure, it can be observed, that for increasing temperature, the density decreases. For example at pressure 400 bar, the density is lower for 154°C than for 20°C. It is also possible to observe the effect of increasing pressure on the drilling fluid density. From the plots, it is observable that increasing pressure clearly increase the density as well.
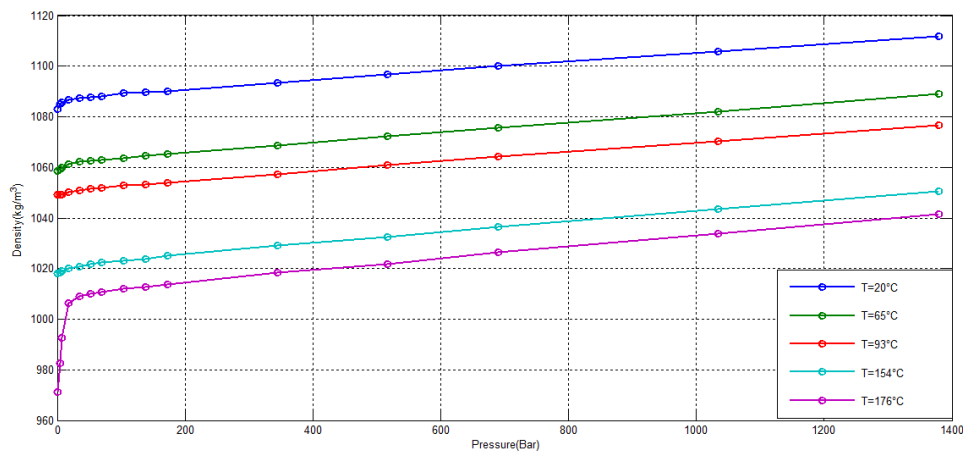
Figure 4-1: Density variations as a function of temperature and pressure

An increase in pressure will always cause an increase in fluid density. For temperature, the density will in most cases decrease with increasing temperature. However, there are some cases where this is not true. An example of this is for water. For water, the density increase between 0°C and 4°C, but when the temperature exceeds 4°C, the density again decrease with increasing temperature. In the table below, this effect can be seen.

Table 4-1: Water density as a function of temperature

Water temperature [°C]	Water density [$\frac{g}{cm^3}$]:
0	0.9998425
+1	0.9999015
+2	0.9999429
+3	0.9999672

17

| +4 | 0.999975 |
| +5 | 0.9999668 |

As mentioned several times, the temperature affect the density of the drilling fluid in both the annulus and in the drillpipe. Therefore, to estimate the equivalent circulating density (ECD) under conditions with high temperatures, it requires information about the downhole temperature. For this, sensors could be used, but the use of models give several advantages. A temperature model is useful, because with such a model it is possible to calculate the temperature for the entire well, and study the effect of the different parameters of the fluid temperature. The effect on the ECD increases with depth and temperature in the well when the difference between the temperature in the formation and the mud increase.

4.3: DENSITY MODELLING IMPORTANCE

To know the correct fluid density is important for several reasons. Drilling fluid density is the key factor for determining the hydrostatic pressure in a well. To determine the hydrostatic pressure, this equation is used:

$$P = \rho g h \hspace{4cm} (\text{ 4-1 })$$

Where P is the hydrostatic pressure, ρ is density of the drilling fluid, g is gravitational acceleration and h is the vertical depth in the well. Correct hydrostatic pressure in a well is very important. Often the mud weight/drilling fluid density is selected to be between the pore pressure and fracture pressure. Where the pore pressure would be the limit for low mud weight, and the fracture pressure would be the limit for high mud weight. Pore pressure is the pressure of the fluids in the pores of a formation. The fracture pressure is the pressure that will cause the formation to fracture hydraulically. If the mud weight is too high, several problems can occur. An example of this is stuck pipe or fracture, which again can cause mud losses. Too low mud weight on the other, can cause problems like collapse and kick. According to Aadnøy, by keeping the mud weight close to the level of the in-situ stress, most of the problems in the borehole could be minimized.[33]

As the density varies, it affects the buoyancy factor. The buoyancy factor is again connected to the weight of the drillpipe, which again will affect the torque and drag force in the well. These effects will be studied later. Some of the other problems related to the density of the mud, will now be presented:

- Borehole collapse: If the mud weight in the well is too low, collapse of the borehole could occur. By increasing the mud weight, this problem could be avoided. This is because a higher mud weight will balance the rock stress.[34] A consequence of borehole collapse could be that fragments from the collapse is filling the wellbore, this could lead to a stuck pipe situation.
- Clay swelling: As for the case with borehole collapse, if a too low mud weight, problems could occur. Another of these problems is clay swelling. Clay swelling is a type of problem where clay swells (increase in volume) due to clay absorbing water from the drilling fluid. This makes the clay swell into the wellbore and thereby reduces the wellbore diameter. A reduced wellbore diameter could lead to problems like a stuck pipe. Prevention methods for clay swelling include using an inhibited mud system. Different salts could be added, like potassium or calcium, in order to reduce the chemical attraction of the water to the shale.[35]

18

- Differential sticking: If the mud weight in the well is too high, differential sticking may occur. The drillstring cannot be rotated in this mode. This is a problem where the pressure in the well is higher than the formation pressure, because of low reservoir pressure, high-pressures in the well or both of these two conditions.[36] This has the consequence of creating high contact forces over an area, and this makes the drillstring pressed against the wellbore wall and potentially stuck. Differential sticking is considered as the greatest drilling problem in the world when concerning time and money spent.[37] To avoid differential sticking, the mud weight should not be too high. However, it should neither be too low to avoid potential collapse problems.
- Lost circulation: Lost circulation is the event where drilling fluid is lost to the formation. One of several reasons for lost circulation is too high mud weight. Other factors for lost circulation could be: Mechanically weak and fractured formation, seepage loss and cementing.[38] To control a potential loss of drilling fluid, different lost circulation materials (LCM) may be used. Lost circulation is an expensive event and could potential lead to a severe situation. This is because the loss of mud and wellbore pressure, initiation of flow could be the result. Inflow of formation fluids could again lead to a kick situation, and if not correctly handled, a blowout could be a worst-case situation. To avoid lost circulation, generally, the mud weight should be below the value where lost circulation would occur.

If there for example is a lost circulation situation, a potential kick situation can develop. The definition of kick is influx of formation fluid into the well. Formation fluid could be oil, gas or water. It happens in situations where the pressure in the well is lower than the formation pressure. Generally, three parameters needs to be in place for a kick to occur:[39]

- Wellbore pressure < Pore pressure
- Reasonable permeability
- Presence of formation fluid

When these parameters are in place, there could be several reasons for a kick:[40]

- **Insufficient mud weight:** As mentioned, the pressure in the well should be higher than the formation pore pressure in order to control the formation pressure. If the pressure in the well, because of insufficient mud weight, decreases below the formation pressure, formation fluid will start to enter the wellbore from the formation. As discussed, the pressure in the well is due to the fluid that is used in the well. Therefore both changed density of the mud or losses of mud to the formation, would affect the pressure in the well.
- **Swabbing effects:** If pulling out of the hole too rapidly, a vacuum could be created. This vacuum could make formation fluid enter the wellbore.
- **Improper fill up:** Can cause fluid level drop in the well, which again can lower the wellbore pressure below the pore pressure.
- **Gas cut mud:** Gas have lower density than drilling mud, and if drilling through a gas-bearing zone, the density of the drilling fluid could be reduced. This could lower the wellbore pressure below the pore pressure.
- **Lost circulation:** As discussed above, if there is too high mud weight in the well compared with the pressure of the formation, loss of circulation fluid could occur. The loss of circulation fluid could lower the wellbore pressure in the well below the pore pressure and a kick could occur.

From the mentioned problems that can occur from wrong mud weight, the need for accurate density modelling is clear. The problems mentioned above, could both be financial damaging and be an integrity problem. A kick could, if not controlled correctly, develop to a blowout, that is a very severe situation with the potential for e.g. loss of human lives, rig and environmental pollution.

4.4: DENSITY MODEL

The density of drilling fluid is dependent of the pressure and temperature in the well, it would be expressed as: $\rho = \rho(P, T)$. This could also be expressed as a function of depth:[41]

$$\frac{d\rho}{dz}(p, T) = \frac{\partial \rho}{\partial p}\frac{dp}{dz} + \frac{\partial \rho}{\partial T}\frac{dT}{dz} \qquad (4\text{-}2)$$

Different models for density calculation exist. The density model used in this thesis is based on the work by Kaasa et al.[42] and is expressed as:

$$\rho = \rho_0 + \frac{\rho_0}{\beta}(p - p_0) - \rho_0\alpha(T - T_0) \qquad (4\text{-}3)$$

Where the isothermal bulk modulus of the liquid (β) and the cubical expansion coefficient of the liquid (α) is defined as:

$$\beta = \rho_0(\frac{\partial p}{\partial \rho})_T \qquad (4\text{-}4)$$

$$\alpha = -\frac{1}{\rho_0}(\frac{\partial p}{\partial T})_p \qquad (4\text{-}5)$$

p_0, ρ_0 and T_0 are defined as the reference point for the linearization.

The isothermal bulk modulus of the liquid (β) is connected to the stiffness of the fluid. It relates to compressibility of liquid (c) by this relation: $c=1/\beta$. The bulk modulus is used to determine the dynamics of the hydraulic system, by describing what kind of pressure transients is the dominating. It is said that the pressure transient is in the interval between seconds to minutes, and for the temperature dynamics, it is in the interval between minutes to hours.[43] Therefore, for temperature, it is much slower than for pressure, and in that way, by knowing the bulk modules the dynamics of the flow can be determined.

If there is a case with normal temperature and normal pressure, as in many wells, the effect of temperature differences in a well for the density changes, can be neglected for transient effects.[44] This has to do with the fact that the cubical expansion coefficient of the liquid (α) is small and thereby also the changes in density is small. However, for HPHT wells there can be large temperature gradients, which causes quicker temperature transients.[45] Therefore, for a HPHT, it is especially important to consider the effect on density by variations in pressure and temperature. In this thesis, cases with high temperature will be considered to determine the effect on the density.

According to Kaasa et al[46], the accuracy for the model reduces with increasing values for the temperature and pressure. It is said to be accurate for most drilling fluids in the interval between 0 to 500 bar in pressure and 0 to 200 °C for the temperature.

The isothermal bulk modulus of the liquid (β) and the cubical expansion coefficient of the liquid (α) in the density model can be calculated by using linear least squares method. This will now be performed.

4.5: SIMULATION RESULTS

In the following, a MATLAB model is used to investigate the density model. Two plots is presented. One plot illustrating the true density measurements as a function of pressure and temperature. The second plot illustrates the differences between the true density measurements and values for the density calculated by using the linearized density model presented earlier. For the model initial data/reference points for the linearization is defined. Reference points for the density (ρ_0), temperature (T_0) and pressure (P_0) is defined as:

$$\rho_0 = 1083 \ \frac{kg}{m^3}$$

$$T_0 = 20°C$$

$$P_0 = 1 \ bar$$

The complete dataset used and the MATLAB code, can be found in Appendix D.1. The dataset used, varies in pressures from 1 bar to 1378,95 bar and the temperatures used is: 20°C, 65°C, 93°C, 154°C and 176°C. A high pressure well is defined at 690 bar (10 000 psi) and the value of 1378,95 bar is not a particular realistic well pressure scenario, but it is included to have an idea how the density varies for very high pressures. In addition, it is important to keep in mind the above mentioned information that for the density model, the accuracy decreases for pressures above 500 bar. For the varying pressures and temperatures, respectable densities are given. With the dataset in place, it is possible to calculate the so-called best-fit coefficients α and β. As mentioned previously, the isothermal bulk modulus of the liquid (β) is related to the compressibility of liquid (c) by this relation: $c=1/\beta$. So by calculating the compressibility, the isothermal bulk modulus can be calculated to be: $\beta = 4,4983 * 10^9 \ Pa = 44983 \ bar$. The cubical expansion coefficient of the liquid, is found to be: $\alpha = 4,5429 * 10^{-4}$. With α and β in place, the linearized density can be found. The two figures below illustrates the plotted density. Figure 4-2 illustrates the density as a function of pressure and temperature, and figure 4-3 illustrates the differences between the true density measurements and values for the density calculated, by using the linearized density model.
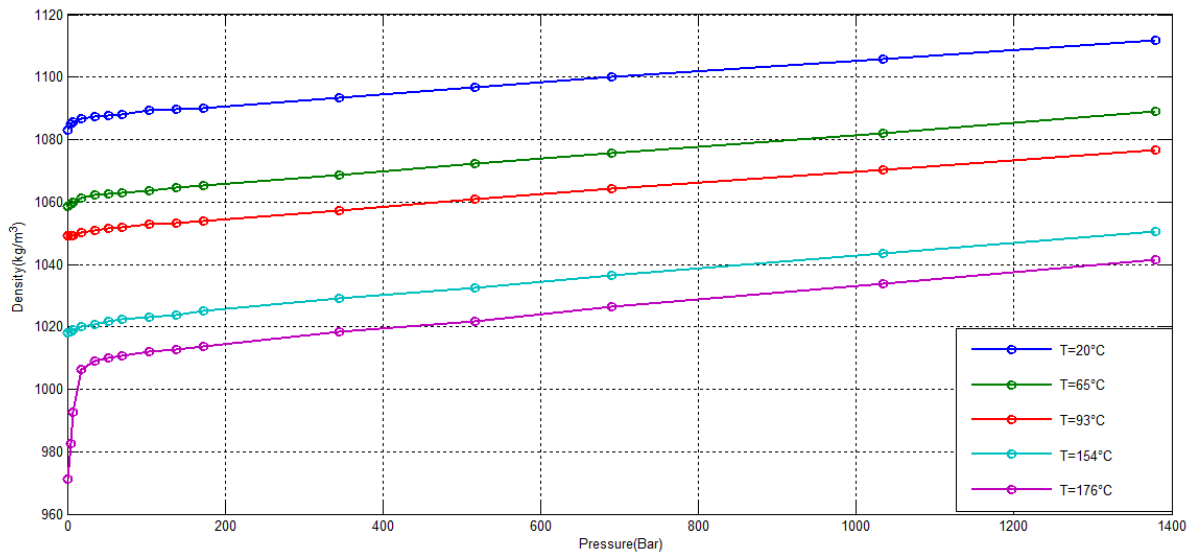
Figure 4-2: Density as a function of pressure and temperature
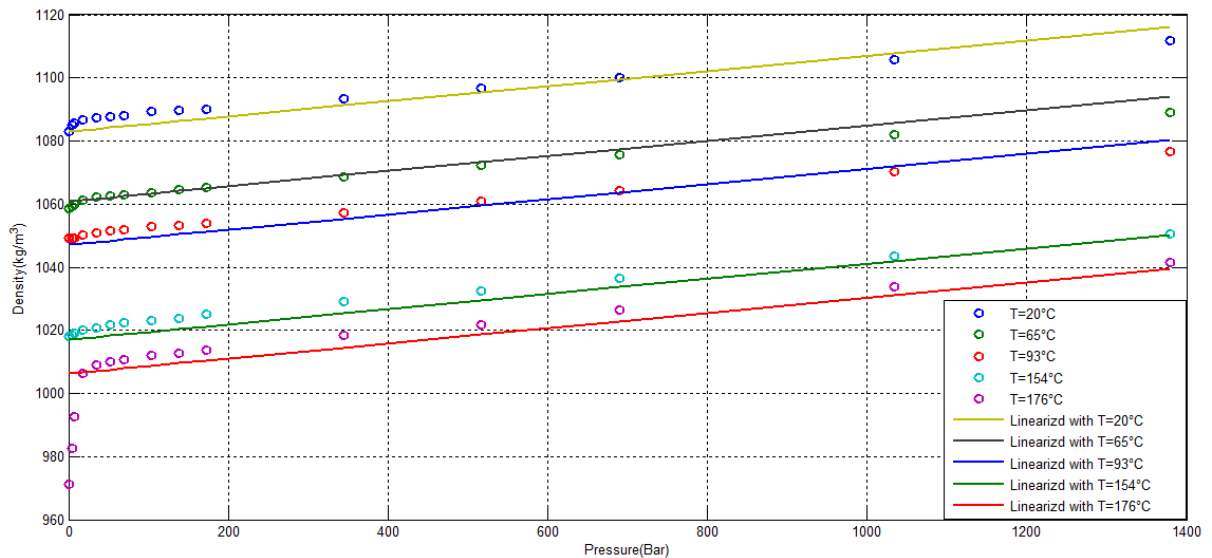
Figure 4-3: Density difference between true density and the linearized density

As seen from the figures above, increasing pressure have the effect on density by increasing it. For increasing temperature, the drilling fluid density decreases. If the two figures above are analyzed, it can be observed that the differences between the density measurements for true density and for linearized density are small, almost negligible. Another observation from the density plots is the noticeable effect of temperature on the density. If the density is studied for a constant pressure, example 172 bar, and temperatures 20°C and for 93°C, it can be seen that for 20°C and 172 bar the density equals to 1090, 1 $\frac{kg}{m^3}$ and for 93°C and 172 bar the density equals to 1053, 7 $\frac{kg}{m^3}$. So, when the temperature changes with 73°C the density changes with 36,4 $\frac{kg}{m^3}$. To illustrate this density mismatch better, the hydrostatic pressure is calculated. For a 1500 m deep well, the bottomhole pressure mismatch equals to: $P_{Hyd} = \rho g \text{H} = 36, 4 \frac{kg}{m^3} * 9, 81 \frac{m}{s^2} * 1500\ m$= 5, 36 bar. It is observed; by neglecting the

22

temperature effect, the mismatch in bottomhole pressure is noticeable. It would especially be of magnitude in deep wells. For example in a 6000 m deep well, the mismatch in bottomhole pressure would be 21,4 bar. The effect of the pressure on the density, can be studied as well. If the density variations is studied for a constant temperature e.g. 93°C and varying the pressure from 1 bar up to 689,5 bar the density is 1049 $\frac{kg}{m^3}$ for 1 bar and 1064 $\frac{kg}{m^3}$ for 689,5 bar. It is observed that the drilling fluid density increases with increased pressure.

From working with the density model, some important observation could be mentioned. One of these observations is the importance of the temperature effect on the fluid density. This also confirms the importance of the temperature model presented earlier. By being able to predict the temperature in the well, it is possible to see how it affects the density of drilling fluid.

4.6: BACKGROUND OF THE VISCOSITY MODEL

Another property of drilling fluid, in addition to density, is viscosity. Viscosity is a property of a fluid that tell something about the fluid resistance to flow.[47] To illustrate the concept of viscosity, a small example from daily life could be mentioned. For example, it could clearly be observed that syrup has a much higher viscosity than water. This has to do with the fact that syrup has higher resistance to flow than the water, i.e. higher viscosity.

Viscosity is dependent of several parameters like temperature, pressure and shear rate. Viscosity is highly temperature dependent. Therefore, to be able to know how a fluid will act under influence of these conditions is of great importance. Viscosity is measured in PaS (pascal second) in SI unit, but often the unit centipoise (cP) is more commonly used.

The viscosity of a material is dependent on what type of material it is, as observed in the syrup/water example. The viscosity of that material is again dependent on the temperature. For example if the syrup, mentioned above, is heated, it will flow more easily, i.e. the viscosity of liquid decreases with increasing temperature, and opposite the viscosity increases with decreasing temperature. For example, the viscosity of water at temperatures between 0-100 °C decreases from 1.79 cP to 0.28 cP with the increase in temperature. This statement will also be backed up by experimental data of a water-based mud sample presented later. During normal conditions, the viscosity of a liquid is said to not be affected by pressure and can in many cases be neglected. However, if the pressure is very high, liquids can have increased viscosity.[48] For gases, the viscosity increase with increasing temperature and is said to be almost independent of pressure increase/decrease.[49]

Viscosity is defined as the shear stress divided by the shear rate.[50]

$$\mu = \frac{\tau}{\gamma}$$
(4-6)

Where μ is the viscosity [PaS], τ is the shear stress [Pa] and γ is the shear rate [sec^{-1}]. A measurement of viscosity need to have the shear rate specified to be meaningful.

4.7: RHEOLOGY MODEL

The viscosity of a fluid is, as for the density, a function of pressure and temperature, as well as the time. It could be expressed as: $\mu = \mu$(P,T,t), where μ is viscosity, P is pressure, T is

temperature and t is the time variable. For increasing temperature, the viscosity of drilling fluid decrease considerably.[51] This will be demonstrated with a rheology experiment later.

According to Kaasa et al[52], and as mentioned above, normally the effect of the pressure on viscosity can be neglected because of its minor effect. The effect of the temperature on the other hand is not neglible. The effect of temperature on the viscosity can be expressed as:

$$\mu = \mu_0 e^{-\lambda(T-T_0)} \tag{4-7}$$

Where μ is the absolute viscosity at temperature T, μ_0 is the visocisty at T_0 (reference temperature) and λ is a constant parameter that is dependent on the fluid.

Rheology is the study of flow and deformation of fluids. Fluids can be classified by their rheological behavior.[53] Fluids can be separated into Newtonian fluids and non-Newtonian fluids. For non-Newtonian fluids, there are seven major rheological models.[54] These are: Bingham plastic model, Power Law model, API model, Herschel-Bulkley model, Unified Model and Robertson-Stiff. Rheological models purpose is to try to help in describing the fluid flow in the best way. The figure below illustrates some of the different rheological models that exist.
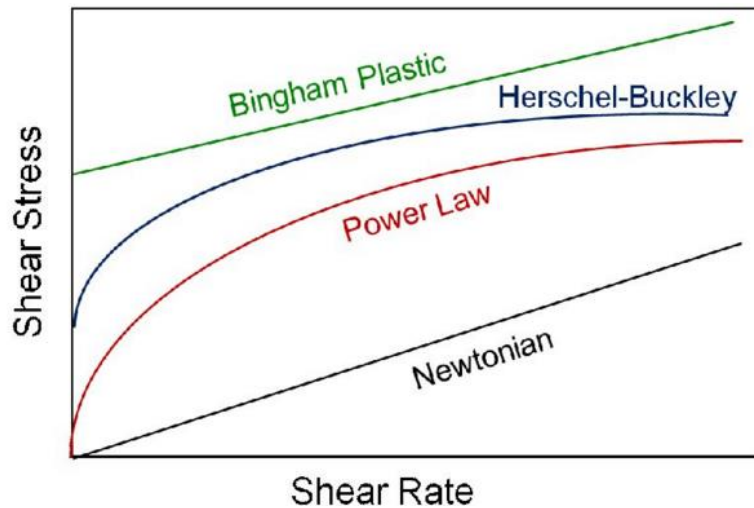
Figure 4-4: Different rheology models [55]

As mentioned, fluids can be classified as Newtonian fluids and non-Newtonian fluids. The difference between such fluids, and rheological models for the two fluids, is presented below:

Newtonian fluids: Newtonian fluids are fluids that follow Newton's law of viscosity, and is given as:[56]

$$\tau = \mu\gamma \tag{4-8}$$

Fluids with constant viscosity during changing shear rates is called Newtonian fluids. An example of a Newtonian fluid is water. For Newtonian fluids, the shear stress is directly proportional to the shear rate.

Non-Newtonian fluids: Non-Newtonian fluids are fluids that do not follow Newton's law of viscosity. Non-Newtonian fluids are fluids where the viscosity varies with varying shear rates. For this type of fluid, the shear stress is not directly proportional to the shear rate.

Most drilling fluids, is said to be non-Newtonian. For non-Newtonian fluids, there are different rheological models, the most important will be explained briefly:

- **Bingham Plastic Model:** This model is given by this equation:[57]
$$\tau = \mu_p \gamma + \tau_y.$$ (4-9)

  Where μ_p represent the plastic viscosity, γ is the shear rate and τ_y is the yield point. The plastic viscosity is the slope of the graph in the linear part, and tell how much the graph increases or decreases. The Bingham model, could be used to describe a fluid that shows yield stress and a Newtonian component. The yield stress would be the amount of applied shear stress that is needed to make the fluid flow. Once the fluid have reached its yield stress, the fluid will act as a Newtonian fluid with the shear stress increasing. The fluid acting as a Newtonian fluid, means that the shear stress of the fluid increases linearly. The Bingham model is said to not be a good representation of the behavior of the drilling fluids at very high shear rate or at very low shear rates. High shear rates could occur at the bit and low shear rates in the annulus.[58]
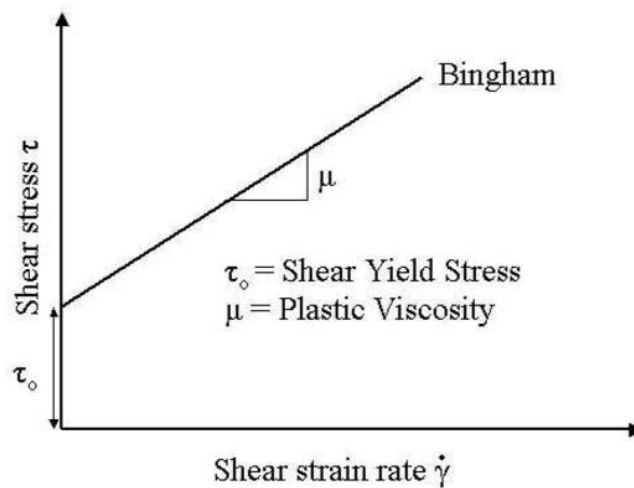
Figure 4-5: Bingham plastic behavior[59]

- **Power Law Model:** The Power law model is given by this equation:[60]

$$\tau = k\gamma^n \qquad (4\text{-}10)$$

Where γ represent the shear rate, k is the consistence index and n is the flow behavior index. Estimation for k and n can be found by: [61]

$$n = 3.32\log(\frac{R_{600}}{R_{300}}) \qquad (4\text{-}11)$$

$$k = \frac{R_{300}}{511^n} = \frac{R_{600}}{1022^n} \qquad (4\text{-}12)$$

Where R_{300} and R_{600} are measurements at 300 rpm and 600 rpm. To convert from rpm to shear rates, this formula could be used:

$$\gamma = 1,703 * rpm \qquad (4\text{-}13)$$

This means for 300 rpm and 600 rpm, the shear rates would be respectively 511 s^{-1} and 1022 s^{-1}. From the model, it is seen that the Power law model consider the relationship between the viscosity and shear rate, this could be a better fit than for the Bingham model, where an assumption is made that it is a linear relationship between the shear rate and the shear stress.

- **Herschel-Bulkley Model**: The Herschel-Bulkley model is given by this equation:[62]

$$\tau = \tau_y + k\gamma^n \qquad (4\text{-}14)$$

Where τ_y represent the yield point, γ is the shear rate, k is the consistence index and n is the flow behavior index. k and n is above described how they can be found. It can be observed that this model combines the Bingham model and the Power Law model. This model do consider both the yield stress point and include the power law term that consider the relationship between the viscosity and shear rate. This is one

reason why the Herschel-Bulkley model is often used to describe drilling fluid in an oil well.[63]

4.8: VISCOSITY EXPERIMENT

4.8.1: Viscosity experiment background

In order to obtain more knowledge and information about the rheology behavior for drilling mud, an experiment including different water-based mud samples were performed. The experiment was conducted on a rheometer. From the rheometer, different data were measured and displayed. Some of the data available from the experiment were shear rate, shear stress and viscosity. For all the measurements, the shear rates were varied in the same interval for all samples. A short explanation of shear rate and shear stress is given below.

Shear stress: The shear stress (τ) is defined as the shear force divided by area acted on by the shear force:

$$\tau = \frac{F}{A} \qquad\qquad (\text{4-15})$$

It is the force per unit area, which is required to sustain a constant rate of fluid movement.[64] Shear stress is measured in Pascal.

Shear rate: It is the rate of shear applied on a fluid. The shear rate is the velocity gradient measured across the diameter of a type of shape, like pipe or annulus.[65] As it will be explained from the experiments later, fluids that are shear dependent will change their viscosity with changing shear rates. Shear rates are measured in sec^{-1}.

For most drilling fluids, the viscosity varies with the shear rate. This effect will be illustrated in the experiment conducted. In the experiment, the viscosity was tested for different shear rates in order to investigate the effect of the different shear rates.

4.8.2: Rheometer

The viscosity experiment was conducted on a rheometer. A rheometer is an instrument that can measure a fluid response to applied forces. For the experiment, the rheometer was connected to a computer with a software program able to read the measurements from the rheometer. All the measurements were recorded in the computer software. The data retrieved from the experiment were shear rate, shear stress, viscosity, speed, torque and temperature. The experiment was carried out on an Anton Paar MCR 302 rheometer. The figure below is an illustration of the type of rheometer that the viscosity experiment was performed on.

Figure 4-6: Anton Paar MCR-302[66]

4.8.3: Viscosity experimental results

The samples used for the experiment were mixed properly before measurement started, and samples were handled carefully due to potential errors for the measurements. To the extent possible, the time from the samples were mixed to they were placed in the rheometer for testing, were minimized to avoid external effects on the samples, like unwanted temperature effects. In total 10 samples were tested. Half of the samples were bentonite based and the other half of the samples were chalk based. Different additives were added to both the bentonite samples and the chalk samples. Additives used were Polypac, Duotec, CMC EHV and CMC LOVIS. The concentration of additives were varied in order to investigate the effect of the additives on the measured variables.

Below is a table of the 10 different mud samples that were tested in the rheometer.

Table 4-2: Viscosity samples

Sample:	Bentonite	Polypac	Duotec	CMC EHV	CMC LOVIS	Chalk
1	6,8 g	0,6 g	Duotec 0,3	-	-	-
2	9,0 g	0,6 g	Duotec 0,3	-	-	-
3	6,8 g	0,3 g	Duotec 0,3	-	-	-
4	6,8 g	0,6 g	Duotec 0,6	-	-	-
5	6,8 g	-	-	0,34 g	0,4 g	-
6	-	0,6 g	0,3 g	-	-	9,49 g
7	-	0,6 g	0,6 g	-	-	6,8 g
8	-	0,6 g	0,3 g	-	-	6,8 g
9	-	0,3 g	0,3 g	-	-	6,8 g
10	-	-	-	0,34 g	0,4 g	6,8 g

Below is a table (table 4-3) with viscosity and shear stress for the 10 different samples. For the experiment, the shear rates were varied between 4,24 S^{-1} to 1020 S^{-1} for all the samples.

28

The temperatures were varied between 25 °C to 150 °C, with an increase of 25 °C for each measuring interval. Due to the extent of the data amount, it is chosen to only present data for temperatures 25 °C and 150 °C, and shear rates 4,24 S^{-1} and 647 S^{-1}. To present the data for these temperatures and shear rates, gives a good presentation of the viscosity and shear stress development with increasing temperatures and shear rates. Plots for all of the samples can be found in Appendix B and Appendix C.

If the data are analyzed, it is observed that there are differences in terms of viscosity and shear stress for the different samples. Samples 1 to 5 are made out of bentonite and samples 6-10 are out of chalk. It can be observed that the viscosity generally is higher for the bentonite samples than for the chalk samples.

It can be observed that the highest viscosities is for sample 2 and 4. For sample 2, the amount of bentonite was increased, resulting in an increase in the viscosity as well. For sample 4, the amount of Duotec was increased compared to sample 1. By increasing the amount of Duotec with twice as much compared to sample 1, it is observed that the viscosity almost triples. For the chalk samples, the lowest viscosity is found for sample 10, where the sample additives are CMC EHV and CMC LOVIS.

From the data and as mentioned before, it is possible to see that the viscosity decreases with increasing shear rates and increasing temperatures. This is true for all samples. From the data, it can also be seen that the shear stress increases with increasing shear rates, and the shear stress decreases with increasing temperature.

Table 4-3: Viscosity and shear stress at different temperatures and shear rates

Sample	Viscosity [mPaS], 25°C & Shear Rate 4,24 [1/S]	Viscosity [mPaS], 25°C & Shear Rate 647 [1/S]	Viscosity [mPaS], 150°C & Shear Rate 4,24 [1/S]	Viscosity [mPaS], 150°C & Shear Rate 647 [1/S]	Shear Stress [Pa], 25°C & Shear Rate 4,24 [1/S]	Shear Stress [Pa], 25°C & Shear Rate 647 [1/S]	Shear Stress [Pa], 150°C & Shear Rate 4,24 [1/S]	Shear Stress [Pa], 150°C & Shear Rate 647 [1/S]
1	429	18	394	5,35	1,82	11,7	1,67	3,46
2	1020	31,7	740	11,9	4,31	20,5	3,14	7,69
3	622	20,6	480	7,53	2,64	13,4	2,04	4,88
4	1270	37	735	8,98	5,41	23,9	3,12	5,81
5	864	20,6	464	8,03	3,66	13,3	1,97	5,19
6	121	10,4	8,27	1,32	0,513	6,74	0,0351	0,851
7	416	16,9	8,72	1,52	1,76	10,9	0,037	0,985
8	128	10,2	8,46	1,32	0,545	6,6	0,0359	0,852
9	92,8	7,74	11,5	1,18	0,393	5,01	0,0488	0,763
10	14,8	5,55	8,53	1,15	0,0626	3,59	0,0362	0,742

The data from the experiment is plotted. One plot with the shear stress against the shear rate and one plot for the viscosity against the shear rate. By using regression-analysis on the experimental data, coefficients are found that can be used to estimate the Reynolds number, which again is important for several reasons, like determining the type of fluid flow.

The Bentonite fluid can be described using the Bingham plastic model. It is defined as:

$$\tau = \tau_y + \mu_{pl}\gamma \qquad\qquad\qquad (\,4\text{-}16\,)$$

Where τ_y is the yield stress, μ_{pl} is the regression coefficient, which tell how much the graph increases or decreases and γ is the shear rate. The Bingham model, as mentioned, could be used to describe a fluid that shows yield stress and a Newtonian component.

Above some general observations were made for the experimental data for the 10 samples. Ideal all 10 samples should have been analyzed further and in more depth, but due to time restrictions this was not possible. In the further work in this thesis, the focus will be on sample 2.

4.8.4: Analysis of Sample 2

For the analysis of sample 2, a new simulation model is made. This model includes the temperature model previous presented in chapter 3, but some of the variables are updated to better correlate with the experimental data of sample 2. In the simulation model, the inlet temperature is changed from 15,5 °C to 25 °C and the initial viscosity is changed from 45,5 mPaS to 31.7 mPaS. These new variables are the same as from sample 2, from the viscosity experiment. In addition, the geothermal gradient have been increased from 0,0231 $\frac{°C}{m}$ to 0,0455 $\frac{°C}{m}$, this is to increase the bottomhole fluid temperature from about 91 °C to 165 °C. This is done in order to better investigate the full specter of viscosity versus temperature, and also simulate high temperature conditions. The geothermal gradient of 0,0455 $\frac{°C}{m}$ is a high value. It is not normal with that high geothermal gradient, but in this case, it is used to investigate the case with high temperature better.

For Sample 2, the behavior of the mud can be studied. As mentioned above, the shear rates is varied between 4,24 S^{-1} to 1020 S^{-1} for all the samples. The temperatures were varied between 25 °C to 150 °C with an increase of 25 °C for each measuring interval. The graph below shows the decreasing viscosity in mPaS with increasing shear rates. It can also be observed, from the graph, as mentioned earlier, that the viscosity decreases with increasing temperatures.
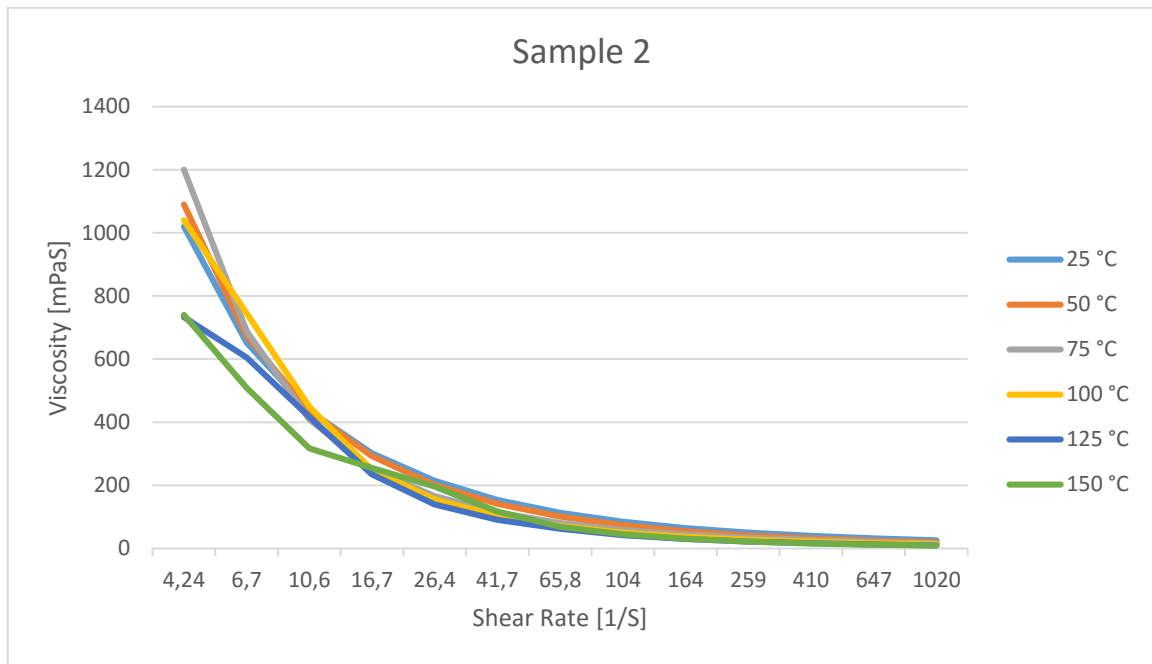
Figure 4-7: Illustrates the decreasing viscosity for increasing temperatures and shear rates

For the samples used in the viscosity experiment, it was not possible to perform density measurements. Therefore, in order to have density measurements, the density dataset presented earlier in chapter 4.5, will be used. This is not the same mud sample, and it is a simplification. The density dataset, presented earlier, gives the density for temperatures 4, 20, 65, 93, 154 and 176 °C, and for different pressures. In the calculation for the viscosity, the standard start temperature used is 25 °C and 1 bar, therefore the density at 25 °C and 1 bar needs to be found. The density data is of a linear type, this allow for the use linear interpolation. The formula for linear interpolation is given below:

$$f(x) = f_1 + (f_2 - f_1)\frac{(x-x_1)}{(x_2-x_1)} \qquad (4\text{-}17)$$

To find the density at 25 °C and 1 bar, density values at 20 °C and 65 °C is used.

$$f(25) = 1{,}083156627 + (1{,}05853027 - 1{,}083156627)\frac{(25-20)}{(65-20}$$

$$f(25) = 1{,}080420365 \text{ s.g.}$$

This density is now used in the temperature model, presented in chapter 3, to calculate the viscosity under varying downhole conditions. The plot below shows the fluid temperature in the annulus and the drillpipe, with the new well parameters like viscosity, density and increased geothermal gradient.
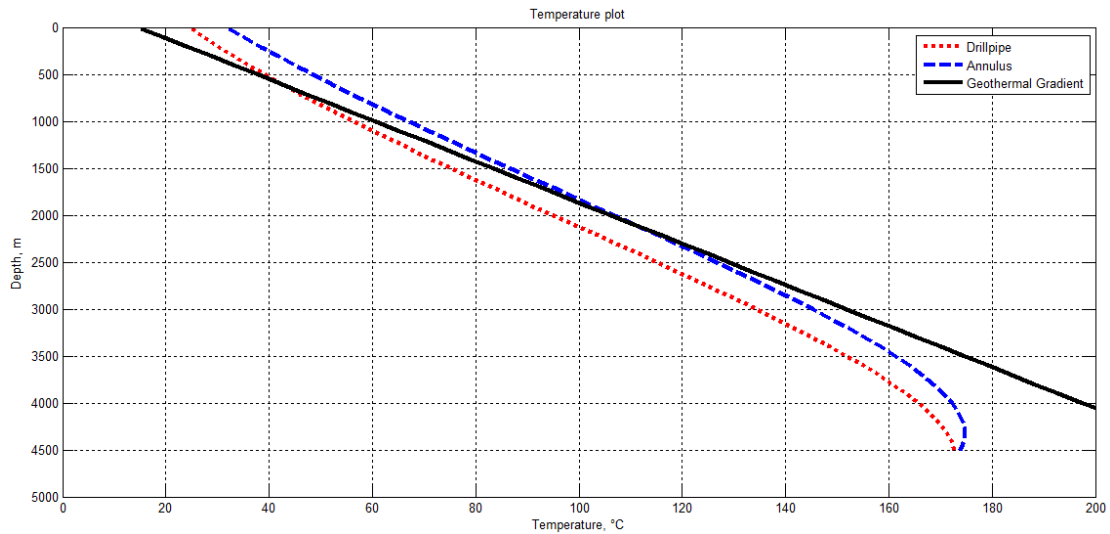
Figure 4-8: Temperature in the drillpipe and annulus

The mud type used in this calculation is of a Bentonite type, named Sample 2 in the experiment measurements. The mud is, as presented above in table 4-3, made out of bentonite (9 gram) and additives Polypac (0,6 gram) and Duotec (0,3 gram). The viscosity is found by a rheometer with different shear rates and temperatures. The viscosity used, is from shear rates 647 S^{-1} and temperatures 25, 50, 75, 100, 125 and 150. Shear rates of 647 S^{-1} were used, because this is a middle value between the highest and lowest shear rates. A shear rate of 647 S^{-1} equals to 380 in rpm. By using the above-mentioned information for shear rate and temperatures, the data was plotted and a linear model was developed. The linear model for this type of mud is as follow:

$$Y = -0,160116X + 33,76 \qquad\qquad (\,4\text{-}18\,)$$

Where X represents the changing temperature, -0,160116 is the "slope" number, that is indicating that the viscosity is decreasing with increasing temperature. The figure below, shows the viscosity against temperature for the bentonite fluid, sample 2. It can clearly be observed that the viscosity decreases with increasing temperature. A linear trend line is added and represents the Y-term presented above. The R^2 symbol, which can be observed in the figure, is a number telling the difference between the real measurements and the linear trend line, in other words, it tells how well the regression equation fits the real measurements. It is a number between 0 and 1, where 1 is an indication of a perfect fit.
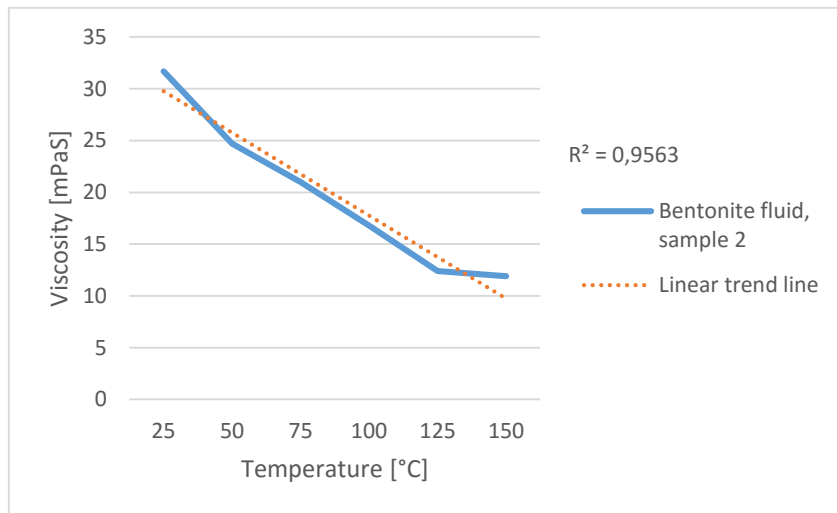
Figure 4-9: Viscosity with increasing temperature

With the temperature behavior of the sample and a model for viscosity as a function of temperature in place, the fluid viscosity of the sample can be simulated. The new simulation model that is developed, allow for simulating the behavior of sample 2 with different temperatures. As for the temperature, the viscosity is divided into 46 segments, each of a length of 100 m. The simulation is performed on MATLAB and the results is plotted, see the figure below. The now found fluid viscosity data, will later be used in the calculation of the pressure in the well.
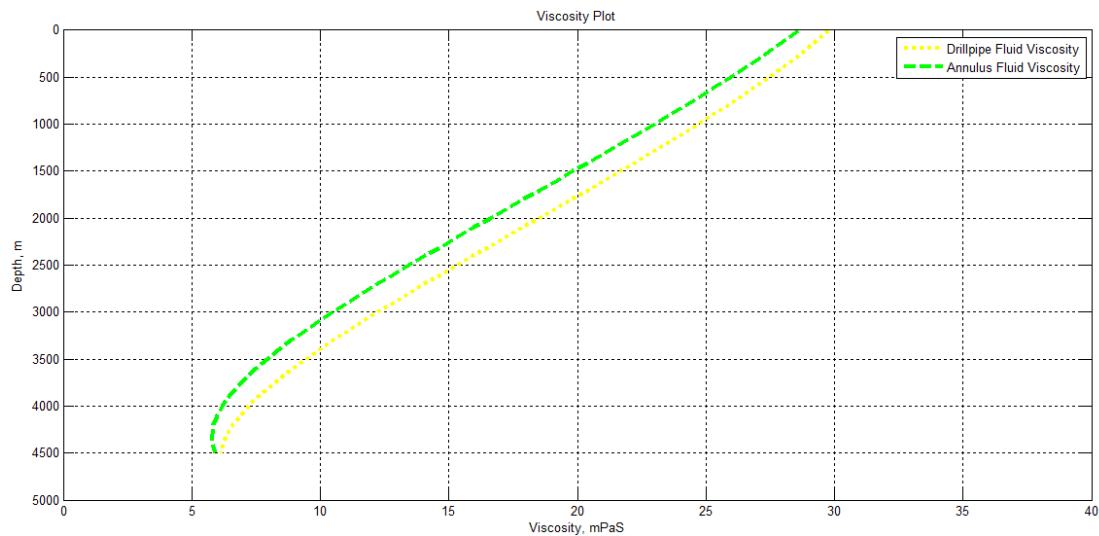
Figure 4-10: Viscosity of sample 2 as a function of temperature with depth

4.9: PRESSURE CALCULATION

4.9.1: Pressure calculation background

The equivalent densities for wells that are circulated and wells that are not circulated, are separated. According to Kårstad & Aadnøy[67], if the well is not circulated, there will be no frictional pressure loss in the well. Potential density variations would then be because of temperature and pressure effects. For temperature, it would be because of thermal expansion. For pressure, it would be because of compression of the drilling fluid. According to Kårstad & Aadnøy[68], for a shallow well, where the mud can be considered almost incompressible, the equivalent circulating density is almost identical to the surface density.

The dynamic fluid pressure loss gradient ($\frac{dP}{dX}$) in a pipe, is a function of several factors. It is a function of factors like the diameter of the pipe, viscosity of fluid, density of fluid, velocity of fluid, roughness of the pipe wall, inclination of pipe and what type of flow regime.[69] For both single- and multiphase flow, it is separated between laminar and turbulent flow. This is important for the calculation of friction pressure drop. To determine whether the flow regime is laminar or turbulent, the Reynolds number is used. It is defined as:

$$Re = \frac{\rho U D}{\mu}$$

(4-19)

Where ρ is fluid density, U is fluid velocity, D is the diameter of the pipe and μ is viscosity of the fluid. Depending on the Reynolds number, it is separated between three different types of flow regimes:

|	
Re ≤ 2000	Laminar flow
2000 < Re ≤ 4000	Transition between laminar and turbulent flow
4000 < Re	Turbulent flow

Laminar flow: Laminar flow is a type of flow where the fluid flows in parallel layers. The layers flow smoothly over each other.[70] As mentioned above, laminar flow exist for a certain value of Reynolds number, below 2000. When the speed of the flowing fluid increase, the flow approaches turbulent flow. Laminar flow generally occur for low velocities and small pipes, and for laminar flow, the shear stress is said to be almost only dependent on the viscosity and independent of the density.[71] When the fluid have high viscosity, the fluid often is laminar.

Transitional flow: Transitional flow is flow in the transition from laminar to turbulent flow. Here the fluid flow have both laminar and turbulent characteristics. As defined above, transitional flow is approximately between Reynolds numbers in the range of 2000 to 4000, so the transition from laminar to turbulent flow is not something that happens suddenly.

Turbulent flow: Turbulent flow is a type of flow regime that is characterized by chaotic motion of the fluid. Turbulent flow exist for Reynolds number above 4000. Turbulent flow is because of its nature of flow, good for transporting fluid cuttings. The friction will be higher for turbulent flow than for laminar flow. Turbulent flow generally occur for high flow rates and larger diameter pipes, and the shear stress for turbulent flow is said to be a function of the density of the fluid.[72] If the viscosity is low, the fluid flow is often found to be in turbulent state.

The pressure gradient ($\frac{dP}{dX}$) consist of three different terms.[73] It consist of the frictional pressure gradient, hydrostatic pressure gradient and acceleration pressure gradient. The total pressure gradient can be expressed as:

$$\left(\frac{dP}{dX}\right) = (\frac{dP}{dX})_f + (\frac{dP}{dX})_h + (\frac{dP}{dX})_a \qquad (4\text{-}20)$$

How much each of these three different gradient effects the total pressure gradient is different for single- and multi phase flow. In this thesis, the focus is drilling scenario, and it is assumed only drilling fluid in the well and single phase flow.

Hydrostatic pressure gradient:

The hydrostatic pressure gradient can be calculated by this formula:

$$(\frac{dP}{dX})_h = \rho g cos I \qquad (4\text{-}21)$$

Where ρ is the drilling fluid density, g is the gravitational acceleration constant and I is the inclination measured from the vertical direction. Inclination is the angle between the tangent to the wellbore and the vertical. Hydrostatic pressure is pressure from a fluid in equilibrium because of gravity.

Acceleration pressure gradient:

If the flow in a well, is single phase stationary flow and the velocity of the flow changes because of larger or smaller pipe, there will be a pressure change. This is called the acceleration pressure gradient and it given as:[74]

$$(\frac{dP}{dX})_a = -\rho U \frac{dU}{dx} \qquad (4\text{-}22)$$

For the work in this thesis, the acceleration pressure will be neglected. If there in a well, is no change in diameter of the pipe, no acceleration pressure will be seen.

Frictional pressure gradient:

Because of the fact that the fluids are viscous, there will be energy loss when the fluid is flowing, this energy loss is due to friction.[75] This friction have the effect of pressure loss. For the frictional pressure gradient, it is distinguished between laminar and turbulent flow. For laminar flow, the fanning friction factor could be used to find the frictional pressure drop. For this model, it is assumed both constant pipe diameter and constant velocity of the flow. It is defined as:

$$\left(\frac{dP}{dX}\right)_f = \frac{4}{D} * \frac{16}{Re}\frac{1}{2}\rho U^2 \text{ or (dP)} = \frac{2f\rho L U^2}{D} \qquad (4\text{-}23)$$

The term $\frac{16}{Re}$ equals f and is the fanning friction factor.

If the flow is turbulent, there will be a different value for f. The expression of f will depend upon the value of the Reynolds number, and it will also depend whether or not it is a smooth pipe or a rough pipe. Generally for turbulent flow, the friction in the well become larger. This is because the velocity profile gets more uniform, that causes larger velocity fall-off towards the wall of the pipe and lager shear.[76]

Some commonly used turbulent friction factors could be mentioned:[77]

- Smooth pipe friction factor by Drew, Koo and McAdams, valid for Reynolds number in the intervall: $3000 < Re < 3*10^6$

$$f = 0.0056 + 0.5Re^{-0.32}$$ (4-24)

- Rough Pipe friction factor by Nikuradse with relative roughness $\frac{\varepsilon}{D}$:

$$\frac{1}{\sqrt{f}} = 1.74 - 2log_{10}\left(\frac{2\varepsilon}{D}\right)$$ (4-25)

- Rough Pipe friction factor by Colebrook & White:

$$\frac{1}{\sqrt{f}} = 1.74 - 2log_{10}\left(\frac{2\varepsilon}{D} + \frac{18.7}{Re\sqrt{f}}\right)$$ (4-26)

- Rough Pipe friction factor by Haaland (1983)

$$\frac{1}{\sqrt{f}} \approx -1.8 - log_{10}\left((\frac{\varepsilon/D}{3.7})^{1.11} + \frac{6.9}{Re}\right)$$ (4-27)

A MATLAB model is made to calculate the friction factor. In the model, equation 4-23 is used if the Reynolds number is below 2000. If turbulent flow and smooth pipe, equation 4-24 is used and if turbulent and rough pipe, the formula by Haaland, equation 4-27, for rough pipe is used to calculate the friction factor.

For the relative roughness factor $\frac{\varepsilon}{D}$, it decreases with smoothness of the pipe. There will be different values for the roughness ε depending on what type of material that is used in the pipe. Some typicall values for ε is giving in the table below:[78]

Table 4-4: Roughness of materials

Material	ε (ft)
Extruded steel	$5*10^{-6}$
Commercial steel	$1.55*10^{-4}$
Cast iron	$8.5*10^{-4}$
Glasss	$1*10^{-6}$
Galvanized iron	$5*10^{-4}$

In the calculation of frictional pressure in this thesis, the roughness factor for commerical steel is used. As seen from table 4-4 this roughness factor equals to $1{,}55*10^{-4}$ ft.

According to Aadnøy:[79]

- The inner side of the drill string is often in turbulent flow
- In the annulus, the section along the BHA may be in turbulent flow or in laminar flow
- The rest of the annulus and riser is usually in laminar flow

So, if the pressure loss for the whole system should be found, equations both for laminar and turbulent flow should be used.

4.9.2: Pressure calculation results

In order to calculate the pressure in the well, a MATLAB model is made based on the above mentioned method to calculate pressure in a well. This pressure model can be seen in the Appendix D.7

First step in the model is to calculate the Reynolds number, in order to determine whether the flow is laminar, transitional or turbulent. As mentioned, depending on the type of flow, there will be different equations for calculating the pressure. The Reynolds number in the simulation model calculates the Reynolds number, both in the annulus and in the drillpipe.

$$Re = \frac{\rho U D}{\mu}$$

(4-28)

To calculate the Reynolds number the fluid density, velocity of fluid flow, diameter and fluid viscosity is required for both the annulus and the drillpipe.

- The fluid density is assumed a constant number in the pressure calculations. The fluid density as a function of depth, will be calculated in the next section. The density for both the drillpipe and annulus is found previously by interpolation to be $1080,4 \frac{kg}{m^3}$.
- The viscosity for the annular fluid and the fluid in the drillpipe, is calculated in section 4.8.4 as a function of temperature for 46 segments. This fluid viscosity will be used in the calculation of the Reynolds number.
- The velocity of the fluid in the annulus and the drillpipe, is calculated based on the same areas for the annulus and drillpipe and circulation rate that is used in the temperature model calculations. The circulation rate equals to $300 \frac{bbl}{hour}$. This equals to $0,01335 \frac{m^3}{s}$. Area of the annulus equals 0,0154546 m² and area of the drillpipe equals 0,0205929 m². This gives the velocities:

$$\text{Velocity annulus: } Ua = \frac{0,01335}{0,0154546} = 0,864 \frac{m}{s}$$

(4-29)

$$\text{Velocity drillpipe: } Upipe = \frac{0,01335}{0,0205929} = 0,648 \frac{m}{s}$$

(4-30)

- For the diameter, there will be different diameter in the annulus and in the drillpipe. Same diameters, of both the well and the drillpipe outside and inside diameter, is used as previous in this thesis. The inside diameter in the drillpipe equals to 0,161925 m. The diameter in the annulus equals diameter of the well subtracted the outside diameter of the drillpipe: 0,219075 − 0,168275 = 0,0508 m.

$$\text{Diameter drillpipe: } D_{pipe} = 0,161925 \, m$$

$$\text{Diameter annulus: } D_{annulus} = 0,0508 \, m$$

The Reynolds number for the annulus and the drillpipe can now be calculated. This is done in MATLAB. Based on the Reynold numbers, it is determined whether the flow is either laminar or turbulent. The friction factor for the corresponding Reynolds number for both the drillpipe and the annulus can be calculated. The friction factor is also based upon if the pipe is either

smooth or rough, as explained in the section above. The MATLAB file then calculates the friction factor based on this information. The friction factor is then used to calculate the friction pressure. The friction pressure is, as mentioned earlier, found by using this formula:

$$(dP) = \frac{2f\rho LU^2}{D}$$

(4-31)

The hydrostatic pressure also needs to be calculated, this is done by using this formula:

$$\left(\frac{dP}{dX}\right)_h = \rho g cos I$$

(4-32)

The friction pressure and hydrostatic pressure is calculated in 46 segments for both the annulus and the drillpipe. The pressure is calculated with assuming 1 bar as initial pressure in the annulus. Further, the pressure in the annulus is calculated by adding the frictional pressure and the hydrostatic pressure for each cell with depth until the bottom of the well is reached. The drillpipe pressure is found by assuming that in the bottom of the well, the annular pressure equals the drillpipe pressure. Annular pressure is set as initial drillpipe pressure. Then the drillpipe pressure is found by subtracting the initial drillpipe pressure, in the bottom of the well, with the hydrostatic pressure, the frictional pressure is added because it works opposite way. The total pressure in the well is plotted and can be seen in the figure below. As it can be observed, from the figure, the pressure increases with a little over 10 bar per 100 m. As it also can be observed, the pressure in the annulus and the drillpipe equals to 489,7 bar in the bottom of the well. As it can be observed, from the figure, the pressure difference between the drillpipe and the annulus increases from the bottom of the well upwards. In this part of the pressure calculation, only the fluid viscosity is a function of depth. Later, the pressure will be found with variable fluid density. This variable fluid density will affect the pressure in the well.
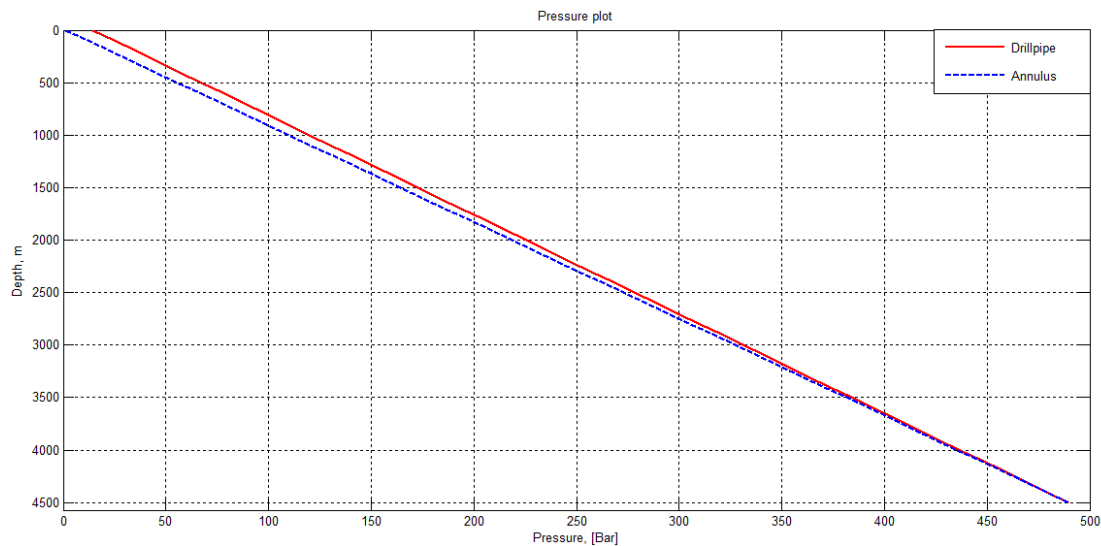

Figure 4-11: Pressure in the drillpipe and annulus

4.10: UPDATED DENSITY

From the density modelling simulation, in section 4.5, the isothermal bulk modulus of the liquid (β) and the cubical expansion coefficient of the liquid (α) is found. β equals $4,4983*10^9$ Pa and α equals $4,5429*10^{-4}$. This together with the density model can be used

38

to find the fluid density in the well for different temperatures and pressures. The density model, as defined previously, equals:

$$\rho = \rho_0 + \frac{\rho_0}{\beta}(p - p_0) - \rho_0 \alpha (T - T_0) \qquad\qquad (\,4\text{-}33\,)$$

β and α is known, the pressure and temperature needs to be updated. From the pressure model, defined in the section above, the new pressure can be found based on the varying frictional pressure. From the temperature model, defined in chapter 3, the temperature as a function of depth is in place.

The dataset used to calculate the isothermal bulk modulus of the liquid (β), and the cubical expansion coefficient of the liquid (α) gives the fluid density for temperatures 4, 20, 65, 93, 154 and 176 °C, and for different pressures. In the calculation of the other variables, like temperature and viscosity, the standard start temperature used is 25 °C and for pressure 1 bar is used, therefore the density at 25 °C and 1 bar needs to be found. This value have been calculated previously using linear interpolation. The density by linear interpolation is found to be 1080,42 $\frac{kg}{m^3}$.

To sum up, the variables needed in the density model is now as follow:

$$\rho_0 = 1080{,}42\ \frac{kg}{m^3}$$

$$T_0 = 25\,°C$$

$$p_0 = 1\ bar$$

$$\beta = 4{,}4983 * 10^9\ Pa$$

$$\alpha = 4{,}5429 * 10^{-4}$$

$$p = variable\ of\ depth$$

$$T = variable\ of\ depth$$

All the variables needed for the density model is now in place. A model to simulate the density is made in MATLAB. As for the pressure and temperature, the density is found with depth and is divided into 46 segments, each of 100 m. As mentioned, the pressure and temperature with depth that is used, is those temperatures and pressures simulated previously, respectively in section 4.8.4 and section 4.9.2. The density will be modelled for both the fluid in the annulus, and for the fluid in the drillpipe. It is to expect different density of the fluid in the annulus and in the drillpipe, because as observed earlier, there are different temperatures and pressures in the annulus and the drillpipe. The plot below shows the fluid density in the annulus and in the drillpipe. The blue dashed line illustrates the fluid density in the annulus and the red solid line illustrates the fluid density in the drillpipe.
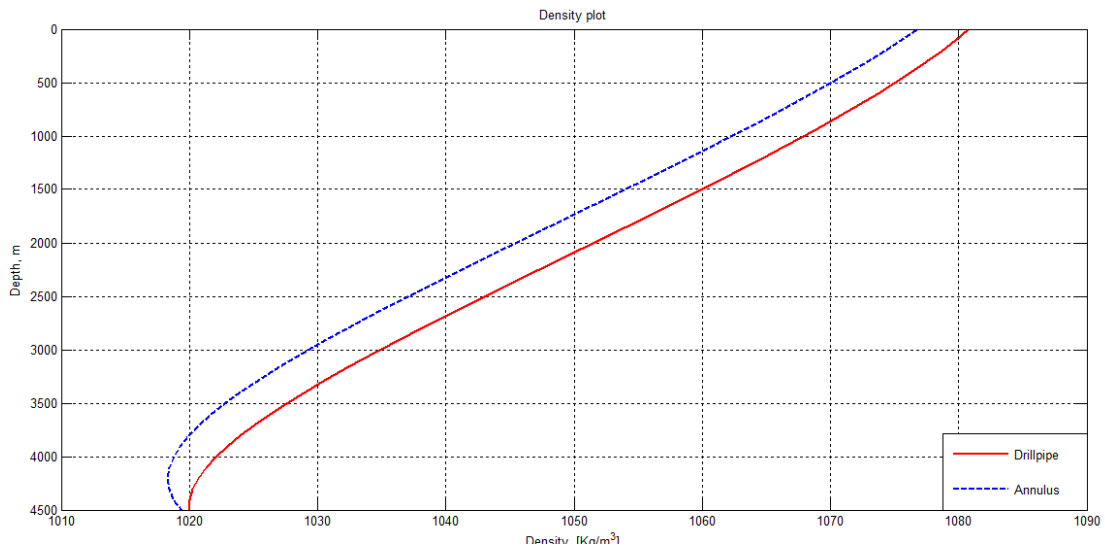
Figure 4-12: Density modelled for the annulus and the drillpipe

As it is possible to observe from the plot of the density, the density in the drillpipe is above the density in the annulus for all depths. It can also be observed that the density at the bottom of the well is $1019,4 \frac{kg}{m^3}$ in the annulus and $1020,0 \frac{kg}{m^3}$ in the drillpipe. At top of the well the density is $1076,8 \frac{kg}{m^3}$ in the annulus and $1080,7 \frac{kg}{m^3}$ in the drillpipe. In other words, the density in annular fluid have decreased with $57,4 \frac{kg}{m^3}$ from the top to the bottom of the well. In the drillpipe the density of the fluid have decreased with $60,7 \frac{kg}{m^3}$ from the top to the bottom of the well.

4.11: UPDATED PRESSURE

In order to investigate the fluid density effect on the pressure in the well, the new calculated densities are used in the pressure model presented in section 4.9. In the pressure calculation in section 4.9, the fluid densities in both the annulus and in the drillpipe were kept constant at $1080,42 \frac{kg}{m^3}$. In the new pressure calculation, the fluid densities are those found above, where the fluid density in the annulus varies between $1076,8 \frac{kg}{m^3}$ to $1019,4 \frac{kg}{m^3}$ and for the drillpipe the fluid density varies between $1080,7 \frac{kg}{m^3}$ to $1020,0 \frac{kg}{m^3}$. Below is a plot of this new pressure with varying density of fluid in the annulus and in the drillpipe.
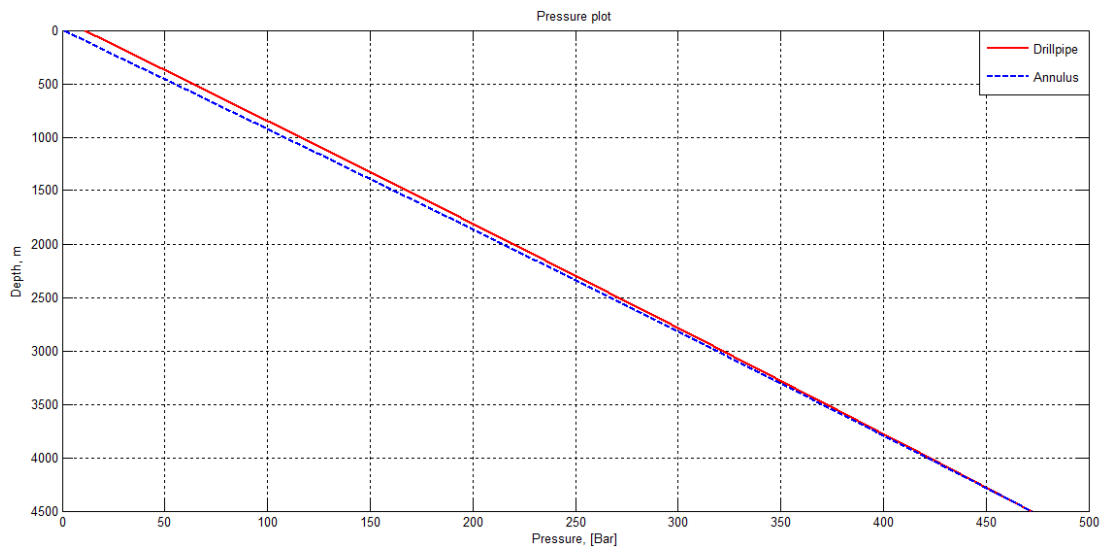
Figure 4-13: Pressure in the well with varying density of fluid with depth

When comparing the case with constant density to the case with varying density with depth, it is possible to observe pressure differences. When the density is constant 1080,42 $\frac{kg}{m^3}$, the bottomhole fluid pressure equals to 489,66 bar in both the annulus and in the drillpipe. When the density is varying with depth, the bottomhole pressure equals to 472,57 bar in the annulus and in the drillpipe. In other words, for the annulus and drillpipe, the pressure reduces with 17,09 bar when considering density variations with depth. Therefore, if the density variations is not considered, the bottomhole pressure in the well is largely overestimated. An overestimation of the bottomhole pressure could lead to several severe consequences, like having insufficient well pressure. It is assumed a higher pressure than what actually is the case. The consequences of insufficient well pressure, as discussed in section 4.3, could be inflow into the well and a kick situation could arise. The plot below shows the pressure for different fluid densities. In the plot, the red line represent the pressure in the drillpipe for constant density. The blue line represents the pressure in the annulus for constant density. The green line represent the drillpipe pressure for variable density and the black line represents the pressure in the annulus for variable density. As mentioned above, it is possible to observe from the figure that the pressure for variable density is lower than for the pressure with constant density.
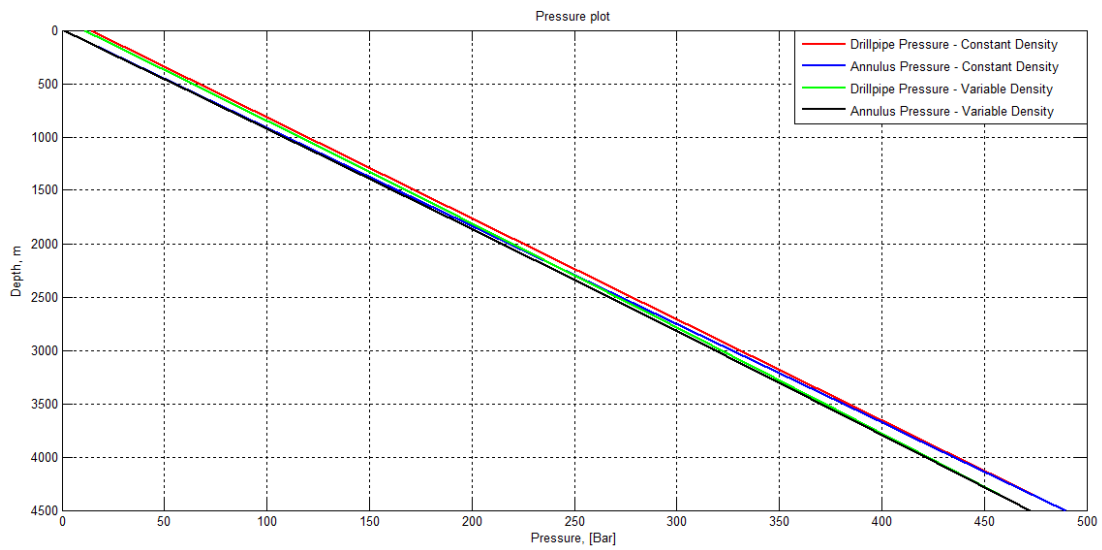
Figure 4-14: Pressure in annulus and drillpipe with constant density and variable density

4.12: RECALCULATED DENSITY

This new pressure, calculated above, is implemented in the pressure model to calculate the density under the influence of both temperature and pressure, where the pressure is calculated using variable density values. The model that is used for this purpose, is the same as before:

$$\rho = \rho_0 + \frac{\rho_0}{\beta}(p - p_0) - \rho_0 \alpha (T - T_0) \qquad (\text{4-34})$$

The variables ρ_0, β, p_0, α and T_0 is of same value as defined previously. The pressure is now a function of varying density, which give a more correct value of the pressure. The pressure is then used to calculate the density more precisely. The fluid density is simulated in MATLAB. The plot of the new densities are illustrated below.
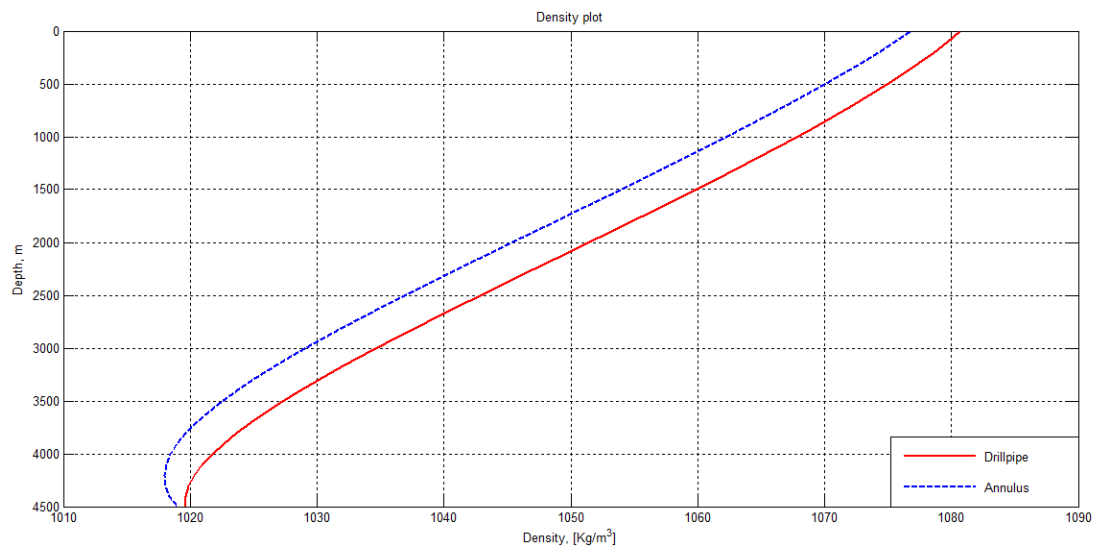
Figure 4-15: Density in annulus and drillpipe

42

As it could be observed from figure 4-15 above, if compared with figure 4-12, the density is almost identically as for the case when the density is calculated using pressure that is calculated for constant density. Actually, when comparing the exact value of the densities, both for the annulus fluid and the drillpipe fluid for the two cases, the largest difference in density is just $0,4 \frac{kg}{m^3}$. Most of the values are in the range $0,1$-$0,3 \frac{kg}{m^3}$. In other words, the density difference is almost negligible for the two cases. Again, the two cases it is being talked about is: one case where the density is calculated, by using a pressure that is calculated using constant density in the first place. The second case, is the case where the first calculated density is used to recalculate the pressure. This pressure is again used to calculate the density. As it was possible to observe, the density difference between the two cases were almost negligible. Even though this new fluid density shows small difference compared with the original, this new density is the density that will be used in the further calculations.

Chapter 5: Torque & Drag model

5.1: INTRODUCTION TO TORQUE & DRAG

Knowledge about torque and drag force is important for several reasons. Torque and drag force is considered key limiting factors for how deep it is possible to drill, especially when drilling horizontally. Torque and drag force is friction between the drillstring and the wellbore. Torque and drag can have some negative consequences for a well. In order to keep them as low as possible, torque and drag modelling is performed. Later equations for estimating torque and drag will be presented. Equations both for straight inclined wellbore sections and for curved wellbore sections will be presented, both cases, with and without combined motion.

5.2: BACKGROUND OF TORQUE & DRAG

Having accurate models for torque and drag is important in several phases of drilling. It is important to make sure that the torque and drag force is not exceeding certain limits, because then several problems could occur. Torque and drag modelling can be used to detect several problems like differential sticking, poor hole cleaning or if there is a so-called dogleg in the well. Also during the planning phase of a well, torque and drag modelling could be used to optimize the wellpath.

Drag force is the extra load compared to free rotating drillstring weight. When pulling out of the wellbore, the drag force is normally positive and when running into the wellbore, the drag force is normally negative.[80] Drag is a force that is primarily caused by friction that is generated by the drillstring being in contact with the wellbore sides.

Torque is a term that, when used in connection with drilling, describes the moment that is required to rotate a pipe. It could be called the rotating friction, meaning that the torque is the moment (force*arm) used to overcome the rotational friction and the friction on the bit with formation.

As it will be presented later, there are models for torque and drag force in both straight inclined wellbore sections and curved wellbore sections. In an ideal vertical well, the torque loss would almost be zero and in a curved/deviated well, the torque loss could be large.[81] For a vertical well (inclination equal zero), there will be no torque loss because the normal force can be neglected. For a horizontal well (inclination equals 90°), there will be a maximum torque loss. This is because there will also be a max value of the normal force. Because of the fact that torque increases as more deviated the well gets, torque could be a limiting factor for how long the well could be. For drag in straight inclined wellbore sections, the friction is caused by the normal weight component. For drag in curved wellbore sections on the other hand, this is a tension dominated process according to Aadnøy.[82] This involves that the normal force between the drillstring and the wellbore hole is closely connected to the axial pipe loading.

Generally, for drag force, the case is often that the force for hoisting/pulling the pipe is higher than when running into the hole/lowering (slack-off). This will be demonstrated later in the thesis. As it also will be demonstrated, the drag force is reduced when rotating.

There are several ways to reduce the torque and drag, like optimizing the wellpath, bit selection and optimal mud.[83] The simplest way is considered optimizing the mud, which

44

involves generally using either oil-based mud or synthetic mud as a replacement for water-based mud. This is because oil-based mud and synthetic mud have better lubrication capabilities than water-based mud. It should also be noted that it is possible to add lubricants to water-based mud to reduce torque and drag.

5.3: BUOYANCY

5.3.1: Buoyancy background

To be able to obtain the effective weight of a drillstring in a well filled with fluid, the weight of the drillstring needs to be multiplied with the buoyancy factor. Buoyancy is a force that acts upward, opposite of the gravitational force, and according to Archimedes' principle, buoyancy is equal to the weight of the fluid that is displaced by the object being submerged. The buoyancy factor is given by:[84]

$$\beta = 1 - \frac{\rho_o A_o - \rho_i A_i}{\rho_{pipe}(A_o - A_i)}$$

(5-1)

Where ρ_o and ρ_i is outside and inside density respectively, A_i and A_o is the inside and outside area and ρ_{pipe} is the density of the pipe used. If there is a case with same inside and outside fluid, the above expression simplifies to:

$$\beta = 1 - \frac{\rho_o}{\rho_{pipe}}$$

(5-2)

According to Aadnøy[85], the first equation is normally used in operations where different outside and inside fluid is used, for example, in cementation operations. The second equations is used in drilling operations, where same inside and outside fluid is used.

From the equations above, it is possible to see that the density of the mud is connected to the buoyancy factor. A mud with heavy density will decrease the effective weight of the drill string. It is important to correct the weight of the drillpipe for buoyancy. This is done by multiplying the weight of the pipe by the buoyancy factor.

$$w = \beta w_{drillpipe}$$

(5-3)

5.3.2: Buoyancy calculation

From the density simulation part, the fluid density was found for varying temperatures and pressures, see section 4.12. The density was found from top of the well to the bottom of the well. The well was divided into segments of each 100 m long. The well is 4500 m deep, i.e. the well will be divided into 46 segments. The fluid density is calculated, for both the annulus and in the drillpipe. Later, there will also be performed simulation with segments of length 30 m, this is to better fit the length of a pipe that is 30 m of length. As mentioned, the MATLAB models are easily updated to simulate for the number of segments that is desirable.

The well dimensions are as follow:

- Well diameter: $D_{well} = 0,219075\ m$
- Drillpipe inner diameter: $D_{inner\ drillpipe} = 0,161925\ m$
- Drillpipe outer diameter: $D_{outer\ drillpipe} = 0,168275\ m$

45

This gives the different areas for the annulus and drillpipe:

Area annulus: $A_{annulus} = \frac{\pi}{4} * (0,219075^2 - 0,168275^2) = 0,01545458 \; m^2$ (5-4)

Area drillpipe: $A_{drillpipe} = \frac{\pi}{4} * 0,161925^2 = 0,02059291 \; m^2$ (5-5)

From this, along with the given density of the mud in the drillpipe and in the annulus, and that density of the drillpipe is given as 7850 $\frac{kg}{m^3}$, it is possible to calculate the buoyancy factor for different inside and outside mud, using the formula for buoyancy factor presented above. From the figure below, it is possible to see the calculated buoyancy factor for the different depth segments. It can be observed, that the buoyancy factor increases with depth, as the density decreases with depth.

The buoyancy factor for the 46 segments varies between 0,8699 at the bottom of the well to 0,8609 at the top of the well. This means, if there for example is an object of 1000 kg displaced in the drilling fluid in the well, the weight of this object at top of the well would be 860,9 kg, and at the bottom of the well the weight would be 869,9 kg. It can then be noticed a weight difference between the top of the well and the bottom of the well, of 9 kg.

To illustrate the buoyancy factor changes with depth, it is plotted against depth.
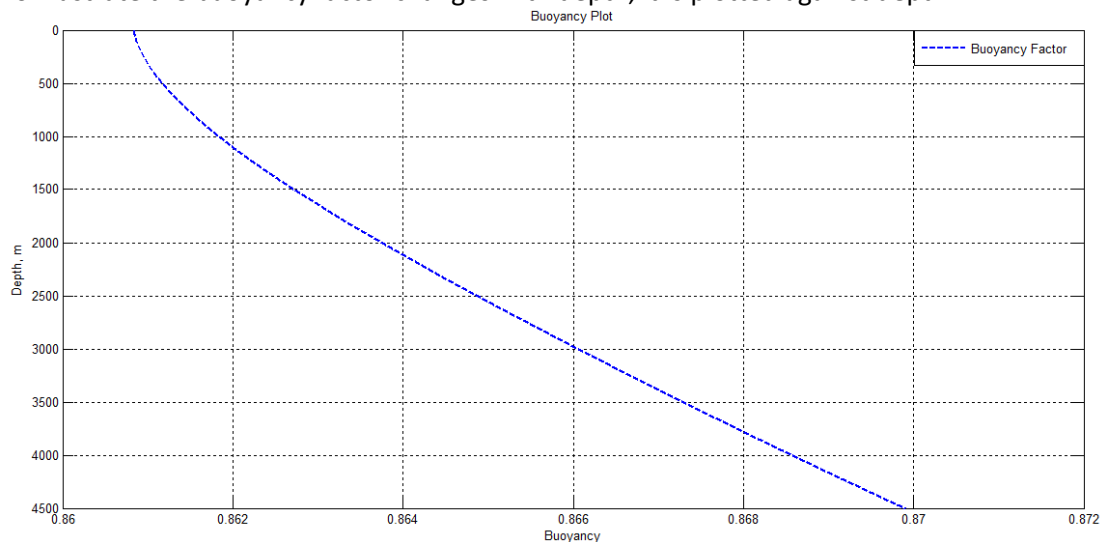
Figure 5-1: Buoyancy factor with depth

For the torque and drag simulation later, the torque and drag will be considered for varying buoyancy factor with depth and a constant buoyancy factor. The constant buoyancy factor is calculated for the density at the top of the well, where the density equals to 1080,5 $\frac{kg}{m^3}$. The constant buoyancy factor is calculated using this formula:

$$\beta = 1 - \frac{\rho_o}{\rho_{pipe}} = 1 - \frac{1080,5}{7850} = 0,8624$$ (5-6)

5.4: TORQUE & DRAG MODELS

In this section, equations for torque and drag in the wellbore will be presented. It will be presented equations for straight inclined wellbore sections without pipe rotation, equations for curved wellbore sections without pipe rotation, equations for static load, equations for straight inclined wellbore with combined motion and there will be presented equations for curved wellbore with combined motion. The equations presented in this section, is based on the work of Aadnøy,[86] and it assumes a soft string model, which involves that pipe bending stiffness is neglected. For torque and drag modelling, an element of the drillstring will be considered in the well. This element or segment is assumed filled with drilling fluid.

For straight inclined wellbore sections without pipe rotation:

$$\textbf{Drag force: } F_2 = F_1 + \beta \Delta L_{pipe} w (cos\alpha \pm \mu sin\alpha) \qquad (\text{ 5-7 })$$

In the equation above the symbol ± can be noticed. The plus sign (+) indicates hoisting of the pipe and the minus sign (-) indicates lowering of the pipe. The plus sign indicates that force is added because of friction from pulling out of the hole. For the minus sign, gravity acts when lowering into the hole. Friction acts the opposite direction of the movement. The term $cos\alpha$ defines the weight of the pipe and the term $\mu sin\alpha$ defines the additional friction force that is needed to move the pipe.

$$\textbf{Torque: } T = \mu r \beta w \Delta L_{pipe} sin\alpha \qquad (\text{ 5-8 })$$

For curved wellbore sections without pipe rotation:

$$\textbf{Drag force: } F_2 = F_1 e^{\pm \mu |\theta_2 - \theta_1|} + \beta w \Delta L_{pipe} (\frac{sin\alpha_2 - sin\alpha_1}{\alpha_2 - \alpha_1}) \qquad (\text{ 5-9 })$$

$$\textbf{Torque: } T = \mu r F_1 |\theta_2 - \theta_1| \qquad (\text{ 5-10 })$$

Static hook load:

The static hook load could alos be found. The static hook load represent the state of free rotating weight of the string. It is simply the buoyed unit weight of the pipe multiplied with the projected vertical height of the well. It is regardless of the wellbore orientation.[87] The static hook load could be given as:

$$\textbf{Static load: } F = \omega \beta \Delta L_{pipe} cos\alpha \qquad (\text{ 5-11 })$$

Torque and drag – combined motion:

According to Aadnøy,[88] when considering combined motion, the presented equations above for torque and drag needs to be updated, and the frictional capacity can be divided into the direction of axial motion and rotation. High rotational speed is said to reduce the frictional drag. Axial motion would be motion up or down.

The angle between the axial and tangential velocity can be defined as:[89]

$$\psi = tan^{-1}\left(\frac{V_h}{V_r}\right) = tan^{-1}(\frac{60 V_h}{2\pi N_r r}) \qquad (\text{ 5-12 })$$

Where V_h is the axial velocity in $\frac{m}{s}$, V_r is the tangential pipe speed, N_r is the rotary pipe speed in rpm and *r* is the radius of the pipe in meter.

According to Tveitdal[90] if:

$$\psi = 0° \rightarrow Rotation\ only$$

$$\psi = 90° \rightarrow Axial\ motion\ only$$

Aadnøy[91] defines the equations for torque and drag for combined motion:

For straight inclined wellbore sections for combined motion:

$$\textbf{Drag force: } F_2 = F_1 + \beta\Delta L_{pipe}w(cos\alpha \pm \mu sin\alpha) * sin\ \psi \qquad (\ 5\text{-}13\ )$$

$$\textbf{Torque: } \text{T} = \mu r\beta w\Delta L_{pipe}sin\alpha cos\ \psi \qquad (\ 5\text{-}14\ )$$

For curved wellbore sections for combined motion:

$$\textbf{Drag force: } F_2 = F_1 + F_1(e^{\pm\mu|\theta_2 - \theta_1|} - 1)\ sin\psi + \beta w\Delta L_{pipe}(\frac{sin\alpha_2 - sin\alpha_1}{\alpha_2 - \alpha_1}) \qquad (\ 5\text{-}15\ )$$

$$\textbf{Torque: } \text{T} = \mu r F_1|\theta_2 - \theta_1|\cos\psi \qquad (\ 5\text{-}16\ )$$

For the force: F_2 equals the force at the top and F_1 equals the force at the bottom. Inclination of the wellbore is the angle between the tangent to the wellbore and the vertical. It is important that the angels used, in the different models, should be given in radians, and not in degrees.

5.5: DEMONSTRATION OF TORQUE CONCEPT

During a simulation of torque, a simple hypothetical wellpath is considered. For the simple hypothetical wellpath, the well will be vertical (zero inclination) from 0 m to 2500 m. The next section will be a straight inclined section. The straight inclined section ends at 4500 m. This simple wellpath with a section of zero inclination, i.e. perfect vertical, and a straight inclined section, is used to illustrate some fundamental concepts with torque. This concept is that in a perfectly/ideal vertical well, i.e. where the inclination is zero, the torque loss would be zero. There will only be some small torque loss, which is because of viscous forces from the mud.[92] In an inclined well, especially in a curved well, the torque loss could be much higher. The figure below illustrates the torque for the hypothetical, unrealistic well. From 0 m to 2500 m where the well is perfectly vertical, it can be observed that the torque is constant, i.e. there is no torque loss. In other words, the torque observed at 2500 m would be the same as the applied torque at surface on the drillstring. Realistically, the amount of torque that is applied on the drillstring at surface would be lower downhole, because torque is lost through the wellbore because of friction. As it can be observed from the figure, from 2500 m, the amount of torque decreases, or said in an other way, the torque loss increases. This is because, as mentioned, from 2500 m, the well is straight inclined and friction increases, i.e. the torque increases. It can be observed, as deeper the well gets, the lower the torque. In order to have sufficient torque at the bit to be able to drill forward in a satisfying way, torque losses have to be accounted for in the calculations of required torque.
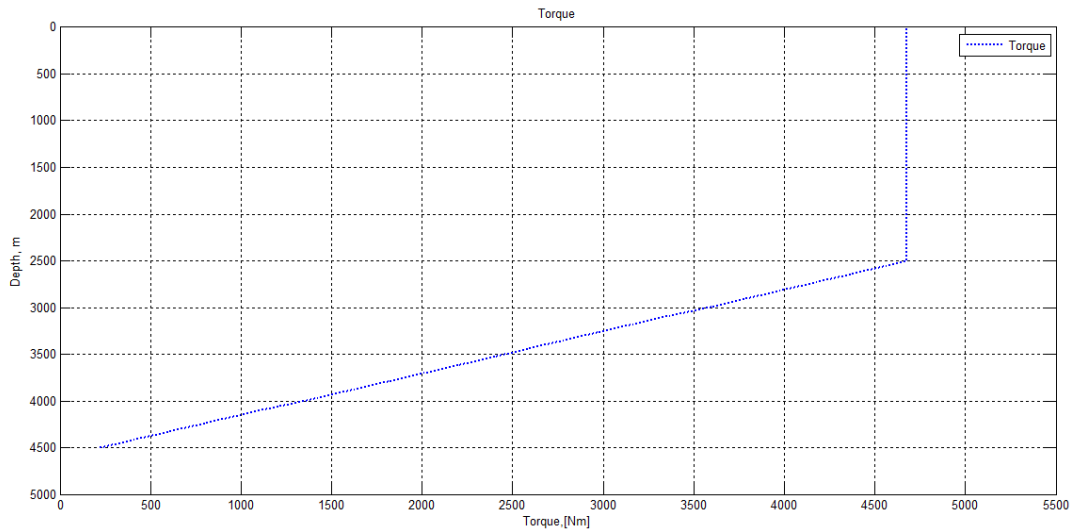
Figure 5-2: Hypothetical well illustrating torque concept

A well with zero inclination, that is perfect vertical, is not a realistic case and is included just to illustrate the concept behind torque. A more realistic case have been simulated and will be presented in the case study later.

5.6: DLS-FILTER

The following section about the DLS filter is based upon and inspired by the work by Terje Tveitdal.[93]

According to Aadnøy,[94] the properties of the friction is different for a straight inclined section and a curved section. Aadnøy states that for a straight inclined section, friction is dependent on pipe weight, because only the normal weight component contributes to friction. For straight inclined sections, the pipe tension do not contribute to the normal pipe force. For curved wellbore sections, Aadnøy states that because the normal contact force between the drillstring and the borehole is highly dependent on the axial pipe loading, it is a tension dominated process. For curved wellbore sections, it can generally be said that more friction is created than for straight inclined wellbore sections.

Since the properties of the friction is different for a straight inclined section and a curved section is different, there are different models for torque and drag depending on the section of the wellbore is straight inclined or if the wellbore is curved. Therefore, to know whether the section of the wellbore is straight inclined or curved, is of great importance to be able to calculate the torque and drag force. According to Tveitdal,[95] in order to determine if a wellbore section is straight inclined or curved, a so called dogleg severity filter (DLS-filter) can be used. Later the application of the DLS-filter will be demonstrated by determining if the wellbore section is straight inclined or curved for a given wellpath. First a further description of the DLS-filter will be given.

The DLS-filter considers the radius of a curve and the radius of segments above and below. A reference line is used, and from this reference line a distance (*h*) is calculated. The radial clearance between the drillstring and borehole is found, and this clearance is compared with the distance *h*. This is used to determine whether the equations for straight inclined wellbore or curved wellbore should be used. According to Tveitdal, if the radial clearance is

49

less than *h*, the equation for curved wellbore should be used, and if the radial clearance is larger than *h*, the equation for straight wellbore should be used.
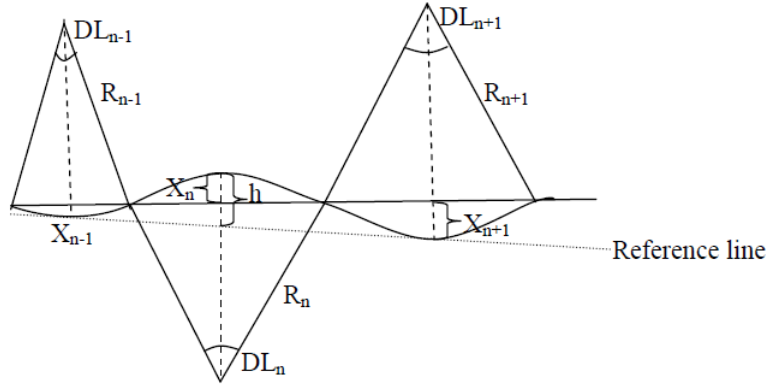

Figure 5-3: Illustration of the concept of the DLS-filter[96]

As observed from the figure above three survey points are given. The radius (R_{n-1}, R_n, R_{n+1}) of these three points needs to be found. The formula to do so is given below:

$$R_{n-1} = \frac{\Delta L_{n-1}}{DL_{n-1}} \tag{5-17}$$

$$R_n = \frac{\Delta L_n}{DL_n} \tag{5-18}$$

$$R_{n+1} = \frac{\Delta L_{n+1}}{DL_{n+1}} \tag{5-19}$$

Further, the height can be calculated using the radius calculated above. The equations for calculating the height is given below:

$$x_{n-1} = R_{n-1}\left(1 - \cos\left(\frac{DL_{n-1}}{2}\right)\right) \tag{5-20}$$

$$x_n = R_n\left(1 - \cos\left(\frac{DL_n}{2}\right)\right) \tag{5-21}$$

$$x_{n+1} = R_{n-1}\left(1 - \cos\left(\frac{DL_{n+1}}{2}\right)\right) \tag{5-22}$$

An approximation of the height difference from the reference line and the point in the "middle" (x_n) can be calculated. The formula to calculate this is given below:

$$h = \frac{1}{2}(x_{n-1} - x_{n+1}) + x_n \tag{5-23}$$

The radial clearance can then be calculated. The radial clearance is given as diameter of large pipe (D) subtracted diameter of small pipe (d). The small pipe is found inside of the large pipe, as the figure below illustrates.

50
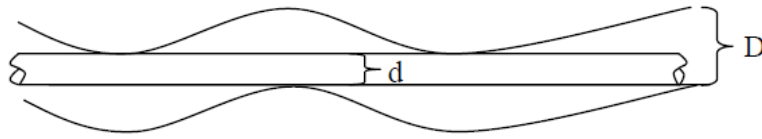
Figure 5-4: Illustration of small pipe inside large pipe[97]

As mentioned, the radial clearance (D-d) is compared with the height (*h*). The conditions for straight inclined wellbore and curved wellbore section is given below:

If *h*< (D-d) → Wellbore section is considered straight inclined

If *h*> (D-d) → Wellbore section is considered curved

From the equations above, it is observed that the absolute change in direction or the so-called dogleg (β) is required in the calculations of the radius. To find the dogleg angle, this equation can be used for the different survey points:

$$\beta = Cos^{-1}(CosI_1 CosI_2 + SinI_1 SinI_2 Cos(A_2 - A_1)) \qquad (\text{ 5-24 })$$

Where β is the dogleg, I_1 and I_2 is inclination for survey point 1 and 2, and A_1 and A_2 is azimuth for survey point 1 and 2. It is important that the dogleg angle is in radians, and not in degrees, when used in the DLS-filter. In order to calculate the dogleg angle, inclination and azimuth is required. The two terms could breifly be explained:

- Inclination is the angle between the tangent to the wellbore and the vertical.[98] For a trajectory that is vertical the inclination is 0°, and for a horizontal wellbore the inclination would be 90°.
- Azimuth of a wellbore is the angle between the projection of the tangent to the wellbore projected onto a horizontal plane and a horizontal referance direction. The angle is measure from 0° to 360°. It is measured clockwise from north direction.[99]

Both inclination and azimuth is measured by measurement while drilling (MWD) tools. Inclination, azimuth and measured depth is measurements that is measured every connection, i.e. every 30 m. Measured depth (MD) is measured along the wellpath. It could be found be counting the number of used drillpipe stands. The three measurements could be used to describe the well as a curve in 3 dimensions. If imagine two surveys points, *p1* and *p2*, as can be illustrated on the figure below, the points refers to two survey points, and *ΔL* is the measured depth between the two survey points. The change in angle, dogleg, can be observed on the figure, and denoted as *Ɵ* in the figure.
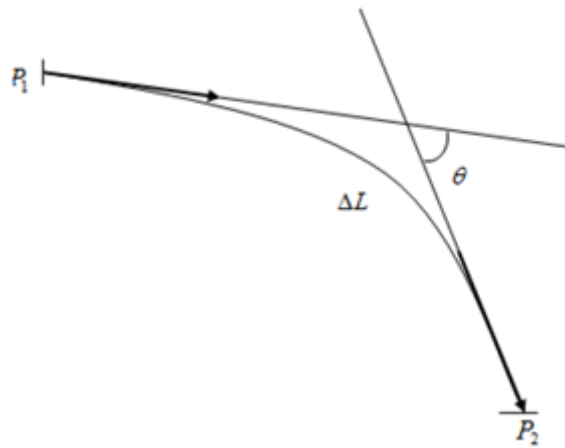
Figure 5-5: Change in direction between two survey points over a length ΔL[100]

The model presented above for determining wheter a well section is either straight inclined or curved, is implemented in MATLAB. The MATLAB code for the DLS-filter can be found in appendix D.11. Later in the case study, the DLS-filter will be demonstrated. There a dataset, with given wellpath, consisting of measurements like is measured depth, true vertical depth, inclination and azimuth is given. From these parameters, the dogleg is calculated along with measured depth between the survey points (dMD). From the dMD and the dogleg (β), the three different radius presented above will be calculated. These three radius values is used to calculate h. These values of h will be compared with the radial clearance (D-d). The simulation program will check the value of h with the radial clearance. As mentioned above, if h< (D-d) the wellbore section is considered straight inclined and if h> (D-d) the wellbore section is considered curved.

Chapter 6: Case study

In order to implement and demonstrate the models, along with confirming the theory presented, a case study have been performed. Below, a flow diagram can be seen, that illustrates the relationship between the models, presented in the above sections. From the flow diagram, it can be seen that the first step is data input to the temperature model. The temperature model calculates the fluid temperature in the drillpipe and in the annulus. This fluid temperature, is then used in the viscosity model to calculate the viscosity of the fluid in the drillpipe and in the annulus with depth. Then the viscosity, along with data inputs, is used to calculate the pressure in the drillpipe and in the annulus with depth. Then, as seen from the flow diagram, both the pressure and the temperature, from the temperature model, is used to calculate the density of the fluid in the drillpipe and annulus with depth. After that, a loop follows, where the density of the fluid is returned back to the pressure calculation, in order to calculate the pressure more precisely. The loop then return the new calculated pressure back to the density model, where the density of the fluid is calculated, as a function of both varying temperature and pressure with depth. The density of the fluid in the drillpipe and annulus, is then used to calculate the buoyancy factor with depth. From the flow diagram, it can be observed, that a set of wellpath data is run through the DLS-filter in order to determine whether the wellpath is straight inclined or curved. This information, along with the buoyancy factors, is then either sent to the equations for torque and drag for straight inclined wellbore or equations for torque and drag for curved wellbore. Finally, the torque and drag force is calculated for the different segments in the well.
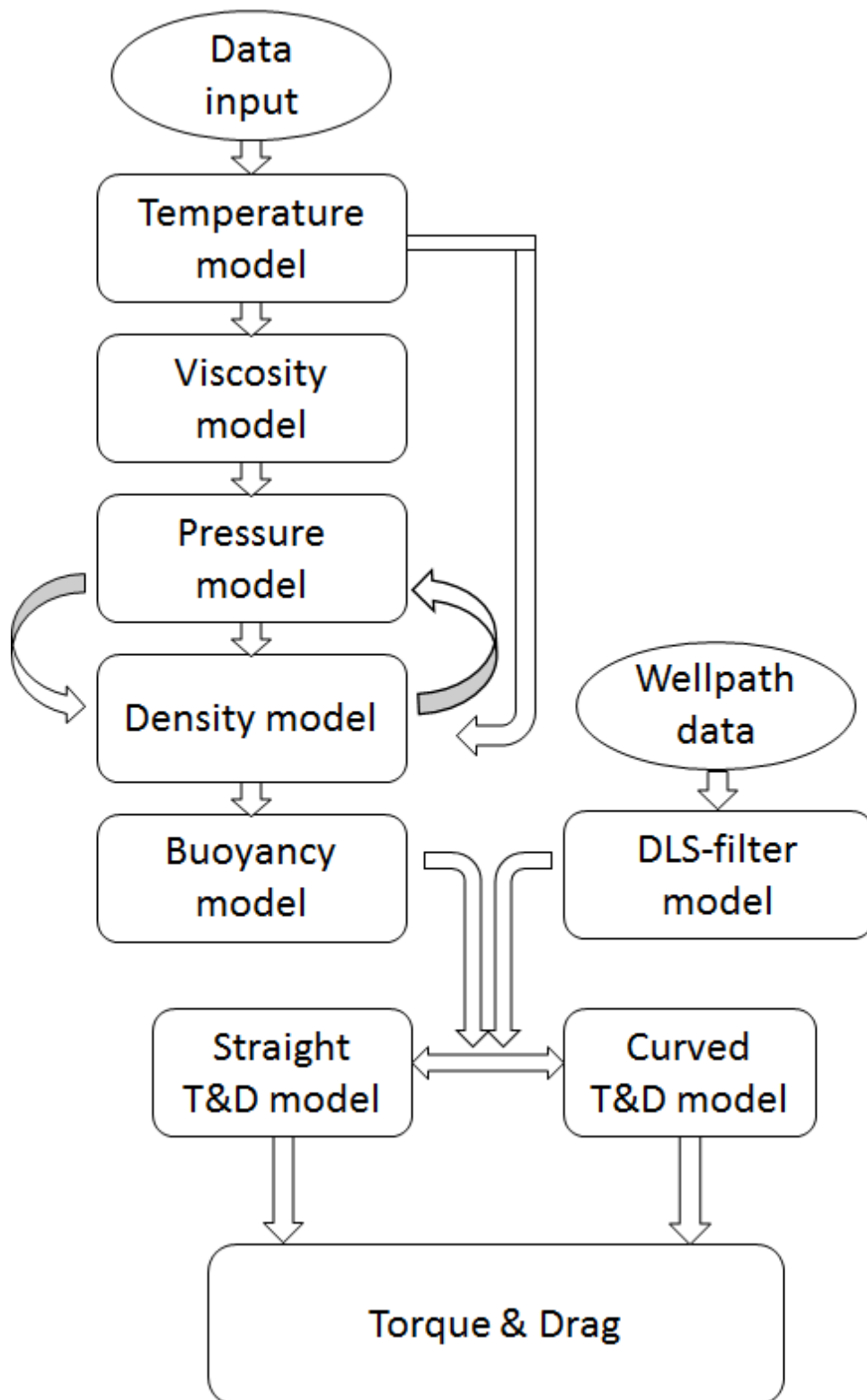
Figure 6-1: Flow diagram illustrating the relationship between the presented models

The original simulated well, used in the different models presented in the above sections, have a depth of 4500 m. The well that is going to be used in the case study, for the simulation of the different properties, have a depth of 3942 m TVD and 4110 m MD. The same models are used, but instead of simulating to a depth of 4500 m, it is simulated to 3942 m. To better fit one pipe length, that normally is 30 m of length, the well will be divided into segments of each 30 m, instead of the previously used 100 m. This is simply updated in the models. The well is divided into segments of each 30 m MD. This implies that there will be 137 segments. As done previously, the other parameters like temperature, pressure, density, viscosity and buoyancy is also found for desired segments, in this case 137 segments.

To give an idea how the well looks like, a vertical section is made. It presents the well in a plane that is defined by the well center and target. On the Y-axis, TVD values are plotted and on the X-axis, horizontal displacement values are plotted. To find the horizontal displacement this formula is used:

$$H = \sqrt{\Delta N^2 + \Delta E^2}$$

(6-1)

Where ΔN and ΔE represent the change in north- and east coordinates. To calculate ΔN and ΔE the minimum curvature method is used. Eriksen[101] gives the equations to find ΔN and ΔE:

$$\Delta N = \left(\frac{1}{2}\right) * \Delta MD * (sinI_1 * cosA_1 + sinI_2 * cosA_2) * RF$$

(6-2)

$$\Delta E = \left(\frac{1}{2}\right) * \Delta MD * (sinI_1 * sinA_1 + sinI_2 * sinA_2) * RF$$

(6-3)

Where ΔMD is measured depth between two survey points. I_1 and I_2 is inclination for survey points 1 and 2. A_1 and A_2 is azimuth for survey points 1 and 2. RF is the ratio factor and can be found using this formula:

$$RF = \tan\left(\frac{\beta}{2}\right)/(\frac{\beta}{2})$$

(6-4)

Where β is the dogleg angle in radians. The dogleg angle have previous been defined in section 5.5. By using these formulas, in combination with values of ΔMD, I_1, I_2, A1, A2 and β from the dataset, the values of ΔN and ΔE can be calculated. When these values are calculated, they can be used to find the horizontal displacement (H). With the horizontal displacement in place, along with the true vertical depths values, a vertical section representing the wellpath can be made. The figure below is illustrating this. It can be observed that the well have a horizontal displacement of 1006 m at TVD.
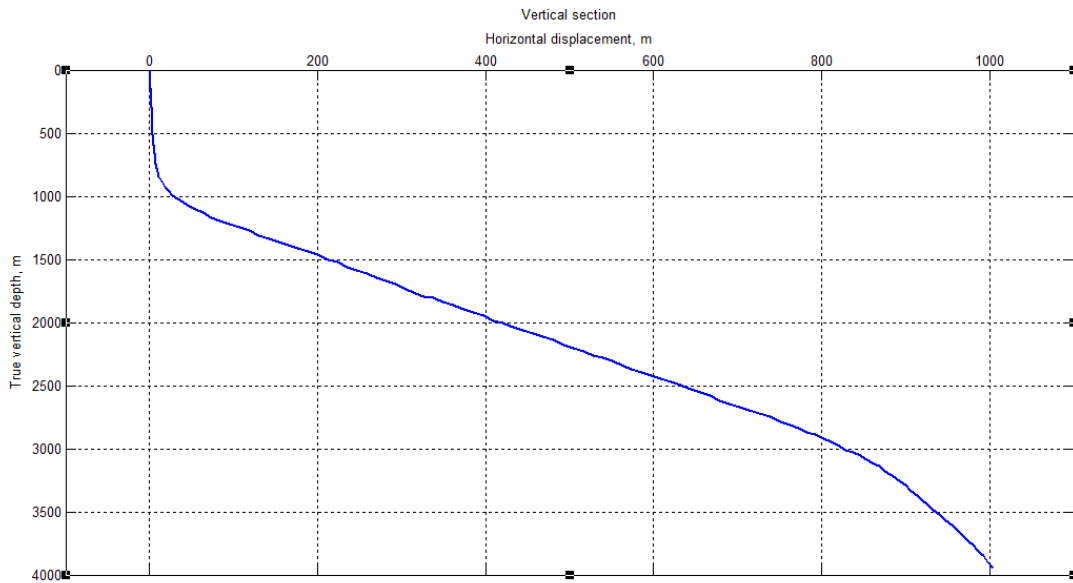
Figure 6-2: Vertical section representing the wellpath used in the case study

In order to further investigate the effect of buoyancy factor on the torque and drag force in the well, a possible "worst-case" situation is simulated. The "worst-case" situation involves simulating a situation where the different parameters affecting the temperature downhole, is set at a typical maximum value. The thermal conductivity of the drilling fluid is changed from $1,73 \frac{W}{mK}$ to $4,5 \frac{W}{mK}$, this is a typical maximum value for the thermal conductivity. The formation thermal conductivity is changed from $2,25 \frac{W}{mK}$ to $5 \frac{W}{mK}$, this is a typical maximum value. Also, the circulation parameters are changed, in order to get a high temperature value of the drilling fluid. The circulation rate is reduced from $300 \frac{bbl}{hour}$ ($0,01325 \frac{m^3}{s}$) to $200 \frac{bbl}{hour}$ ($0,0088 \frac{m^3}{s}$). This is a low value, and it would be rare to circulate in such small amounts, but done here in order to investigate the "worst-case" scenario. It is referred to the sensitivity analysis in section 3.5 and Appendix A to observe the effect of these parameters on the temperature in the well.

For the case study, a constant diameter of the drillstring will no longer be assumed. The drillstring now used, consists of four different pipes, with different inside and outside diameters. The drillstring consists of two different types of drillpipes, a pipe section with heavy weight drillpipe and a section of drill collars. The drillstring configuration, in the 3942 m TVD well, is presented in the table below:

Table 6-1: Drillstring configuration

Type of pipe:	Depth interval: [m]	Outside diameter: [m]	Inside diameter: [m]	Weight: [N/m]
Drillpipe 1:	0-2087,7	0,168	0,127	450
Drillpipe 2:	2087,7-3642,6	0,127	0,1016	290

56

HWDP	3642,6-3764,4	0,127	0,0762	620
Drill collars	3764,4-TD	0,2032	0,0762	2130

The diameter of the well, casing inner diameter, is updated as well. It is assumed that the inner diameter throughout the well equals the diameter of the production casing. In the case study, a 10-3/4 inch (0,27305 m) production casing is assumed. This new well diameter have to be included in the different models. This because new well diameter, along with the pipe diameters, presented in table 6-1 above, will affect the fluid temperature and pressure in the well, and thereby the other parameters like fluid viscosity, fluid density and buoyancy factor. For the interested reader, the sensitivity of the fluid temperature for changes in well diameter, is referred to the temperature model in chapter 3.5 and Appendix A.

From the given well configuration, with well diameter and respective pipe diameters, the areas of flow in the well can be calculated. The calculated areas will be used in the different models to e.g. calculate the buoyancy factor.

$$A_{outside,drillpipe\ 1} = \frac{\pi}{4} * \left(D_{well}{}^2 - D_{outer\ drillpipe\ 1}{}^2\right) = 0,0364\ m^2 \qquad (6\text{-}5)$$

$$A_{inside,drillpipe\ 1} = \frac{\pi}{4} * \left(D_{inner\ drillpipe\ 1}{}^2\right) = 0,0127\ m^2 \qquad (6\text{-}6)$$

$$A_{outside,drillpipe\ 2} = \frac{\pi}{4} * \left(D_{well}{}^2 - D_{drillpipe\ 2}{}^2\right) = 0,0459\ m^2 \qquad (6\text{-}7)$$

$$A_{inside,drillpipe\ 2} = \frac{\pi}{4} * \left(D_{inner\ drillpipe\ 2}{}^2\right) = 0,0081\ m^2 \qquad (6\text{-}8)$$

$$A_{outside,HWDP} = \frac{\pi}{4} * \left(D_{well}{}^2 - D_{HWDP}{}^2\right) = 0,0459\ m^2 \qquad (6\text{-}9)$$

$$A_{inside,HWDP} = \frac{\pi}{4} * \left(D_{HWDP}{}^2\right) = 0,00456\ m^2 \qquad (6\text{-}10)$$

$$A_{outside,drill\ collar} = \frac{\pi}{4} * \left(D_{well}{}^2 - D_{drill\ collar}{}^2\right) = 0,0261\ m^2 \qquad (6\text{-}11)$$

$$A_{inside,drill\ collar} = \frac{\pi}{4} * \left(D_{drill\ collar}{}^2\right) = 0,00456\ m^2 \qquad (6\text{-}12)$$

As mentioned, the new well configuration will affect the different parameters like fluid temperature, density, pressure, viscosity, buoyancy and finally torque and drag. In addition to the new well configuration, some of the parameters affecting the fluid temperature like conductivity, circulation rate and geothermal gradient, is, as mentioned, set at typical high value. This is to investigate a possible "worst-case" situation. The different parameters will now be calculated for the new well configuration and well parameters.

6.1: TEMPERATURE CALCULATION:

The fluid temperature for the new well diameter and drillstring configuration, with four different pipe sections, is to be calculated. As mentioned, some of the parameters affecting the temperature is updated from the previous base case used in the temperature-modelling chapter. The circulation rate is reduced to 0,008833 $\frac{m^3}{s}$ (200 $\frac{bbl}{hour}$) and the conductivity of the drilling fluid and formation is increased. By changing the circulation rate and conductivity, it will have the effect of increasing the fluid temperature, i.e. simulating a more "challenging" situation. The fluid temperature inside the pipes and in the annulus for the four different pipes is calculated and can be observed in the figure below.
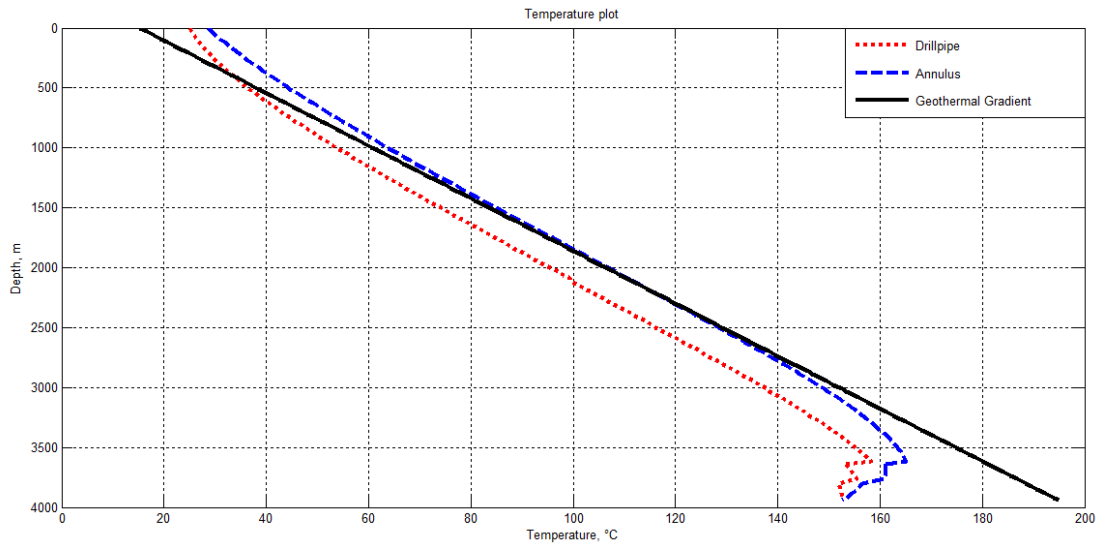
Figure 6-3: Temperature of the fluid inside the pipes and in the annulus

It is observed that the fluid temperature inside the drillpipes and annulus, at bottom of the well, equals to 152,7 °C. As it can be observed from the figure, at transition depths to different type of pipe, the temperature changes. These transitions to new type of pipes is at depths: 2087,7 m, 3642,6 m and 3764,4 m, as also can be seen above in table 6-1. It can be observed that when changing to new type of pipes, the results is reduced temperature.

From the sensitivity analysis in section 3.5 and from appendix A, some general observations were made regarding the temperature behavior for changed inside and outer pipe diameters:

- When the pipe inner diameter decreases the temperature decreases
- When the pipe inner diameter increases the temperature increases
- When the pipe outer diameter decreases the temperature increases
- When the pipe outer diameter increases the temperature decreases

It can from these points above, be observed opposite effects regarding the temperature for changed pipe diameters. It is observed, that for the inner pipe, the temperature increases with increasing diameter and decreases with decreasing diameter. For the outer diameter of the pipe, the temperature decreases with increasing diameter and the temperature increases with decreasing pipe diameter.

If these findings above, is compared with the drillstring configuration in table 6-1 above, it can be observed that from drillpipe 1 to drillpipe 2, both the inside and outside pipe diameter decreases. At transition depth between drillpipe 1 and 2 at depth 2087,7 m, it is observed that the drillpipe temperature decreases slightly, while the annulus temperature seems unaffected. From this, since the temperature decreases in the drillpipe, it is observed that the effect of the decreasing inner diameter is the dominant effect compared to the decreasing outer diameter. Since at mentioned, from the general observations points above, decreasing inner and outer diameter of the pipe, have different temperature effects. From drillpipe 2 to HWDP, the pipe outside diameter is constant, while the inside pipe diameter is decreased. It is from this, expected that the temperature should decrease, since the inner pipe diameter is decreased. If figure 6-3 above is studied, at transition depths from drillpipe

58

2 to HWDP at 3642,6 m, it is observed that the temperature is decreased. This confirms the statement that reduced inner pipe diameter decreases the fluid temperature. From HWDP to drill collars, the pipe outside diameter is increased, while the inside pipe diameter is constant. From this, and the general observations regarding the sensitivity of the fluid temperature for changed pipe diameters, the fluid temperature should be decreased, since increased outer pipe diameter should decrease the fluid temperature. This is also true, if the figure above is studied. It can at transition depth at 3764,4 m be observed reduced fluid temperature both for the drillpipe and in the annulus.

6.2: VISCOSITY CALCULATION:

With the new calculated fluid temperature presented above, the viscosity of the fluid will also change. The same formula, as used before, for calculating viscosity for the specific mud used, with temperature (X), will be used. This formula equals:

$$Y = -0,160116X + 33,76 \qquad\qquad (\,6\text{-}13\,)$$

With this formula, along with the fluid temperature calculated above, the viscosity of the fluid inside the pipes and in the annulus can be calculated. The plotted viscosity of the fluid is illustrated in the figure below.
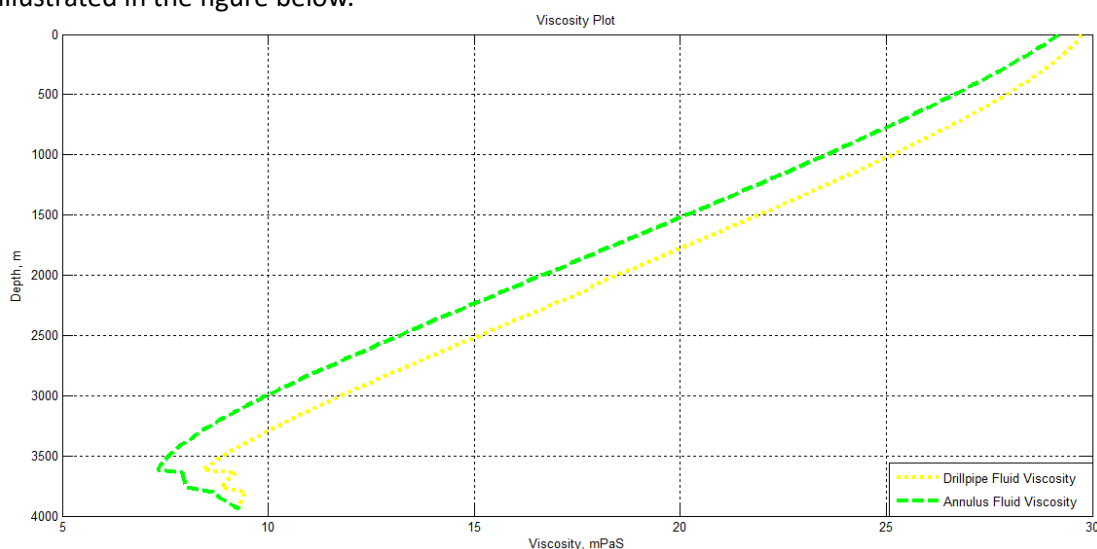

Figure 6-4: Viscosity of the fluid inside the pipes and in the annulus

It can be observed that the viscosity of the fluid in the bottom of the well equals to 9,32 mPaS. As for the temperature, it can be observed that in the transitions to new type of pipes, the viscosity is affected. It can be observed that when changing to new type of pipe, the result is increased viscosity. This has to do with the effect explained above, for the fluid temperature. For the fluid temperature it was observed decreasing temperature at the different transitions to new pipes. This fluid temperature change will affect the fluid viscosity. The effect of changed pipe is most visible for changing from drillpipe 2 to HWDP and from HWDP to drill collars, but it can also be observed viscosity increase in the transition from drillpipe 1 to drillpipe 2. Below, a zoomed view illustrates this. It can be observed that the viscosity in the drillpipe fluid increases, but for the viscosity in the annular fluid it seems unaffected. This has to do with the fact, that at this depth, the temperature for the drillpipe

59

fluid is reduced, while the annular fluid shows minor temperature change as the pipe change.
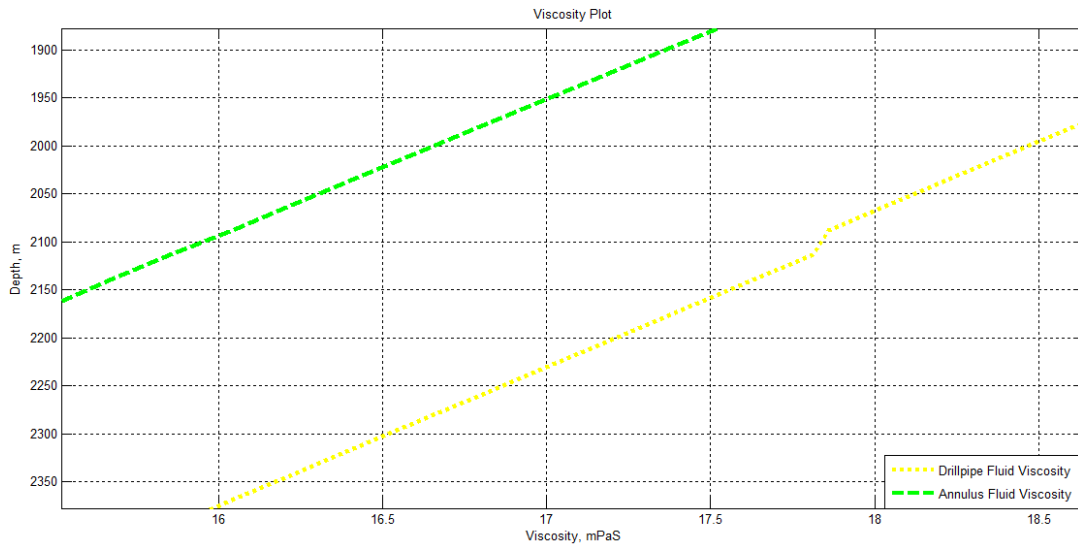
Figure 6-5: A zoomed view of the viscosity at transition depth for drillpipe 1 and drillpipe 2

6.3: PRESSURE CALCULATION:

The new well configuration, is now included in the pressure calculation model. To find the pressure, the Reynolds numbers first needs to be calculated. Since the outer and inner diameter of the pipes and the well diameter have changed, there will be new values for the annular- and pipe diameters, annular- and pipe areas, and the annular- and pipe fluid velocity when calculating the Reynolds numbers. In addition, the new fluid viscosities, calculated above, with changing temperatures, is used in the calculation of the Reynolds numbers. The fluid density is in this pressure calculation kept constant at 1080,4 $\frac{kg}{m^3}$. Below, the pressure will be calculated for densities varying with depth. The Reynolds number is calculated, and the same pressure model, presented previously, is used to calculate the pressures in the well. From the models, the pressure inside the pipes and in the annulus is calculated, and it is plotted in the figure below. The red solid line in the figure, represent the pressure in the drillpipes, and the blue dotted line represent the pressure in the annulus. As it can be seen, the pressure in the drillpipe is higher than for the pressure in the annulus. The bottomhole pressure, equals to 419,3 bar, both for the drillpipes and in the annulus.

60
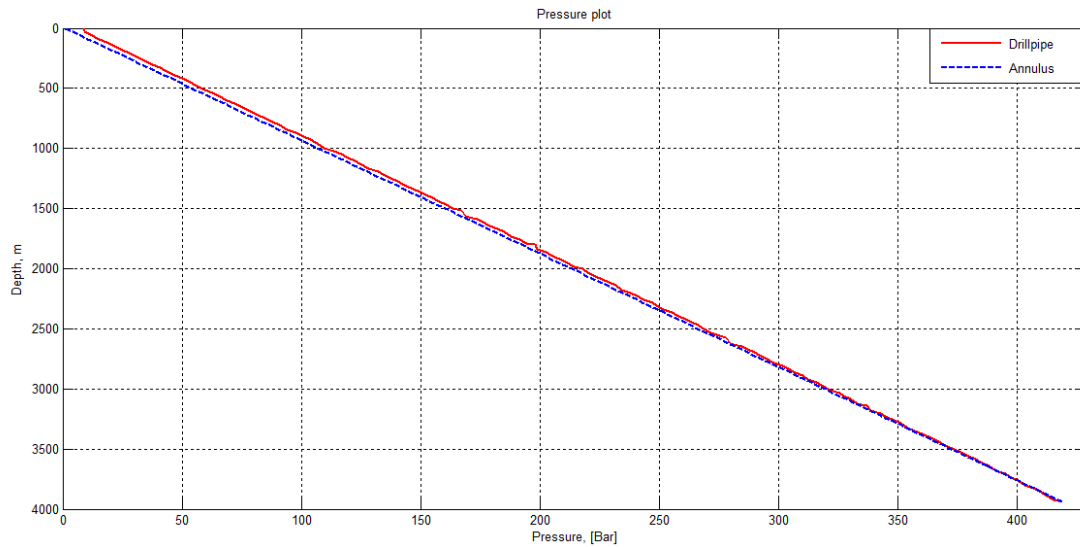
Figure 6-6: Pressure inside the pipes and in the annulus

6.4: DENSITY CALCULATION:

These new pressures for the annulus and inside the pipes can be used in the density model to calculate the new fluid densities in the annulus and the drillpipe. The density model is the same as previously defined:

$$\rho = \rho_0 + \frac{\rho_0}{\beta}(p - p_0) - \rho_0 \alpha (T - T_0) \qquad (\text{6-14})$$

To find the fluid densities, same values for ρ_0, β, p_0, α and T_0 is used, as previous in the thesis. The new values of p and T, that are calculated for the new well configuration, will be used. The density of the fluid inside the pipes and in the annulus is calculated and the results is plotted below. The red solid line represent the fluid density in the drillpipes, and the blue dotted line represent the fluid density in the annulus. For all depths, except bottomhole, the density of the fluid in the annulus is lower, than for the density of the fluid in the drillpipe. Bottomhole fluid density equals to 1027,8 $\frac{kg}{m^3}$, both for annulus and drillpipe. Initial drillpipe fluid density equals to 1080,6 $\frac{kg}{m^3}$, i.e. a decrease of 52,8 $\frac{kg}{m^3}$ from top to bottom of the well. Initial annular fluid density equals 1078,7 $\frac{kg}{m^3}$, i.e. a decrease of 50,9 $\frac{kg}{m^3}$. From the figure, it can be observed same behavior as for the viscosity and temperature, at depths for transitions to new pipe section. It can be observed that the effect from the three transitions to new pipe sections at depths 2087,7 m, 3642,6 m and 3764,4 m, is increased fluid density for all transitions. Especially for the transitions from drillpipe 2 to HWDP and from HWDP to drill collars, the density increase is notable.

61
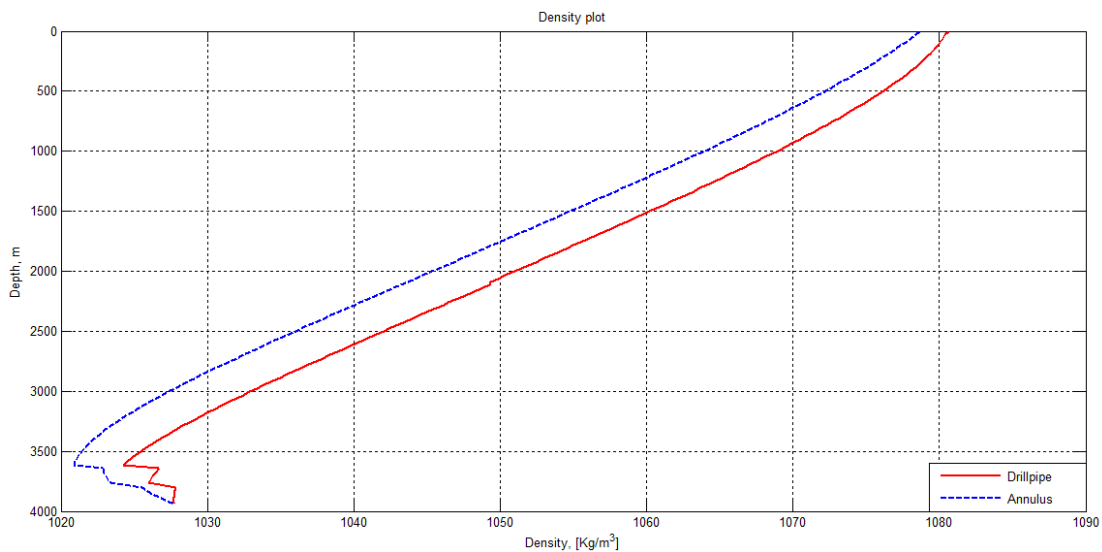
Figure 6-7: Density of the fluid inside the pipes and in the annulus

6.5: RECALCULATION OF PRESSURE AND DENSITY

As it have been done, and explained previously, the density, found above, is now used in the recalculation of pressure with varying density, instead of constant density. This is done to improve the accuracy of the pressure calculation. The new pressure is plotted below.
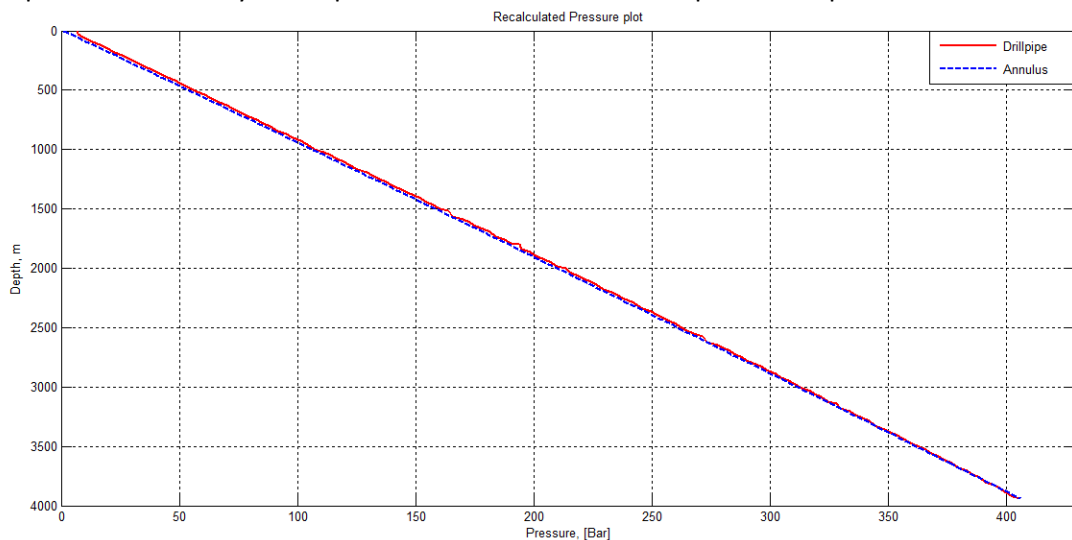

Figure 6-8: Recalculated pressure inside the pipes and in the annulus

From the recalculation of the pressure, it can be observed that the bottomhole pressure in the well have been reduced. As mentioned before, at the bottom of the well, the pressure in the pipe and in the annulus, is the same. Bottomhole pressure in the well with constant density equals to 419,3 bar, and recalculated bottomhole pressure, with varying density, equals to 406,3 bar. It can be observed, a reduction of the bottomhole pressure of 13 bar. As mentioned previously, this mismatch of pressure calculation could have severe consequences regarding e.g. well integrity. The new recalculated pressure is implemented in the calculation of fluid density. Same formula and method, as presented above, is used. The recalculated density of the fluid inside the pipes and in the annulus is plotted in the figure below:

62
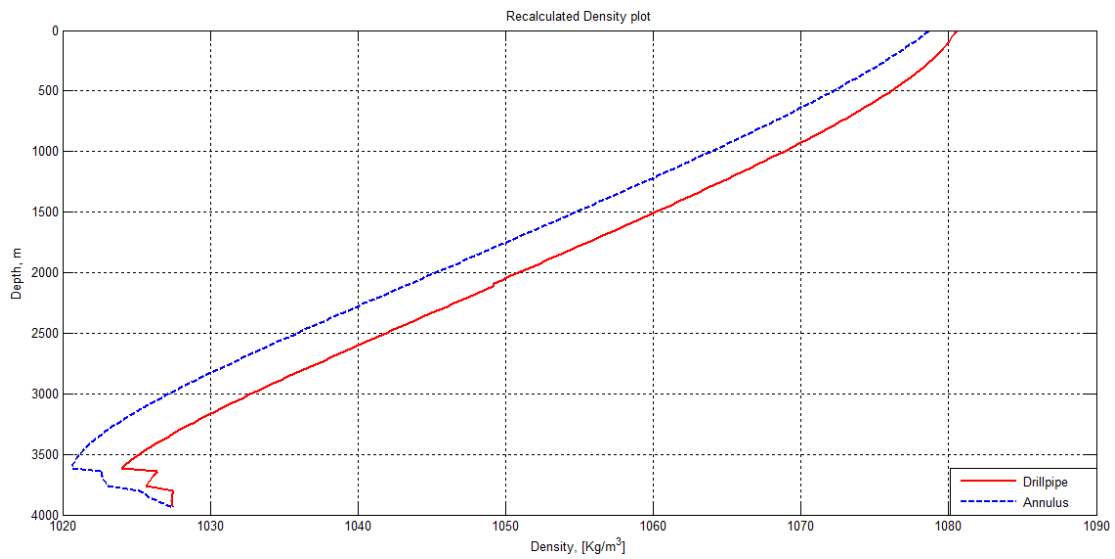
Figure 6-9: Recalculated density of the fluid inside the pipes and in the annulus

Initial bottomhole fluid density equals to 1027,8 $\frac{kg}{m^3}$, both for annulus and drillpipe, calculated with the pressure with constant density. The recalculated bottomhole fluid density equals to 1027,5 $\frac{kg}{m^3}$. In can be observed a density reduction of only 0,3 $\frac{kg}{m^3}$. However, this new recalculated fluid density, is the density that will be used in the calculation of buoyancy factor for the well.

6.6: BUOYANCY FACTOR CALCULATION:

The new densities of the inside pipe fluid (ρ_i) and the annular fluid (ρ_o), along with the new areas calculated, can be used to calculate the buoyancy factors in the well. Above the area inside (A_i) and outside (A_o) for drillpipe 1, drillpipe 2, HWDP and drill collar were calculated. The formula for buoyancy factor for different inside and outside fluid is defined as:

$$\beta = 1 - \frac{\rho_o A_o - \rho_i A_i}{\rho_{pipe}(A_o - A_i)} \qquad (\,6\text{-}15\,)$$

Density of the pipe (ρ_{pipe}) is the same as before and equals 7850 $\frac{kg}{m^3}$. As for all the other parameters, the buoyancy factor will also be calculated for each 30 m MD and in the 4110 m MD deep well, it means the buoyancy will be calculated for 137 segments. Below the buoyancy factor in the well is plotted:
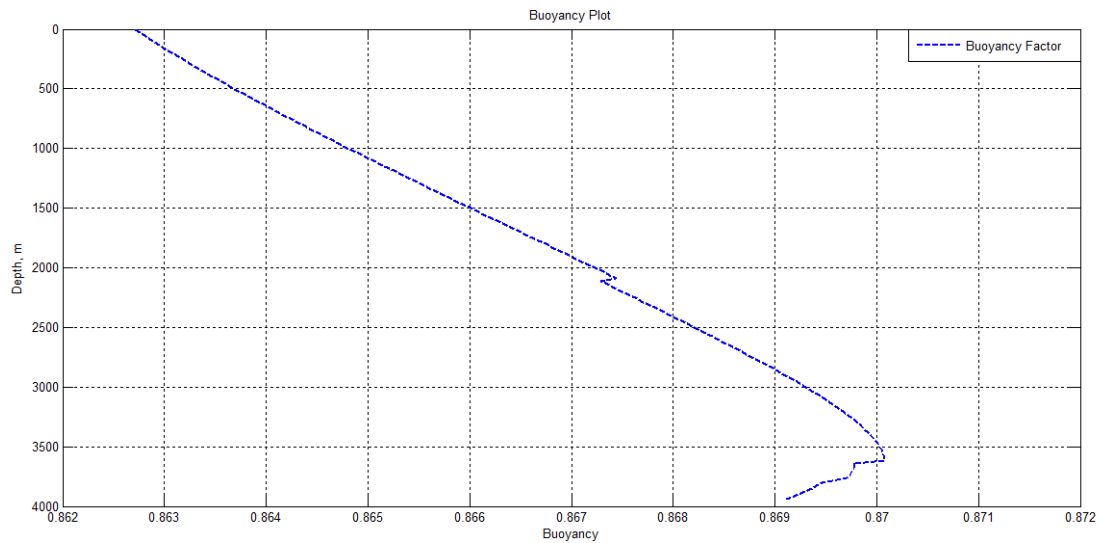
Figure 6-10: Buoyancy factor in the well

By having in mind the different areas and that the fluid density decrease with depth, it can be observed two effects on the buoyancy factor plot. If starting at the top of the well, it can be observed that the buoyancy factor increases with depth. It can also be observed that the buoyancy factor decreases when changing to new pipe sections at depths 2087,7 m, 3642,6 m and 3764,4 m. This have to do with the above mentioned fluid density changes at these depths. At 2087,7 m, where drillpipe 1 ends and drillpipe 2 starts, it can be observed that the buoyancy factor decrease. At 2087,7 m the buoyancy factor equals to 0,8674 and at next pipe stand, 30 m below, at 2117,7 m, the buoyancy factor have decreased to 0,8673. I.e. a decrease of 0,0001. Imagine a 1 ton heavy object, a change of the buoyancy factor of 0,0001 would equal 0,1 kg in changed weight. The change in buoyancy from drillpipe 1 to drillpipe 2, do not follow the trend with increasing buoyancy factor with increasing density, therefore it can be stated that the buoyancy factor decrease, is due to the changes in the respective areas.

In order, to thoroughly illustrate the effect of the area in the pipe and annulus on the buoyancy factor, a small case is presented. In the case, the buoyancy factor for drillpipe 1 and drillpipe 2, with given different areas, but for same density will be studied. The density at 2087,7 m (end of drillpipe 1) will be used for both cases. The inside pipe fluid density equals to 1049,2 $\frac{kg}{m^3}$ and annulus fluid density equals to 1043,6 $\frac{kg}{m^3}$. Density of the pipe equals to 7850 $\frac{kg}{m^3}$.

$$\beta_{Drillpipe\ 1} = 1 - \frac{(1043{,}6 * 0{,}0364) - (1049{,}2 * 0{,}0127)}{7850(0{,}0364 - 0{,}0127)} = 0{,}8674 \qquad (\ 6\text{-}16\ )$$

$$\beta_{Drillpipe\ 2} = 1 - \frac{(1043{,}6 * 0{,}0459) - (1049{,}2 * 0{,}0081)}{7850(0{,}0459 - 0{,}0081)} = 0{,}8672 \qquad (\ 6\text{-}17\ )$$

It can be observed, that the buoyancy factor is reduced from drillpipe 1 to drillpipe 2, as the areas have changed. The actual buoyancy factor at drillpipe 2, 30 m MD below the bottom of drillpipe 1, equals to 0,8673. The difference from actual buoyancy factor of 0,8673 and 0,8672 is due to the decreasing density. Therefore, it can be observed that the decreasing density have an increasing effect on the buoyancy factor.

64

It can be observed an interesting behavior of the buoyancy factor between 3500 m and TD. This is due to the effects of the changing areas and densities discussed above. As mentioned, the buoyancy factor is affected by changes in areas. The effect of density can also be studied. From the density plot, figure 6-9, it can be observed that the density behaves differently, both in the pipes and in the annulus, than for the rest of the well. The density of the fluid inside the pipe shows a decreasing trend, while the density of the fluid in the annulus between about 3500 m and 3942 m, deviates from its decreasing trend and actually starts to increase. These deviations, for both inside the pipe and in the annulus, for the drilling fluid density, could be explained with the temperature behavior in the well between about 3500 m to 3942m. For the annulus, the temperature increases from the bottom of the well to about 3500 m, after this point and upwards, the annular fluid temperature decreases. This temperature increase, from bottom of the well to 3500 m, is due to the temperature effect explained before. This effect is due to the drilling fluid that flows up the annulus and to the top of the well, experience both heat transfer from the annulus and from the outside of the drillpipe. This makes the drilling fluid temperature increase to about 3500 m depth. The temperature inside the pipe shows a decreasing trend from 3500 m to 3942 m. These temperature deviations, for both the annular drilling fluid and the inside pipe fluid, will, as possible to observe, affect the fluid density. The density behavior between 3500 m and TD is also affected by the transitions from drillpipe 2 to HWDP and from HWDP to drill collars. From the density calculation section 6.4, it was seen that the density in the transitions from drillpipe 2 to HWDP and from HWDP to drill collars increased notable. From this, it is observed that the density is increased, by different processes, and thereby the buoyancy factor in the well.

If the buoyancy factor for constant density and the buoyancy factor varying with depth is studied, some observations can be made. The constant buoyancy factor is previously calculated to be 0,8624. If the constant buoyancy factor is used, it is used regardless of the depth. This involves same buoyancy factor will be used at for example 200 m and at 3200 m. For the varying buoyancy factor with depth, it can be observed a maximum value of 0,8701. From this, it can be seen that the highest difference value, by ignoring the varying buoyancy factor with depth could be: 0,8701-0,8624=0,0077. A pipe stand, i.e. 30 m, of a weight $450 \frac{N}{m}$ could be used to visualize this difference better. The weight of the pipe stand would be $450 \frac{N}{m}$ *30 m=13 500 N. In kilo grams this would be 135000/9,81=1376 kg. If this pipe is displaced in the drilling fluid and with a buoyancy difference of 0,0077, the weight difference would be 10,6 kg per pipe stand. The well for the case study consists of 137 pipe stands, so with the weight difference from ignoring buoyancy effect for the whole well would be 137*10,6=1452,2 kg. This is for the case with highest difference value regarding the two buoyancy factors.

6.7: TORQUE AND DRAG:

The well that is used for the simulation of torque and drag force, have a depth of 3942 m TVD and 4110 m MD. The dataset used, have different parameters given like measured depth (MD), true vertical depth (TVD), inclination and azimuth. As explained earlier, this data is used to calculate the dogleg angle. It is important that the dogleg angle is given in radians for the purpose of calculating whether the wellpath is straight inclined or curved. The MD values ranges from 0 m to 4110 m, with an increase of 30 m between each measurement point. The depth of 30 m equals a pipe stand length. The TVD data starts at 0 m and ends at the bottom

of the well at 3942 m. The vertical height between the TVD measurements depends on the inclination of the well. If the inclination equals 0° (perfect vertical) the vertical height between each measurement would be 30 m and if the inclination equals to 90° (perfect horizontal) the vertical height between the measurements would equal to 0 m. The measured depth values are used in the DLS-filter to determine whether the wellbore is straight inclined or curved. The true vertical depth values are used in the different models to determine the fluid temperature, density, viscosity, pressure and buoyancy factor.
The wellpath data is implemented in the MATLAB simulation, and the DLS-filter determines whether the wellpath is either straight inclined or curved. When the DLS-filter have determined whether for which depth the wellpath is straight inclined or curved, the equations for torque and drag for either straight inclined wellbore or curved wellbore will be used.

The drag force and the torque is calculated for the case with hoisting, lowering and static conditions for the drillstring. The different conditions for the drillstring are calculated with the case for constant buoyancy factor, and for the case with varying buoyancy factor with depth. In addition, in the simulation, the torque and drag force is simulated both for the case without pipe rotation and for the case with combined motion. As mentioned, combined motion could be divided into axial motion and rotation. For the case with combined motion the angle between the axial and tangential velocity (ψ) need to be calculated. As presented previously, the equation needed to do so is:

$$\psi = tan^{-1}\left(\frac{V_h}{V_r}\right) = tan^{-1}(\frac{60V_h}{2\pi N_r r}) \tag{6-18}$$

For the axial velocity (V_h) a reasonable number is assumed to be equal to 0,25 $\frac{m}{s}$. The rotary pipe speed is assumed equal to 120 rpm. The radius of the pipe will be different for the different pipe sections. The angle between the axial and tangential velocity can be calculated for the four different pipe sections, i.e. drillpipe 1, drillpipe 2, HWDP and drill collar:

$$\psi_{drillpipe\ 1} = tan^{-1}\left(\frac{60*0,25}{2\pi*120*0,0841}\right) = 13,3° \tag{6-19}$$

$$\psi_{drillpipe\ 2} = tan^{-1}\left(\frac{60*0,25}{2\pi*120*0,0635}\right) = 17,4° \tag{6-20}$$

$$\psi_{HWDP} = tan^{-1}\left(\frac{60*0,25}{2\pi*120*0,0635}\right) = 17,4° \tag{6-21}$$

$$\psi_{drill\ collar} = tan^{-1}\left(\frac{60*0,25}{2\pi*120*0,1016}\right) = 11,1° \tag{6-22}$$

Below is a plot that illustrates the wellpath. The small round circles indicates whether the wellpath is straight inclined or curved. The well configuration consist of a well diameter of 0,27305 m, pipe outer diameters equals to 0,168 m for drillpipe 1, 0,127 m for drillpipe 2, 0,127 m for the HWDP and 0,2032 m for the drill collar. This gives four different relation for the expression D-d:

- For drillpipe 1: D-d=0,104775 m
- For drillpipe 2: D-d=0,14605 m
- For HWDP: D-d=0,14605 m
- For drill collar: D-d=0,06985 m

The condition for straight inclined wellbore, according to the DLS-filter, it that $h<$ (D-d) and for curved wellbore $h>$ (D-d). As possible to observe, from the figure below, the wellpath is considered curved for multiple depths. The wellpath is not straight inclined, i.e. curved, for the points that are offset from the vertical line at 0, i.e. these points, that are circled out in red, are those which represent curved wellpath section. To be clear, the plot below do not illustrate the actual wellpath, but it illustrates, at which depth the wellpath is straight inclined or curved. A small description how to interpret the figure could be given: From the figure it could for example be observed that the wellpath is considered straight inclined from top of the well down to about 800 m, then wellpath is considered curved from 800 m down to about 1200 m, below 1200 m the wellpath is straight inclined etc. The further interpretation of the when the wellpath is considered straight incliend or curved could be observed from the figure.
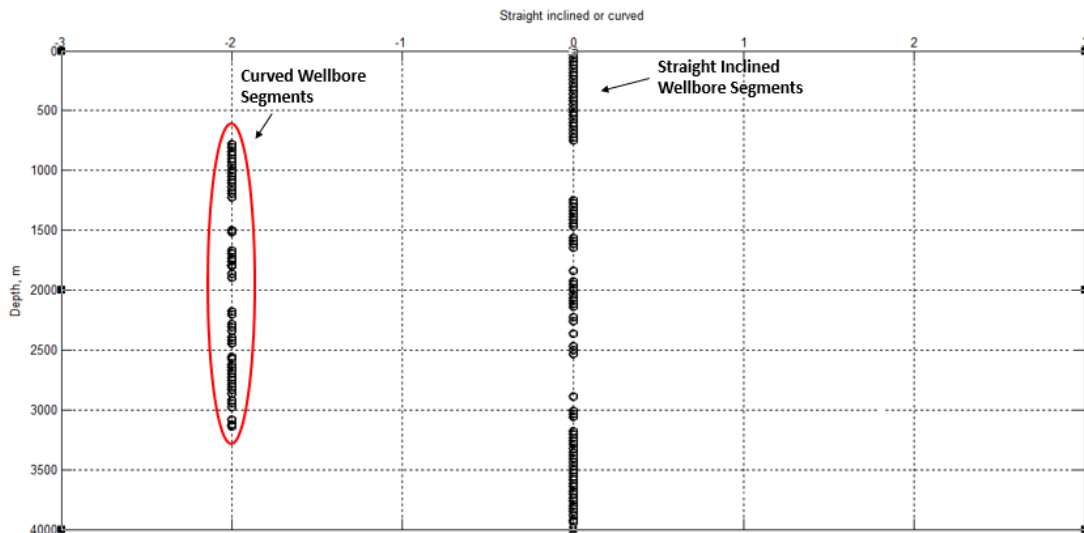

Figure 6-11: Points indicating at which depth wellbore is straight inclined or curved

With the buoyancy factor for the well, calculated in last section, in place, the torque and drag can be calculated for varying buoyancy, not just one constant buoyancy factor through the whole well. The constant buoyancy factor through the whole well equals:

$$\beta = 1 - \frac{\rho_{mud}}{\rho_{pipe}} = 1 - \frac{1080,5}{7850} = 0,8624 \qquad (\,6\text{-}23\,)$$

There will be four different values for the weight of the pipes. The weight is presented in newton per meter $(\frac{N}{m})$.

- Drillpipe 1 weight = 450 $\frac{N}{m}$
- Drillpipe 2 weight = 290 $\frac{N}{m}$
- HWDP weight = 620 $\frac{N}{m}$

67

- Drill collar weight = $2130 \frac{N}{m}$

The friction coefficient is set to 0,2 throughout the whole well.

All the parameters needed to calculate the torque and the drag in the well is now in place. Several cases for the torque and the drag are to be calculated. The different cases are:
- Drag lowering with constant buoyancy factor
- Drag hoisting with constant buoyancy factor
- Drag lowering with varying buoyancy factor
- Drag hoisting with varying buoyancy factor
- Static load with constant buoyancy factor
- Static load with varying buoyancy factor
- Drag lowering combined motion with constant buoyancy factor
- Drag hoisting combined motion with constant buoyancy factor
- Drag lowering combined motion with varying buoyancy factor
- Drag hoisting combined motion with varying buoyancy factor

- Torque with constant buoyancy factor
- Torque with varying buoyancy factor
- Torque combined motion with constant buoyancy factor
- Torque combined motion with varying buoyancy factor

The different situations are plotted and will in the further will analyzed:

6.8: TORQUE ANALYZE

Below there are three plots. One plot illustrating the torque when lowering the drillstring, one illustrating the torque when hoisting the drillstring and one plot illustrating the torque during static conditions. As possible to observe, the wellpath is considered curved for multiple depths. The wellpath is not straight, i.e. curved, for the points that are offset from the vertical line at 0, these points are circled out in red.
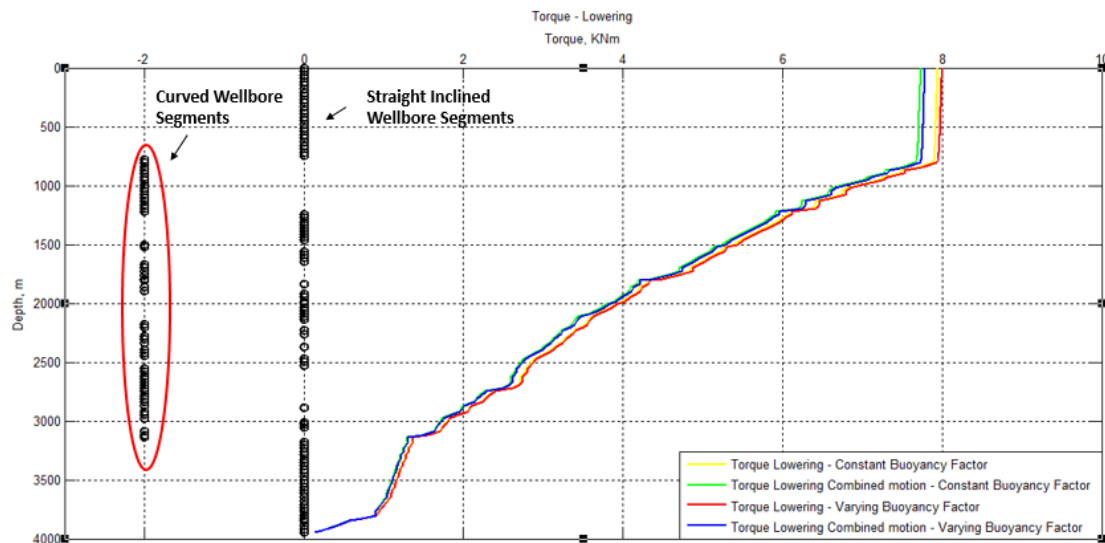

Figure 6-12: Torque when lowering the drillstring

68
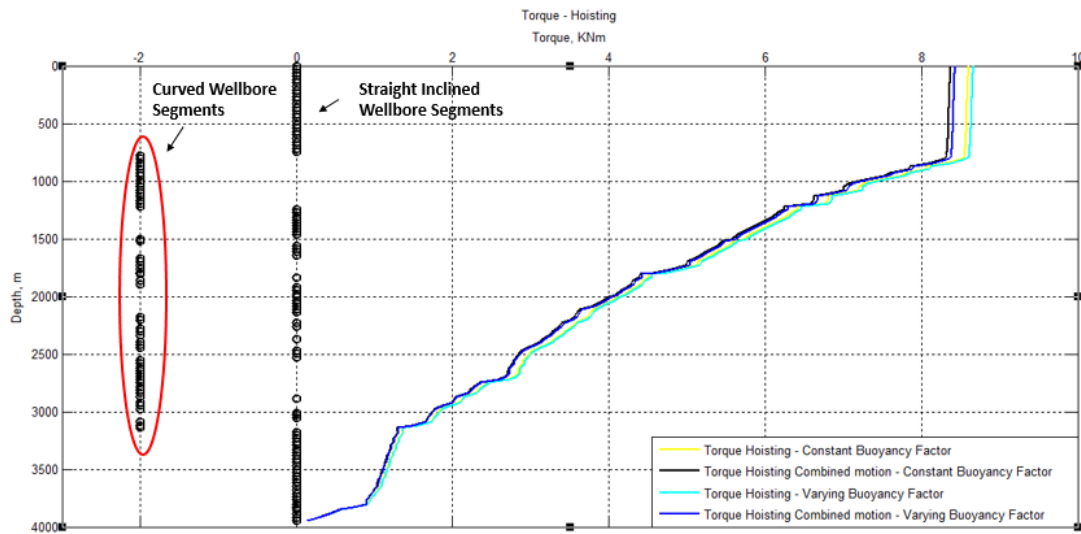
*Figure 6-13: Torque when hoisting the drillstring*
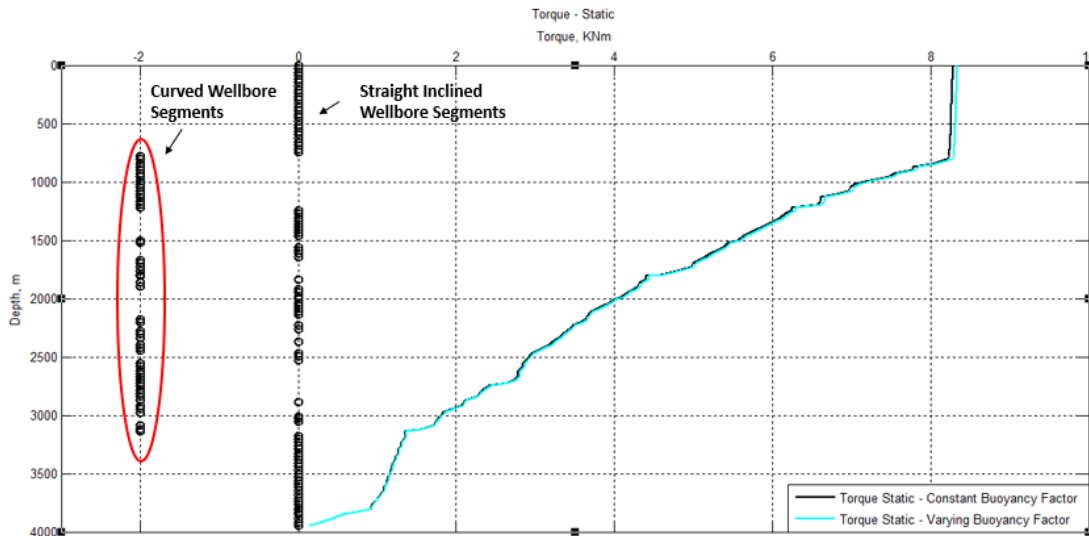
Figure 6-14: Torque during static conditions

From the plots of torque for lowering-, hoisting- and static conditions, it can be observed that the torque is different, for all of the three cases. If the torque at the top of the well is studied, some observations can be made. The torque for the cases with lowering, hoisting and static drillstring is observed, for the case with constant buoyancy and without combined motion. It can be observed that the torque for lowering equals to 7,94 kNm, for hoisting it equals to 8,60 kNm and for static conditions it equals to 8,28 kNm. In other words, it is observable that the torque for lowering is the lowest, hoisting is the highest and static is the middle value.

Regarding the torque in the well, some other interesting general observations, for the three cases, can be made. It can be observed that for the drill collars, at depth 3764,4 m to the bottom of the well, with its high weight of 2130 $\frac{N}{m}$, the torque loss is high. At 177,6 m (drill collar length), the torque is reduced from about 900 Nm to about 137 Nm.

69

Another observation is made in the upper part of the well, from 0 m to about 800 m, the torque loss in the well is low. This could be due to the low inclination in this part of the well. As mentioned before, when low inclination, the torque loss is also low. From 0 m to 800 m the highest inclination in this interval is 1,4°. Below 800 m, the inclination builds up to about 22°. The inclination is around 20-23° to about 2900 m, below this point the inclination drops, and finally reaches 7° at the bottom of the well at 3942 m TVD depth.

If the effect of the buoyancy factor in the well is studied, the cases with a constant buoyancy factor and the case with the varying buoyancy factor with depth, should be studied. The difference in torque is compared at the top of the well. Below, a figure of the torque in the well for the case with lowering-, hoisting- and static conditions for the drillstring, with constant buoyancy factor and varying buoyancy factor, is illustrated. As it can be seen from the figure, for all the three cases for the drillstring, it can be observed lower torque when a constant buoyancy factor is applied. The effect of buoyancy can be studied more in detail, for the three different operational modes for the drillstring:

- **Lowering the drillstring:** At the top of the well, for the case for lowering torque, with constant buoyancy and without combined motion, the torque equals to 7,94 kNm. The lowering torque, with varying buoyancy factor and without combined motion, equals to 7,99 kNm. It can be observed a torque difference of 0,05 kNm, or 50 Nm, for the different cases.
- **Hoisting the drillstring:** At the top of the well, for the case for hoisting torque, with constant buoyancy and without combined motion, the torque equals to 8,60 kNm. The hoisting torque, with varying buoyancy factor and without combined motion, equals to 8,66 kNm. It can be observed a torque difference of 0,06 kNm, or 60 Nm, for the different cases.
- **Static conditions for the drillstring:** At the top of the well, for the case for static torque, with constant buoyancy and without combined motion, the torque equals to 8,28 kNm. The static torque, with varying buoyancy factor and without combined motion, equals to 8,34 kNm. It can be observed a torque difference of 0,06 kNm, or 60 Nm, for the different cases.

From this, a conclusion can be made. It can be concluded that the case with varying buoyancy factor shows higher torque at the surface than for the case for torque with constant buoyancy factor.
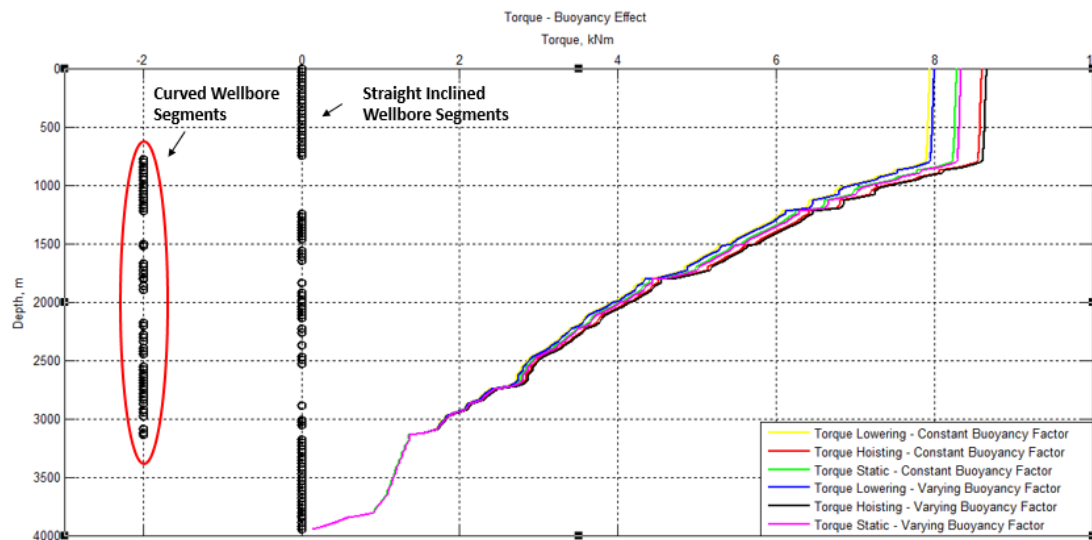
Figure 6-15: Buoyancy effect on the torque in the well

Another observation is the effect of the combined motion on the torque. If the torque at the top of the well is compared for the case for torque with and without combined motion, it can be observed that the combined motion have the effect of reducing the torque in the well. The effect of combined motion for hoisting and lowering torque can be studied:

- **Lowering torque:** For the case with lowering the string, the torque at top of the well, without combined motion and constant buoyancy factor, equals to 7,94 kNm. For the case with lowering the string at top the well, with combined motion and constant buoyancy factor, the torque equals to 7,73 kNm. It can be observed a torque loss of 0,21 kNm due to combined motion.

- **Hoisting torque:** For the case with hoisting the string, the torque at top of the well, without combined motion and constant buoyancy factor, equals to 8,60 kNm. For the case with hoisting the string at top the well, with combined motion and constant buoyancy factor, the torque equals to 8,37 kNm. It can be observed a torque loss of 0,23 kNm due to combined motion.

Below, a figure illustrating the effect of combined motion on the torque can be seen.

71
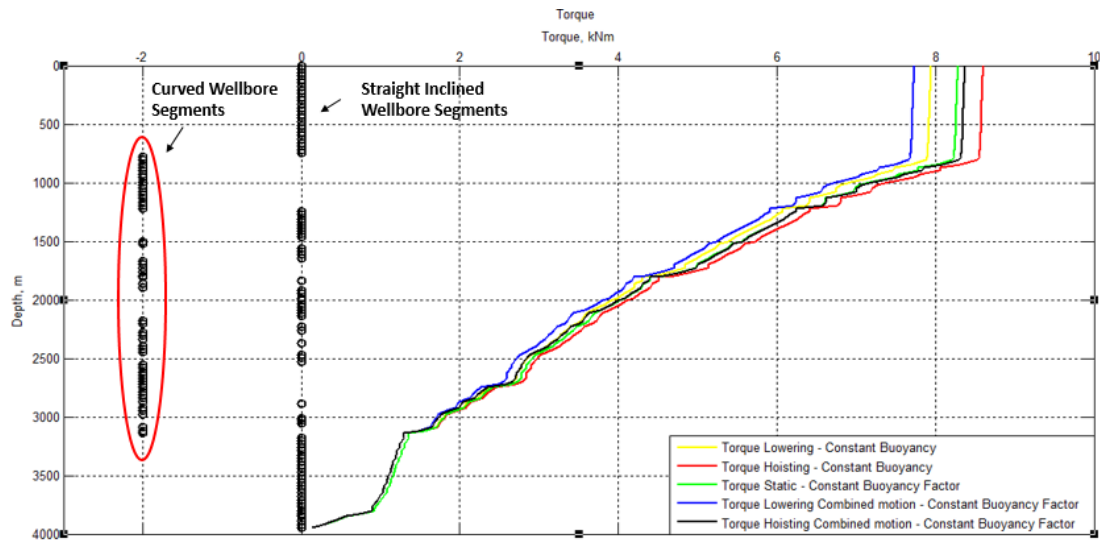
Figure 6-16: Torque in the well

6.9: Drag force analyze:

Below, there are two plots of the drag force in the well. The first plot illustrates the drag force with constant buoyancy factor. The second plot is illustrating the drag force with varying buoyancy factor with depth. In both plots, the drag force for five operational modes are plotted. The drag force is plotted for these operational modes for the drillstring: Drag force lowering, drag force hoisting, static load, drag lowering with combined motion and drag hoisting with combined motion.
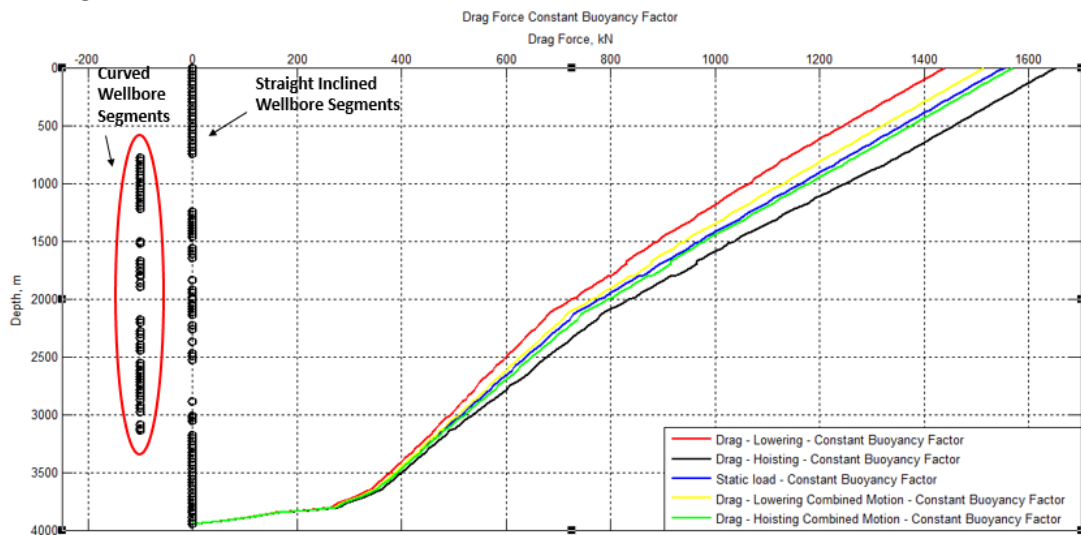
Figure 6-17: Drag force in the well with constant buoyancy factor

72
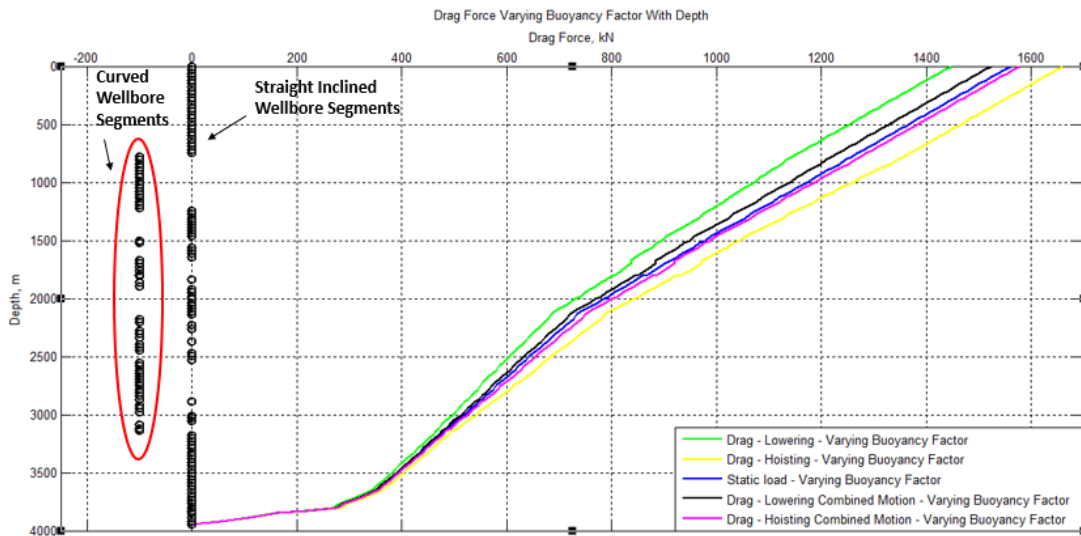
Figure 6-18: Drag force in the well with varying buoyancy factor with depth

Regarding the drag force, some interesting observations can be made. First, it can be observed that the drag force is higher for cases with hoisting than for the cases with lowering of the drillstring. As for the torque, it can be observed that for the drill collar section at depth 3764,4 m to bottomhole, with its high weight of $2130 \frac{N}{m}$, the drag force increases rapidly. From the bottom of the well, the drag force increases from 0 N up 265 kN at 3764,4 m (top of drill collars). This rapid increase in the drag force, could be explained by the drill collars high weight.

It can be observed, from the figures of drag force, that the drag force is connected to the different pipes. For the four types of pipes, it can clearly be observed deviations in the transitions from one type of pipe, to another type of pipe. The transitions can be found at depths: 2087,7 m, 3642,6 m, 3764,4 and 3942 m. These transitions in pipes correlates well with the observed deviations on the figures.

If the effect of the buoyancy factor in the well is studied, the cases with a constant buoyancy factor and the cases with the varying buoyancy factor with depth, should be studied. The difference in drag force is compared at the top of the well. The cases for lowering drag force, hoisting drag force and static load, with constant buoyancy factor and with varying buoyancy factor is compared. For the cases, the top plot is illustrating the case without combined motion and the bottom plot illustrating the case with combined motion.

73
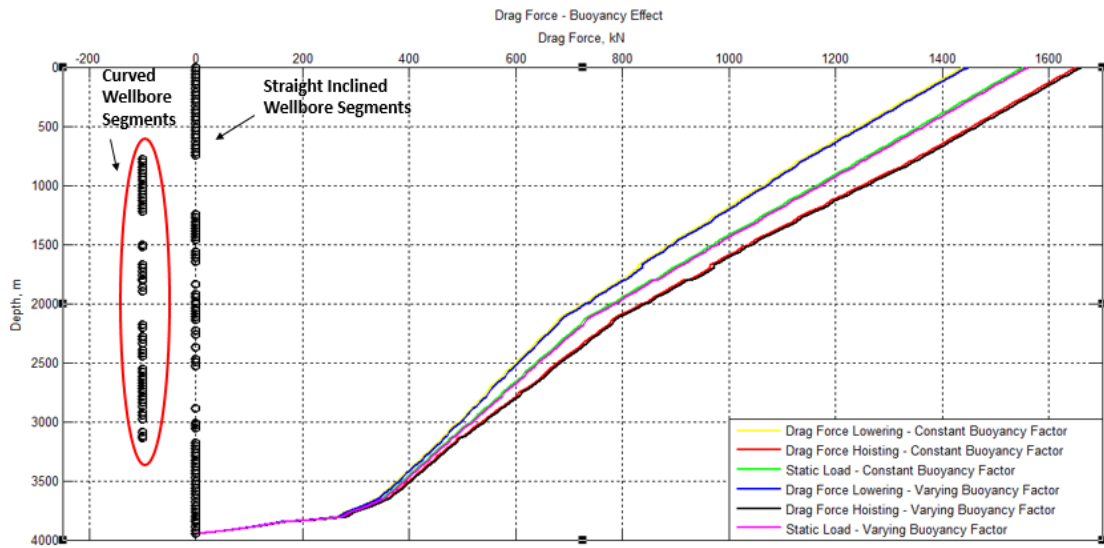
Figure 6-19: Buoyancy effect on drag force in the well without combined motion
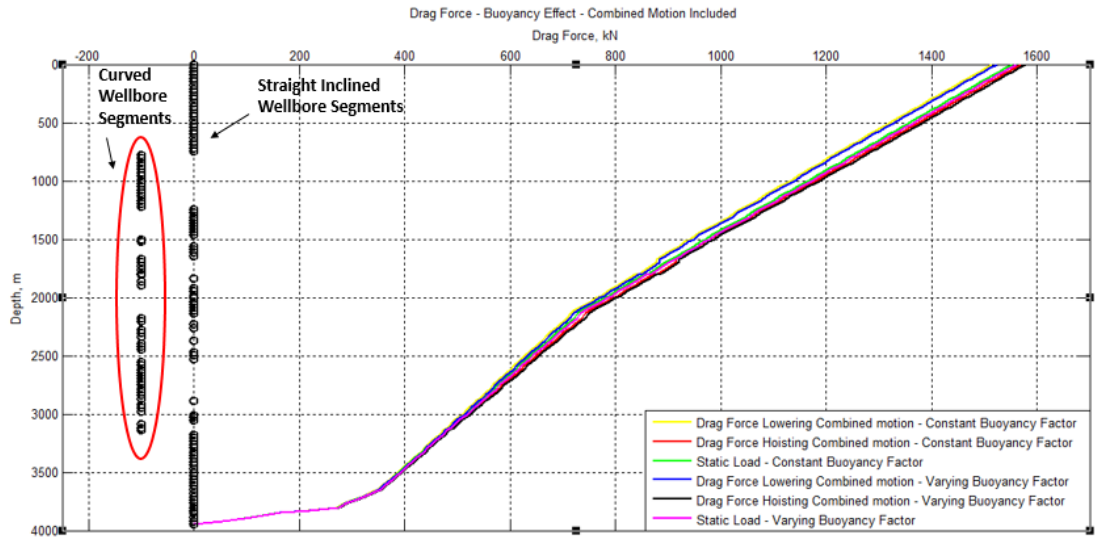
Figure 6-20: Buoyancy effect on drag force in the well with combined motion

Below, is a table illustrating the drag force at the top of the well for the different cases that can be seen from the two plots above. The cases mentioned are; drag force for lowering, hoisting and static condition, with constant buoyancy factor and with varying buoyancy factor and for with and without combined motion. The drag force difference between the cases are calculated. As it is possible to see from table 6-2, the drag force difference is between 7,5 kN and 9,0 kN, for the case with constant buoyancy factor compared to the case with varying buoyancy factor. Therefore, by assuming a constant buoyancy factor throughout the well, could lead to the consequence of miscalculating the drag force.

Table 6-2: Drag force differences in the well

Operational mode	Drag force constant buoyancy factor [kN]	Drag force varying buoyancy factor [kN]	Drag force difference with constant and varying buoyancy factor [kN]
Pure lowering	1440,1	1447,6	7,5
Pure hoisting	1651,9	1660,9	9,0
Static	1552,7	1560,9	8,2
Lowering with combined motion	1515,6	1523,6	8,0
Hoisting with combined motion	1569,8	1578,3	8,5

To illustrate the drag force difference, calculated from table 6-2 above, a plot for the case with pure hoisting of the drillstring, with constant buoyancy factor and varying buoyancy factor, is included. The plot is a zoomed view of the drag force difference at top of the well. The red line is illustrating the hoisting drag force with constant buoyancy factor and the black line is illustrating the hoisting drag force with varying buoyancy factor. It can be observed, from the figure below, that for the case with constant buoyancy factor, the hoisting drag force equals to 1651,9 kN, and for the case with varying buoyancy factor, the drag force for hoisting equals to 1660,9 kN, i.e. a difference of 9,0 kN is observed.
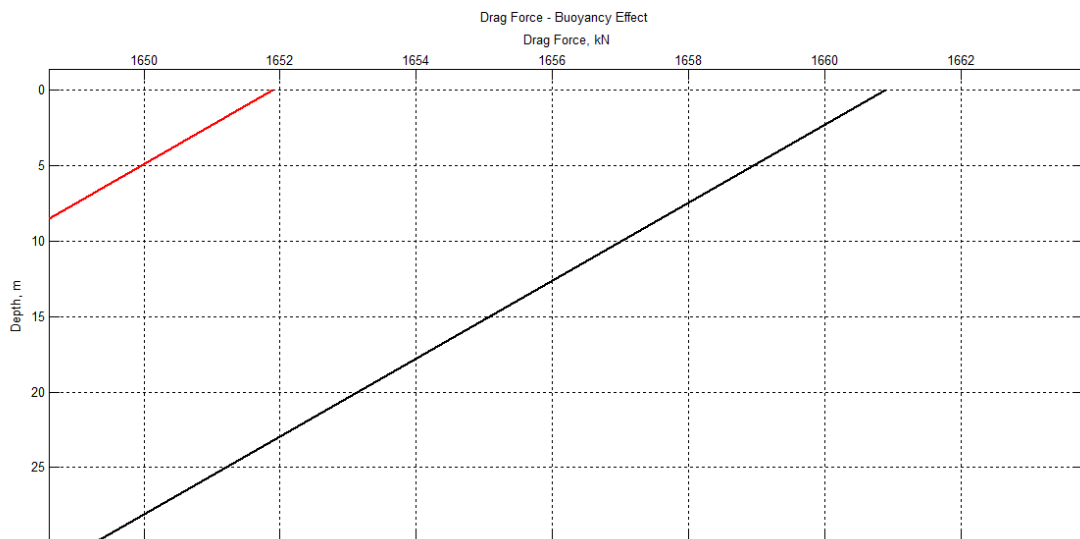
Figure 6-21: A zoomed view for hoisting drag, with constant- and varying buoyancy factor

If the drag force for combined motion is analyzed, some observations can be made. As mentioned, combined motion can be divided into rotation and axial motion. It can be observed, with the effect of combined motion, the drag force for both lowering and hoisting of the drill string, the drag forces approaches the static load of the string. As it can observed from figure 6-17 and figure 6-18, the drag force is in this order, from low to high drag force:
1) Pure Lowering
2) Lowering combined motion
3) Static load

75

4) Hoisting combined motion
5) Pure hoisting

The same order applies for both with constant buoyancy factor and for the cases with varying buoyancy factor. As previously stated, the expected effect of rotation, is that the axial friction is reduced.[102] This has the mentioned effect, that both the drag force for both lowering and hoisting of the string, approaches the static load of the string.
A high rotational speed should reduce the axial friction. The two conditions below for the angle between the axial and tangential velocity must be remembered. A lower value of the angle, a higher reduction of the axial friction will be seen. Low values of the angle can be achieved by high rotational speed or low hoisting or lowering speed. If the angle equals 90°, there will only be axial motion, i.e. no rotation. This again, implies that same values for the drag force will be seen, as for the case without combined motion.

$$\psi = 0° \rightarrow Rotation\ only$$

$$\psi = 90° \rightarrow Axial\ motion\ only$$

As mentioned, by rotation, the axial friction is reduced. From the plots and table 6-2 above, it is possible to observe that axial friction influences the drag force. As the axial friction is reduced, it can be observed that for the case with hoisting, the drag force at top of the well, both for constant buoyancy factor, is reduced from 1651,9 kN to 1569,8 kN. For the lowering of the drillstring, it can be observed that reduced axial friction have the effect of increasing the drag force from 1440,1 kN to 1515,6 kN. The static load at top of the well equals to 1552,7 kN, so it can be observed that both for the case with lowering and for hoisting, both approaches the static load during combined motion.

It can be observed, for both hoisting and lowering, the axial friction in the well is reduced considerably with combined motion. To examine this even further, the rotational speed can be increased. Initial, the rotational speed equals to 120 rpm, this is now increased to 180 rpm. By doing this, the drag force for lowering with constant buoyancy and combined motion increases even further, from 1515,6 kN to 1523,9 kN. The drag force for hoisting with constant buoyancy and combined motion decreases from 1569,8 kN to 1560,8 kN. This goes to confirm that rotational speed decreases the axial friction, and thereby allowing the drag forces for lowering and hoisting, approach the static load. In other words, for combined motion, it can be said that if hoisting or pulling the string, the force required to do so would be less if the string is rotated when pulling the string. The effect of hoisting/lowering speed can also be investigated. Initial the hoisting/lowering speed equals to 0,25 $\frac{m}{s}$, this is now increased to twice as fast, i.e. 0,50 $\frac{m}{s}$. In this case, the rotational speed equals 120 rpm. The observed effect of increasing the hoisting/lowering speed, is that the drag force for lowering with constant buoyancy and combined motion decrease from 1515,6 kN to 1494,3 kN. The drag force for hoisting with constant buoyancy and combined motion is increased from 1569,8 kN to 1593,0 kN. It is observed that the hoisting/lowering speed have the opposite effect on the drag force compared to rotational speed.

Chapter 7: Discussion

In this thesis, several models have been considered in order, to investigate the effect of downhole conditions on the drilling fluid. It have been observed a clear connection between the downhole temperatures and pressures, and the drilling fluid behavior. It have been seen that higher pressure increases the drilling fluid density due to fluids are compressed by pressure. While as higher temperature decreases the drilling fluid density, due to fluids expands when heated. Changes that have been studied, regarding the drilling fluid, includes changes in the drilling fluid density and viscosity variations as a function of temperature and pressure. It was observed that the bottomhole fluid temperature, according to findings in the sensitivity analysis of the temperature model, were more sensitive to changes in the drilling fluid density than for changes in drilling fluid viscosity. It was also seen, that the changes in drilling fluid properties, mentioned above, did again affect properties, like the pressure in the well and the buoyancy factors.

The need for accurate temperature modelling, to investigate drilling fluid behavior, have been demonstrated. The advantages by the temperature model include possibility to calculate the fluid temperatures for the entire well, and study the effect of the different parameters. From the case study, the effect of different sizes of pipes were investigated. It was seen, that the different sizes of pipes affected the drilling fluid temperature. It was observed for the pipes used in the case study, when changing to new type of pipe, the results was reduced temperature. Some general observations were made regarding the temperature behavior for changed inside and outer pipe diameters:

- When the pipe inner diameter decreases the temperature decreases
- When the pipe inner diameter increases the temperature increases
- When the pipe outer diameter decreases the temperature increases
- When the pipe outer diameter increases the temperature decreases

As for the temperature, it was observed for viscosity of the fluid, that in the transitions to new pipes, the viscosity was affected. For the pipes used in the case study, it was observed when changing to a new type of pipe, the result was increased viscosity. This was observed connected to the temperature effect. For the fluid temperature it was observed decreasing temperature at the different transitions to new pipes. This fluid temperature change, affected the fluid viscosity. From the viscosity experiment performed, it was observed differences in terms of viscosity and shear stress for the different samples. Findings were made, stating that the viscosity generally is higher for the bentonite samples, than for the chalk samples. Also, it was observed increased viscosity, with increasing amount of bentonite. The effect of additives to the mud samples were also studied. For example, it was seen by increasing the amount of Duotec with twice as much, the viscosity almost triples. The experiment also confirmed some theory presented. It was seen that viscosity decreases with increasing shear rates and increasing temperatures. This was true for all samples.

For the density of the drilling fluid, it was observed increased density, with new pipe section. For the case study, it was observed that particularly for the transitions from drillpipe 2 to HWDP and from HWDP to drill collars, the density increase was notable. It was also observed that the fluid density decreases with depth, as the fluid temperature increases. For the buoyancy factor, it was shown that the buoyancy factor increases with depth, as the density decreases with depth. For the case study, with different pipe sections downhole, two effects of the buoyancy factor were observed. It was observed that the buoyancy factor increased

with depth, due to density decrease. It was also observed that the buoyancy factor decreased with decreasing outside- and inside diameters.

In the evaluation of torque and drag force several interesting findings were made:
- The effect of the varying buoyancy factor have been evaluated for torque and drag force. Regarding the drag force, it was observed, from the simulation, that generally, the drag force were lower for the cases with constant buoyancy factor than for the cases with varying buoyancy factor with depth. For the different cases, involving pure lowering, pure hoisting, static, lowering with combined motion and hoisting with combined motion, it could be noticed a reduction of drag force from varying buoyancy factor to drag force for constant buoyancy factor, between 7,5 kN and 9,0 kN for the different cases. It was observed, that since the drag force for the cases with constant buoyancy is lower, than for the cases with varying buoyancy factor, the drag force could be underestimated by assuming a constant buoyancy factor through the well. By assuming a constant buoyancy factor throughout the well, it could lead to the consequence of miscalculating the drag force, and several negative consequences as a result.
- Regarding the buoyancy factor effect on torque, it was observed, from the simulation, that generally, the torque for lowering, hoisting and static, is lowered when a constant buoyancy factor is applied. The conclusion made, were that case with varying buoyancy factor shows higher torque at the surface, than for the case for torque with constant buoyancy factor.
- In the torque and drag analysis, the effect of combined motion were investigated. Some clear findings were made. It was observed that the effect of rotation, was that the axial friction in the well was reduced. This had the result that both the drag force for both lowering and hoisting of the string, approaches the static load of the string. It was seen that the axial friction could be reduced by either high rotational speed or low hoisting/lowering speed. It was seen that the drag force in the well, during the different operational modes, were given in this order:

  1. Pure Lowering
  2. Lowering combined motion
  3. Static load
  4. Hoisting combined motion
  5. Pure hoisting

- For torque, is was observed that the rotation have the effect of reducing the torque in the well. The behavior of torque and drag force during combined motion, could be explained with the fact that a high rotation should reduce the axial friction. For the case with lowering the drillstring, it was observed a torque loss of 0,21 kNm due to rotation. For the case with hoisting of the drillstring, it was observed torque loss of 0,23 kNm due to rotation.
- The effect of hoisting and lowering speed of the drillstring, on the drag force were also investigated. It could be seen, that the effect of increasing the hoisting/lowering speed of the drillstring, the drag force for lowering of the drillstring were decreased. While the effect of increased speed on the drag force for hoisting, was increased drag force. In other words, the effect of hoisting and lowering speed, had opposite effect on the drag force, compared to rotation.

In this thesis, some simplifications have been made. These simplifications, along with potential improvements and further work, to aid in the accuracy for the models presented in this thesis, could be mentioned:

- For simplicity in the calculations in this thesis, it is assumed that the both the annulus and drillstring is completely filled with mud. According to Fazaelizadeh[103], during tripping in operations, the annulus is completely filled with mud, but the inside of the drillpipe is initially empty. The drillpipe is typically filled with mud, after running in every few hundred meters. In others words, the drillpipe is not completely filled with mud all the time during tripping in, this again would affect the local buoyancy factor. According to Fazaelizadeh, changes in buoyancy factor during tripping out are negligible. However, the effect of tripping in on the buoyancy factor, are considerations that should be taken into account in the future work, with the process of evaluating torque and drag force using the presented models from this thesis.
- In order to obtain even more realistic and better results, an identical mud sample should have been used for the density and viscosity studies. In this thesis, different muds were used for the different purposes. Only for the viscosity, an actual physical study were performed. The density data were different from the viscosity data, with no connection with the mud sample used in the viscosity experiment. As explained before for the models, same values regarding the temperature and pressure were used for both the viscosity and density studies. Interpolation regarding the density were used, in order to achieve density values at correct temperature and pressure. Ideally, the same mud sample would be used for both the studies, but this was not possible for the work in this thesis.
- For the case study, different sized pipes were used in the well. When different sized pipes are used, this would give an acceleration pressure gradient, and it would affect the frictional pressure gradient. This have not been considered in the calculations in this thesis. In order to obtain as realistic results as possible, this is something that in the further work, with these issues, should be considered.
- In the work with this thesis, the effect of temperature have been evaluated. The effect of varying diameter have also been evaluated. In the further work, it would be interesting to connect these two properties, and even further study their combined effects through thermal expansion. Thermal expansion is the process of materials were changed shape, area and volume due to temperature changes, can be observed. In the further work, it would be interesting to study the process, especially in deep, high temperature wells, this could be a factor to consider.

Chapter 8: Conclusion

Some key findings, presented in this thesis, can be summed up:

- It have been observed a clear connection between downhole temperature and pressure, and the drilling fluid behavior. Higher pressure increases the drilling fluid density, while higher temperature decreases the drilling fluid density.
- For the buoyancy factor, it was shown that the buoyancy factor increases with depth, as the density decreases with depth. The effect of different inside and outside diameters of pipes, have to be considered when calculating the buoyancy factor. It was also observed from the case study, that the buoyancy factor decreased with decreasing outside- and inside pipe diameters.
- From the case study, for the different cases, involving pure lowering, pure hoisting, static, lowering with combined motion and hoisting with combined motion, it could be noticed a reduction of drag force from varying buoyancy factor to drag force for constant buoyancy factor, between 7,5 kN and 9,0 kN for the different cases.
- Regarding the torque, it was observed that generally the torque, for lowering, hoisting and static, is lowered when a constant buoyancy factor is applied. The conclusion made, were that case with varying buoyancy factor shows higher torque at the surface than for the case for torque with constant buoyancy factor.
- Regarding the effect of combined motion, it was observed that with the effect of rotation, the drag force for both lowering and hoisting of the drill string, the drag forces approaches the static load of the string. For torque it was observed that the rotation have the effect of reducing the torque in the well. It was observed, that the effect of hoisting and lowering speed, had opposite effect on the drag force, compared to rotational speed.

References

[1] Aleksander Kristensen, «Flow properties of water-based drilling fluids» (Master thesis, NTNU, 2013)

[2] Schlumberger Oilfield Glossary, «Pack off», Retrieved 19.04.16 from
http://glossary.oilfield.slb.com/Terms/p/pack_off.aspx

[3] Kjell Kåre Fjelde, «Numerical Solution Techniques for Nonlinear Equations and Applications within Petroleum Engineering»

[4] Kjell Kåre Fjelde, «Numerical Solution Techniques for Nonlinear Equations and Applications within Petroleum Engineering»

[5] Hero Santoso Effendi, «Water based mud drilling fluid» *Petroleum Support* (2015)
http://petroleumsupport.com/water-based-mud-drilling-fluid/

[6] Hero Santoso Effendi, «Water based mud drilling fluid» *Petroleum Support* (2015)
http://petroleumsupport.com/water-based-mud-drilling-fluid/

[7] Kjell Kåre Fjelde, «Drilling program & Drilling problems» UiS, 2015

[8] Schlumberger Oilfield Glossary, «Mudcake» Retreieved 19.04.16 from
http://glossary.oilfield.slb.com/Terms/m/mudcake.aspx

[9] Kjell Kåre Fjelde, «Drilling program & Drilling problems» UiS, 2015

[10] Schlumberger Oilfield Glossary, «Oil base mud» Retrieved 19.04.16 from
http://glossary.oilfield.slb.com/Terms/o/oil_base_mud.aspx

[11] Kjell Kåre Fjelde, «Drilling program & Drilling problems» UiS, 2015

[12] Kjell Kåre Fjelde, «Drilling program & Drilling problems» UiS, 2015

[13] Keelan Adamson et al. «High-Pressure, High-Temperature Well Construction» (1998), 45

[14] Eirik Kårstad, «Time-Dependent Temperature Behavior in Rock and Borehole» (Ph.D avhandling nr. 43, Høgskolen I Stavanger, 1999)

[15] Eirik Kårstad, «Time-Dependent Temperature Behavior in Rock and Borehole» (Ph.D avhandling nr. 43, Høgskolen I Stavanger, 1999)

[16] Zoltán Szarka-Elemér Bobok, «Determination of the temperature distribution in the circulating drilling fluid» Geosciences and Engineering, Vol 1, No. 1 (2012), 37

[17] Schlumberger Oilfield Glossary, «high-pressure, high-temperature» Retrieved 03.05.16 from
http://glossary.oilfield.slb.com/Terms/h/high-pressure_high-temperature.aspx

[18] Eirik Kårstad, «Time-Dependent Temperature Behavior in Rock and Borehole» (Ph.D avhandling nr. 43, Høgskolen I Stavanger, 1999)

[19] Eirik Kårstad, «Time-Dependent Temperature Behavior in Rock and Borehole» (Ph.D avhandling nr. 43, Høgskolen I Stavanger, 1999)

[20] Eirik Kårstad, «Time-Dependent Temperature Behavior in Rock and Borehole» (Ph.D avhandling nr. 43, Høgskolen I Stavanger, 1999)

[21] Eirik Kårstad, «Time-Dependent Temperature Behavior in Rock and Borehole» (Ph.D avhandling nr. 43, Høgskolen I Stavanger, 1999)

[22] Essat Can Apak, «A study on heat transfer inside the wellbore during drilling operations» (Master thesis, E.C. Apak, 2006).

[23] Essat Can Apak, «A study on heat transfer inside the wellbore during drilling operations» (Master thesis, E.C. Apak, 2006).

[24] Eirik Kårstad and Bernt S. Aadnøy, «Analysis of Temperature Measurements during Drilling,» SPE paper 38603 (1997).

[25] Essat Can Apak, «A study on heat transfer inside the wellbore during drilling operations» (Master thesis, E.C. Apak, 2006).

[26] Essat Can Apak, «A study on heat transfer inside the wellbore during drilling operations» (Master thesis, E.C. Apak, 2006).

[27] Dan Sui, «Improvement of Wired Drill Pipe Data Quality via Data Validation and reconciliation», International Journal of Automation and Computing

[28] Dan Sui, «Improvement of Wired Drill Pipe Data Quality via Data Validation and reconciliation», International Journal of Automation and Computing

[29] Schlumberger Oilfield Glossary, «Conductivity», Retrieved 18.04.16 from
http://glossary.oilfield.slb.com/Terms/c/conductivity.aspx
[30] G.L. Shires, «Rayleigh number» Retrieved 20.03.16 from:
http://www.thermopedia.com/content/1076/
[31] Edgar Rolando Santoyo-Gutiérrez, «Transient Numerical Simulation of Heat Transfer Processes
During Drilling of Geothermal Wells» (Ph.D, University of Salford, Salford, UK, 1997)
[32] Eirik Kårstad, «Time-Dependent Temperature Behavior in Rock and Borehole» (Ph.D avhandling nr.
43, Høgskolen I Stavanger, 1999)
[33] Bernt S. Aadnøy, *Modern Well Design* (University of Stavanger, Stavanger, Norway: CRC Press, 2010),
244
[34] Bernt S. Aadnøy, *Modern Well Design* (University of Stavanger, Stavanger, Norway: CRC Press, 2010)
[35] Mesfin Belayneh, «Advanced Drilling Engineering and Technology» (2015)
[36] Schlumberger, «Differential Sticking» Retrieved 03.04.16 from
http://www.glossary.oilfield.slb.com/Terms/d/differential_sticking.aspx
[37] Schlumberger, «Differential Sticking» Retrieved 03.04.16 from
http://www.glossary.oilfield.slb.com/Terms/d/differential_sticking.aspx
[38] Mesfin Belayneh, «Advanced Drilling Engineering and Technology» (2015)
[39] Mesfin Belayneh, «Advanced Drilling Engineering and Technology» (2015)
[40] Mesfin Belayneh, «Advanced Drilling Engineering and Technology» (2015)
[41] Eirik Kårstad, «Time-Dependent Temperature Behavior in Rock and Borehole» (Ph.D avhandling nr.
43, Høgskolen I Stavanger, 1999)
[42] Glenn-Ole Kaasa, et al. «Simplified Hydraulics Model Used for Intelligent Estimation of Downhole
Pressure for a Managed-pressure-Drilling Control System» (2012)
[43] Glenn-Ole Kaasa, et al. «Simplified Hydraulics Model Used for Intelligent Estimation of Downhole
Pressure for a Managed-pressure-Drilling Control System» (2012)
[44] Glenn-Ole Kaasa, et al. «Simplified Hydraulics Model Used for Intelligent Estimation of Downhole
Pressure for a Managed-pressure-Drilling Control System» (2012)
[45] Glenn-Ole Kaasa, et al. «Simplified Hydraulics Model Used for Intelligent Estimation of Downhole
Pressure for a Managed-pressure-Drilling Control System» (2012)
[46] Glenn-Ole Kaasa, et al. «Simplified Hydraulics Model Used for Intelligent Estimation of Downhole
Pressure for a Managed-pressure-Drilling Control System» (2012)
[47] Glenn Elert, «Viscosity», *The Physics Hyper Textbook, http://physics.info/viscosity/*
[48] Glenn Elert, «Viscosity», *The Physics Hyper Textbook, http://physics.info/viscosity/*
[49] Glenn Elert, «Viscosity», *The Physics Hyper Textbook, http://physics.info/viscosity/*
[50] Schlumberger Oilfield Glossary, «Viscosity» Retrieved 13.04.16 from
http://glossary.oilfield.slb.com/Terms/v/viscosity.aspx
[51] Glenn-Ole Kaasa, et al. «Simplified Hydraulics Model Used for Intelligent Estimation of Downhole
Pressure for a Managed-pressure-Drilling Control System» (2012)
[52] Glenn-Ole Kaasa, et al. «Simplified Hydraulics Model Used for Intelligent Estimation of Downhole
Pressure for a Managed-pressure-Drilling Control System» (2012)
[53] Aleksander Kristensen, «Flow properties of water-based drilling fluids» (Master thesis, NTNU, 2013)
[54] Mesfin Belayneh, «Rheology, Hydraulics and cutting transport» Advanced Drilling Engineering and
Technology (2015)
[55] Carl Montgomery, «Fracturing Fluids», http://www.intechopen.com/books/effective-and-
sustainable-hydraulic-fracturing/fracturing-fluids#article-front
[56] Mesfin Belayneh, «Rheology, Hydraulics and cutting transport» Advanced Drilling Engineering and
Technology (2015)
[57] Mesfin Belayneh, «Rheology, Hydraulics and cutting transport» Advanced Drilling Engineering and
Technology (2015)
[58] Mesfin Belayneh, «Rheology, Hydraulics and cutting transport» Advanced Drilling Engineering and
Technology (2015)
[59] The concrete portal, «Rheology,» *The concrete portal*,
http://www.theconcreteportal.com/rheology.html

[60] Mesfin Belayneh, «Rheology, Hydraulics and cutting transport» Advanced Drilling Engineering and Technology (2015)

[61] Mesfin Belayneh, «Rheology, Hydraulics and cutting transport» Advanced Drilling Engineering and Technology (2015)

[62] API «Rheology and Hydraulics of Oil-well Drilling Fluids» Seventh edition, 15

[63] API «Rheology and Hydraulics of Oil-well Drilling Fluids» Seventh edition, 15

[64] Schlumberger Oilfield Glossary, «Shear Stress» Retrieved 12.04.16 from http://glossary.oilfield.slb.com/Terms/s/shear_stress.aspx

[65] Schlumberger Oilfield Glossary, «Shear Rate» Retrieved 13.04.16 from http://glossary.oilfield.slb.com/Terms/s/shear_rate.aspx

[66] Anton Paar, «The Modular Compact Rheometer Series» Retrieved 03.05.16 from http://www.anton-paar.com/?eID=documentsDownload&document=18378&L=6

[67] E. Kårstad and B.S. Aadnøy, «Density Behavior of Drilling Fluids During High Pressure High Temperature Drilling Operations» *SPE Paper* 47806 (1998), 4

[68] E. Kårstad and B.S. Aadnøy, «Density Behavior of Drilling Fluids During High Pressure High Temperature Drilling Operations» *SPE Paper* 47806 (1998), 4

[69] Rune W. Time, «Two-Phase Flow in Pipelines» Course compendium (2009), 30

[70] Schlumberger Oilfield Glossary, «Laminar flow» Retrieved 13.04.16 from http://glossary.oilfield.slb.com/Terms/l/laminar_flow.aspx

[71] The Engineering Toolbox, «Pipe stress analysis», *The Engineering Toolbox, http://www.engineeringtoolbox.com/laminar-transitional-turbulent-flow-d_577.html*

[72] The Engineering Toolbox, «Pipe stress analysis», *The Engineering Toolbox, http://www.engineeringtoolbox.com/laminar-transitional-turbulent-flow-d_577.html*

[73] Rune W. Time, «Two-Phase Flow in Pipelines» Course compendium (2009), 30

[74] Rune W. Time, «Two-Phase Flow in Pipelines» Course compendium (2009)

[75] Mesfin Belayneh, «Rheology, Hydraulics and cutting transport» Advanced Drilling Engineering and Technology (2015)

[76] Rune W. Time, «Two-Phase Flow in Pipelines» Course compendium (2009)

[77] Rune W. Time, «Two-Phase Flow in Pipelines» Course compendium (2009)

[78] Rune W. Time, «Two-Phase Flow in Pipelines» Course compendium (2009), 32

[79] Bernt S. Aadnøy, *Modern Well Design* (Stavanger: CRC Press, 2010), 29

[80] Mesfin Belayneh, «Advanced Drilling Engineering and Technology», (2015)

[81] Mesfin Belayneh, «Advanced Drilling Engineering and Technology», (2015)

[82] Bernt S. Aadnøy, *Modern Well Design* (University of Stavanger, Stavanger, Norway: CRC Press, 2010), 244

[83] Terje Tveitdal, «Torque & drag analyses of North Sea Wells using new 3D model» (master thesis, University of Stavanger, 2011)

[84] Bernt S. Aadnøy, *Modern Well Design* (Stavanger: CRC Press, 2010), 243

[85] Bernt S. Aadnøy, *Modern Well Design* (Stavanger: CRC Press, 2010), 243

[86] Bernt S. Aadnøy, *Modern Well Design* (University of Stavanger, Stavanger, Norway: CRC Press, 2010), 244

[87] Bernt S. Aadnøy, *Modern Well Design* (University of Stavanger, Stavanger, Norway: CRC Press, 2010), 244

[88] Bernt S. Aadnøy, *Modern Well Design* (University of Stavanger, Stavanger, Norway: CRC Press, 2010), 244

[89] Bernt S. Aadnøy, *Modern Well Design* (University of Stavanger, Stavanger, Norway: CRC Press, 2010), 244

[90] Terje Tveitdal, «Torque & drag analyses of North Sea Wells using new 3D model» (Master Thesis, University of Stavanger, 2011)

[91] Bernt S. Aadnøy, *Modern Well Design* (University of Stavanger, Stavanger, Norway: CRC Press, 2010), 244

[92] Mesfin Belayneh, «Advanced Drilling Engineering and Technology», (2015)

[93] Terje Tveitdal, «Torque & drag analyses of North Sea Wells using new 3D model» (Master Thesis,

University of Stavanger, 2011)

[94] Bernt S. Aadnøy, *Modern Well Design* (University of Stavanger, Stavanger, Norway: CRC Press, 2010), 244

[95] Terje Tveitdal, «Torque & drag analyses of North Sea Wells using new 3D model» (Master Thesis, University of Stavanger, 2011)

[96] Terje Tveitdal, «Torque & drag analyses of North Sea Wells using new 3D model» (Master Thesis, University of Stavanger, 2011)

[97] Terje Tveitdal, «Torque & drag analyses of North Sea Wells using new 3D model» (Master Thesis, University of Stavanger, 2011)

[98] Erik Leif Eriksen, «The Well Bore Trajectory – Position Calculations» Høgskolesenteret i Rogaland, 1993

[99] Erik Leif Eriksen, «The Well Bore Trajectory – Position Calculations» Høgskolesenteret i Rogaland, 1993

[100] Mohammad Fazaelizadeh, «Real Time Torque and Drag Analysis during Directional Drilling» (PhD. University of Calgary, 2013)

[101] Erik Leif Eriksen, «The Well Bore Trajectory – Position Calculations» Høgskolesenteret i Rogaland, 1993

[102] Bernt S. Aadnøy, *Modern Well Design* (University of Stavanger, Stavanger, Norway: CRC Press, 2010), 256

[103] Mohammad Fazaelizadeh, «Real Time Torque and Drag Analysis during Directional Drilling» (PhD. University of Calgary, 2013)

Appendix A – Temperature sensitivity analysis

Base case plot:	Changed parameter:	Updated plot:
	Circulation rate decreased from 0,01325 m³/s to 0,006625 m³/s	
	Circulation rate increased from 0,01325 m³/s to 0,01988 m³/s	
	Circulation time increased from 44 hours to 66 hours	
	Circulation time decreased from 44 hours to 22 hours	
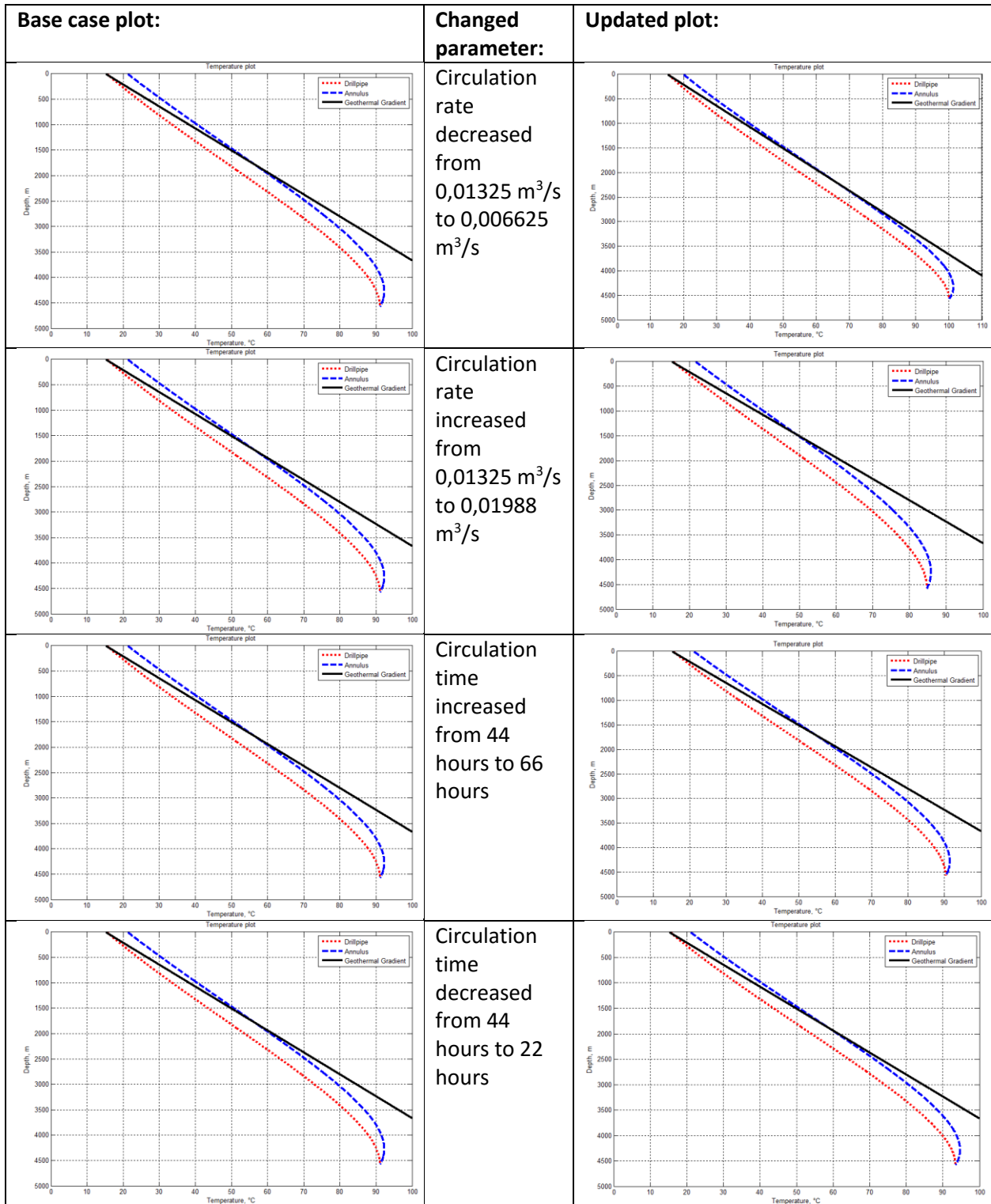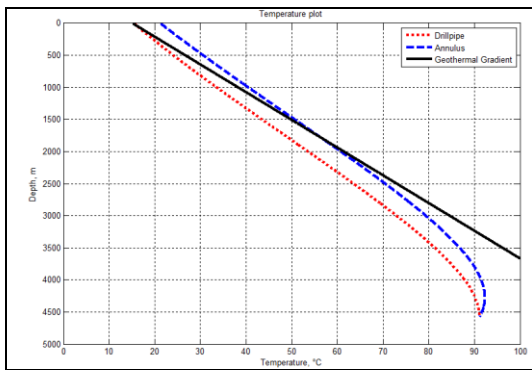
	Drilling fluid density decreased from 1200 kg/m^3 to 600 kg/m^3
	Drilling fluid density increased from 1200 kg/m^3 to 1800 kg/m^3
	Viscosity of fluid increased from 0.04547 Pa*S to 0.068207 Pa*S
	Viscosity of fluid decreased from 0.04547 Pa*S to 0.0227358 Pa*S
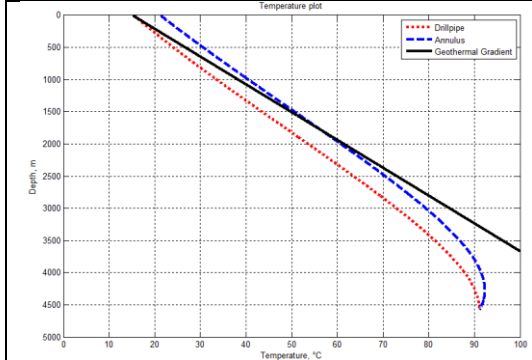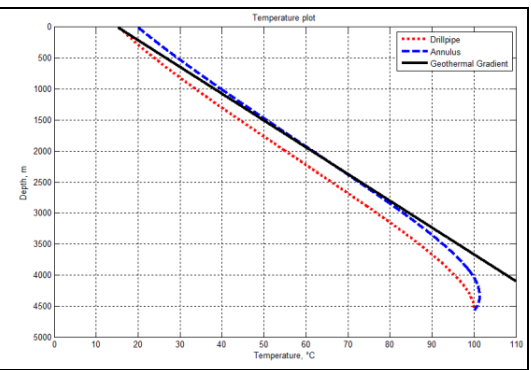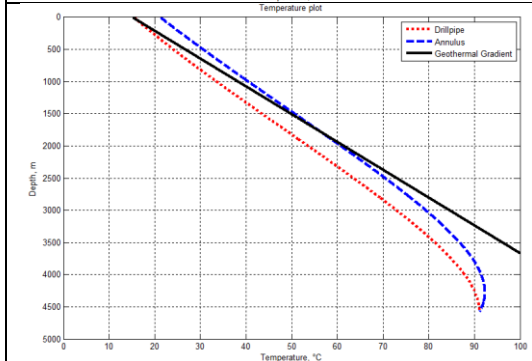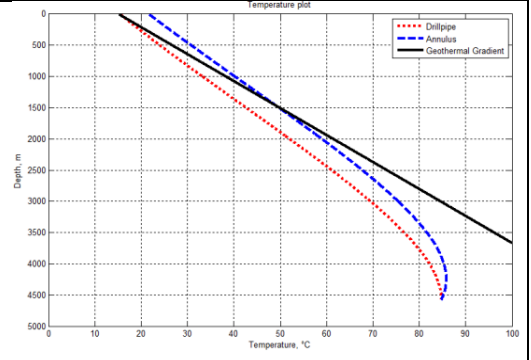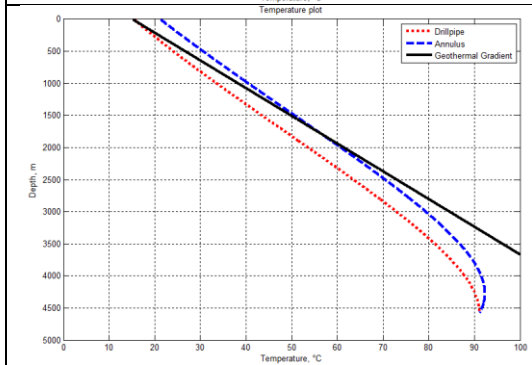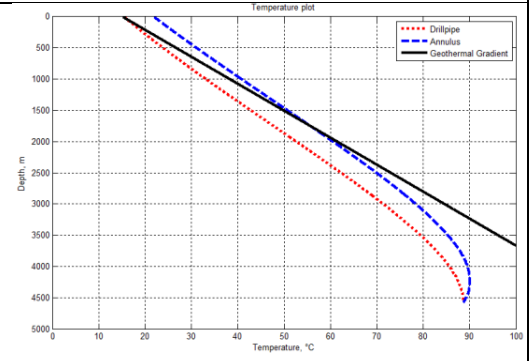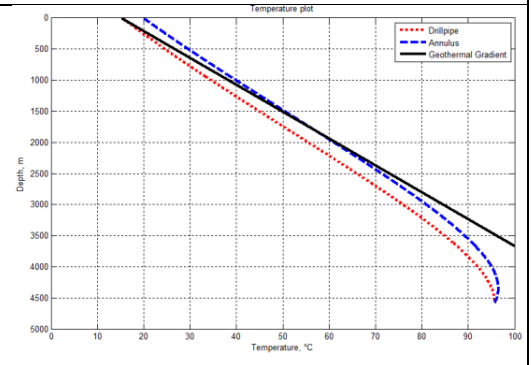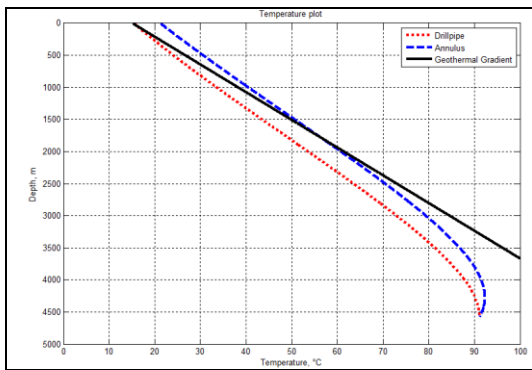
	Geothermal gradient increased from 0,0231 °C/m to 0,0347 °C/m	
	Geothermal gradient decreased from 0,0231 °C/m to 0,0116 °C/m	
	Inlet temperature increased from 15,5 °C to 23,25 °C	
	Inlet temperature decreased from 15,5 °C to 7,75 °C	
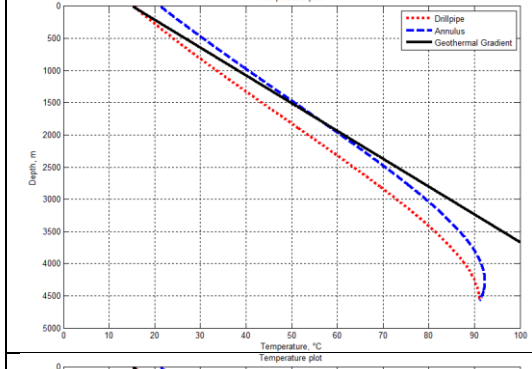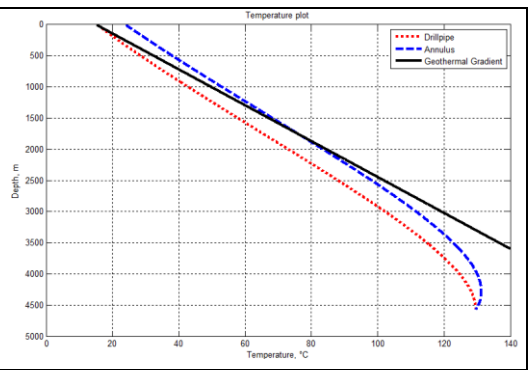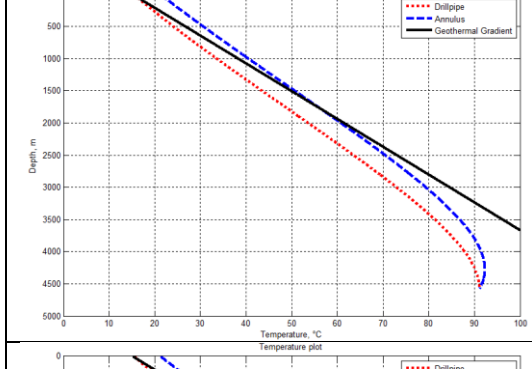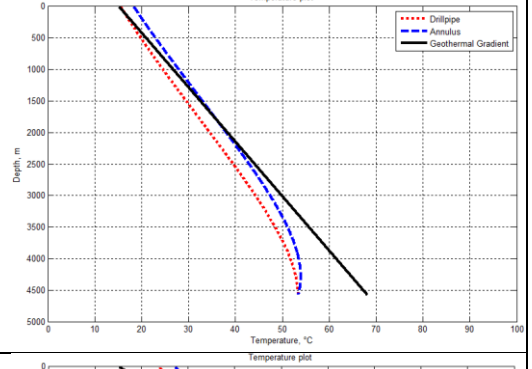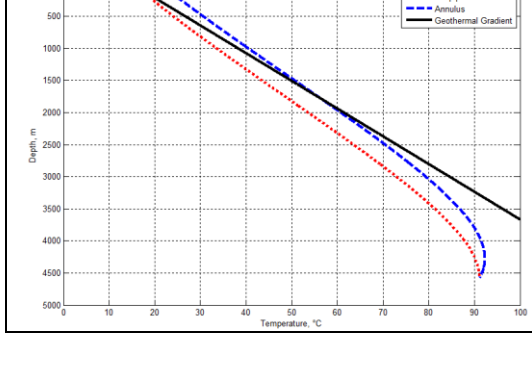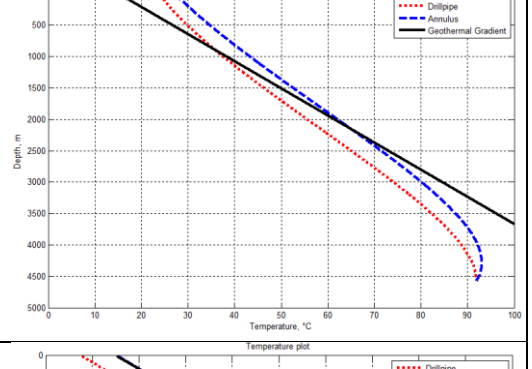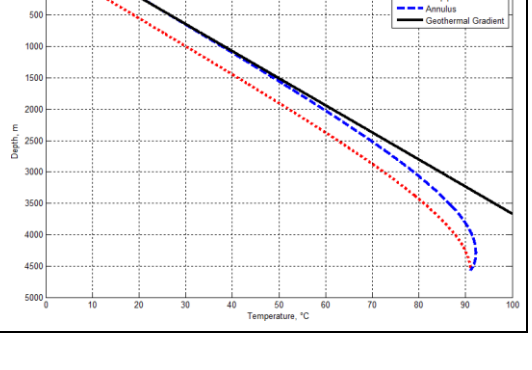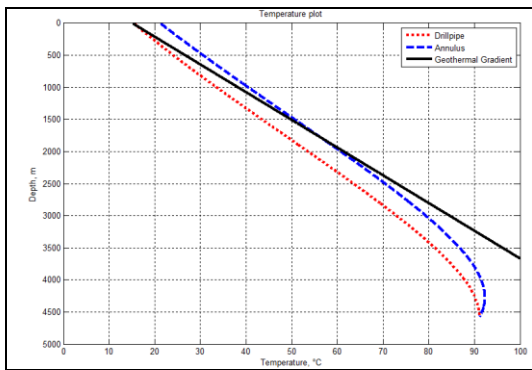
	Conductivity of tubing increased from 34,6 (W/m*K) to 52 (W/m*K)		
	Conductivity of tubing decreased from 34,6 (W/m*K) to 17,3 (W/m*K)		
	Heat capacity of fluid (Drilling fluid specific heat) increased from 1674,7- to 2512,1 J/(kgC		
	Heat capacity of fluid (Drilling fluid specific heat) decreased from 1674,7- to 837,4 J/(kgC		
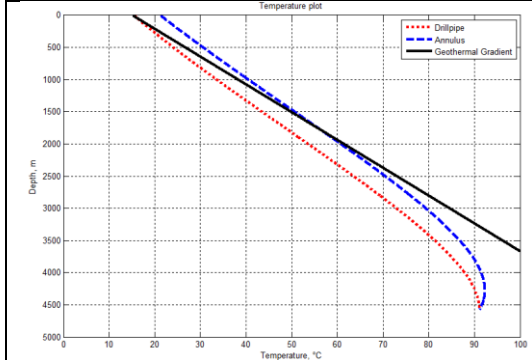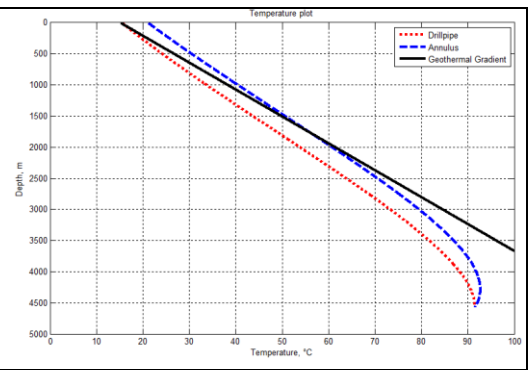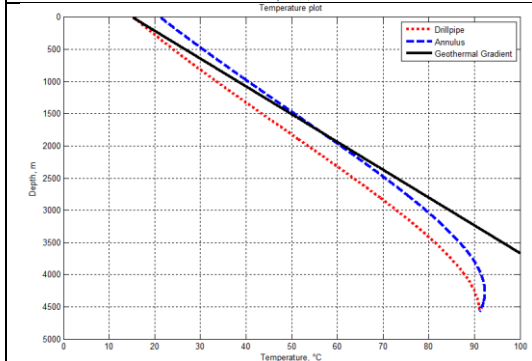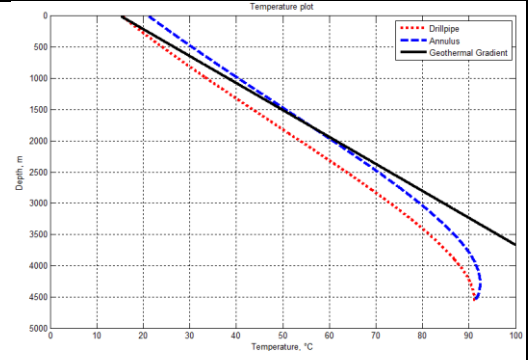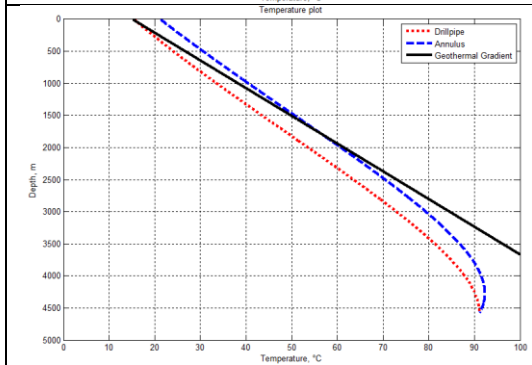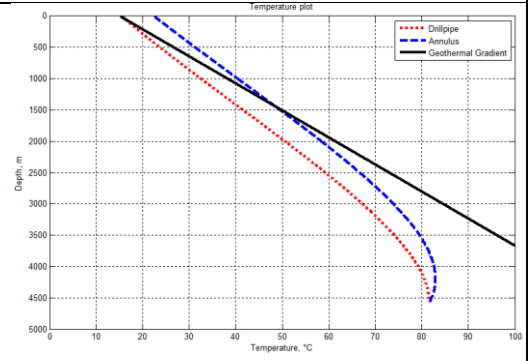
88
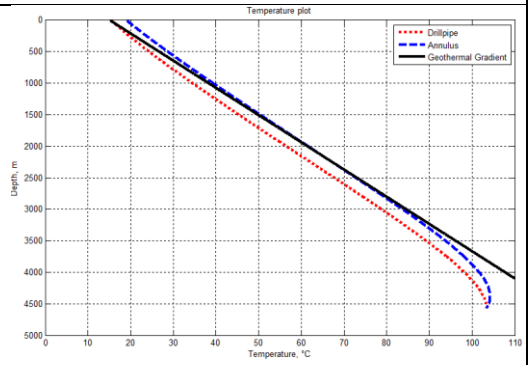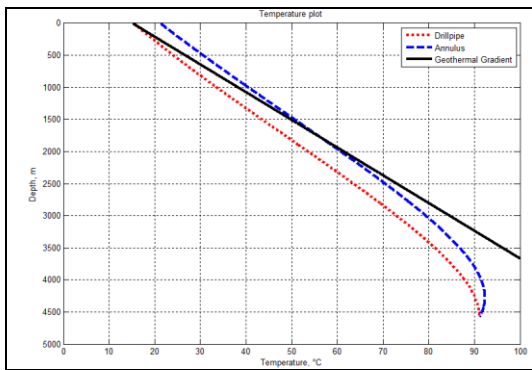
	Earth density increased from 2643 kg/m^3 to 3964,6 kg/m^3	
	Earth density decreased from 2643 kg/m^3 to 1321,5 kg/m^3	
	Tubing inner diameter decreased from 0,16193 m to 0,08096 m	
	Tubing inner diameter increased from 0,16193 m to 0,24289 m	
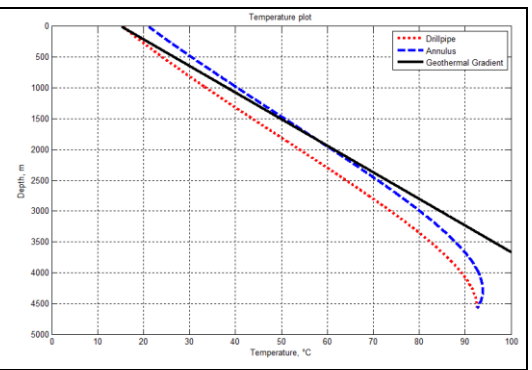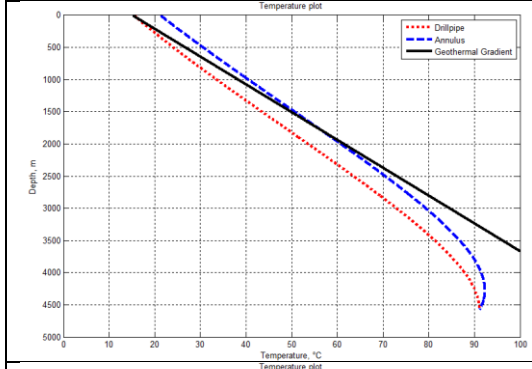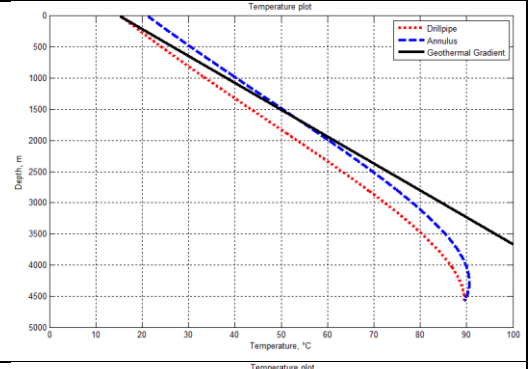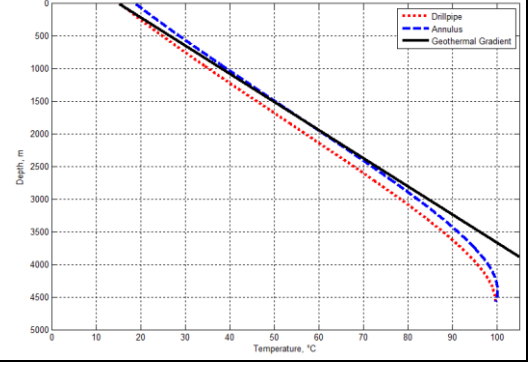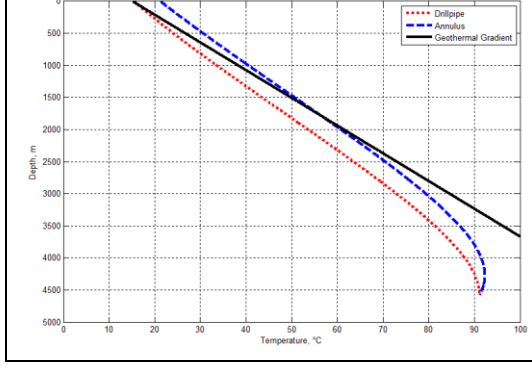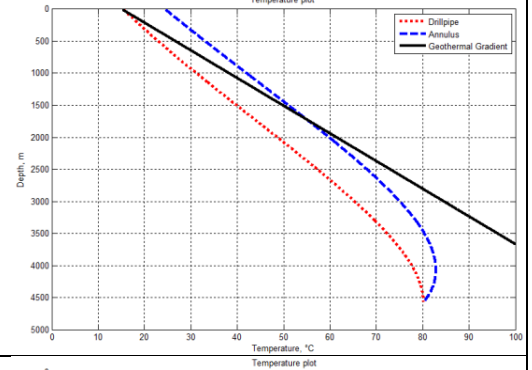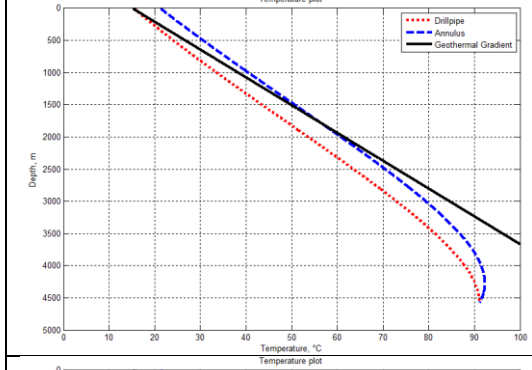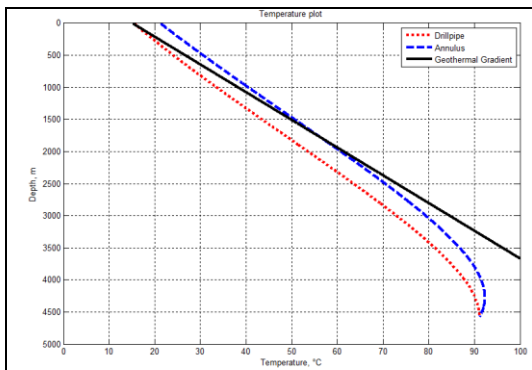
	Tubing outer diameter decreased from 0,168275 m to 0,08414m	
	Tubing outer diameter increased from 0,168275 m to 0,2524m	
	Wellbore diameter decreased from 0,219075 m to 0,10954 m	
	Wellbore diameter increased from 0,219075 m to 0,32861m	
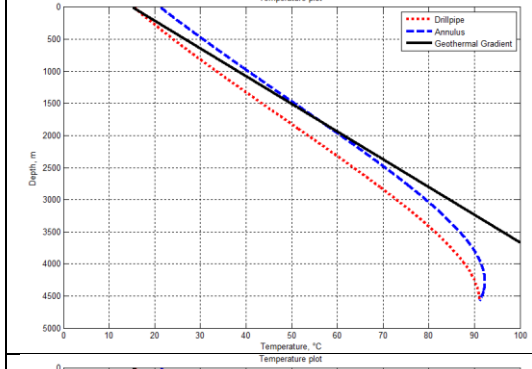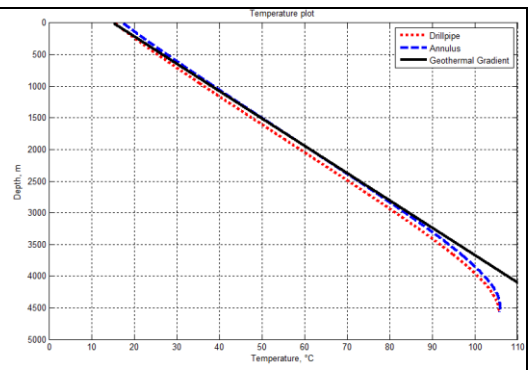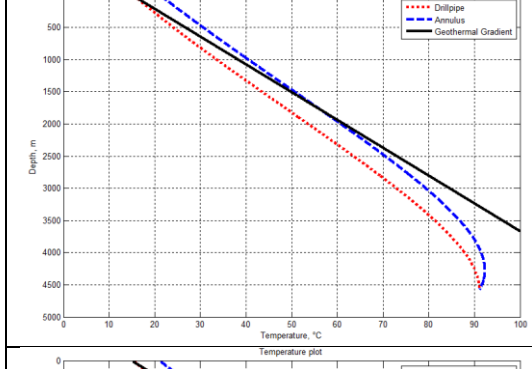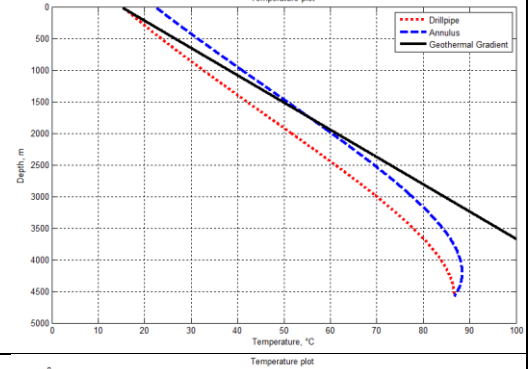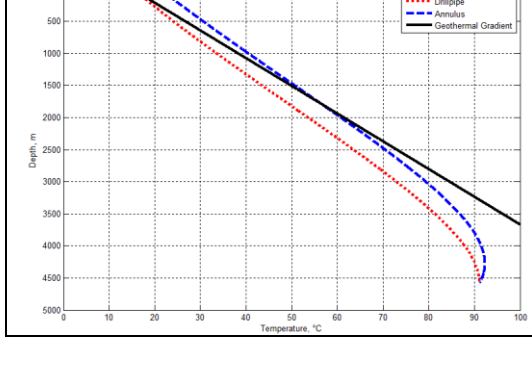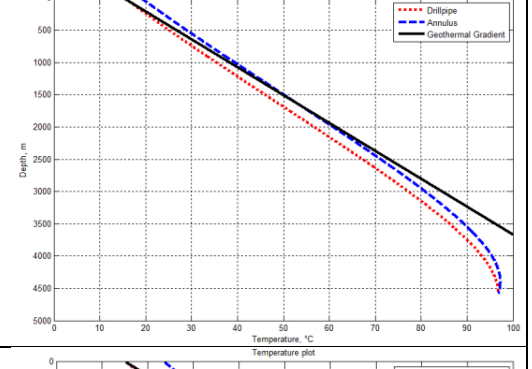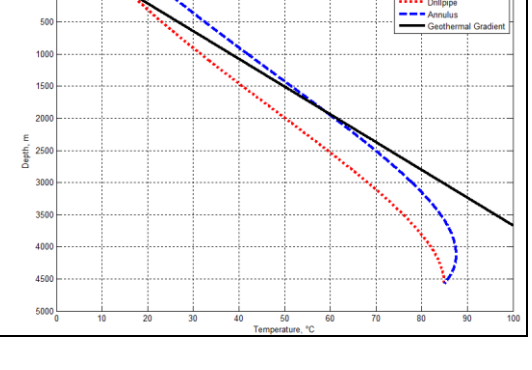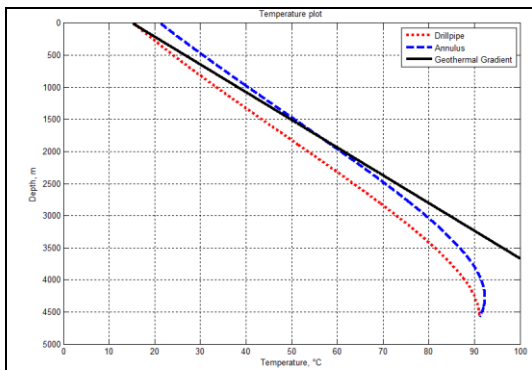
	Temperature surface decreased from 15,3 °C to 7,65 °C	
	Temperature surface increased from 15,3 °C to 22,95 °C	
	Conductivity of earth decreased from 2,25 [W/m*K] to 1,125 [W/m*K]	
	Conductivity of earth increased from 2,25 [W/m*K] to 3,375 [W/m*K]	
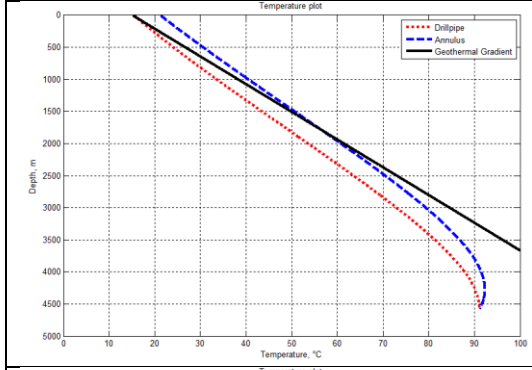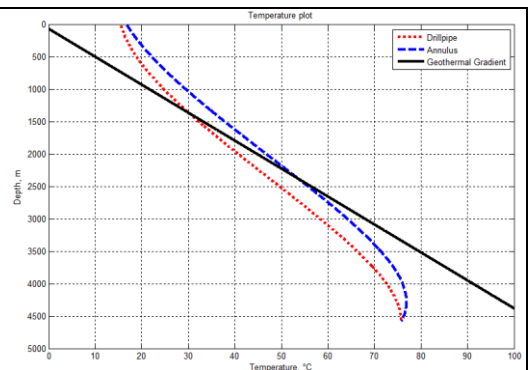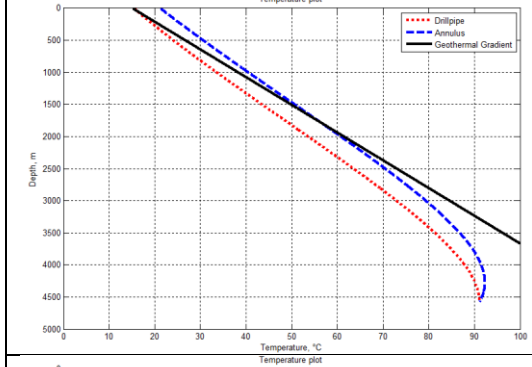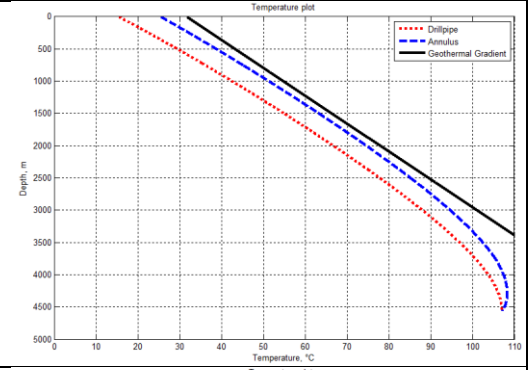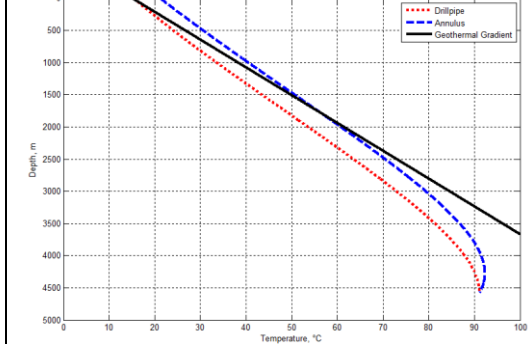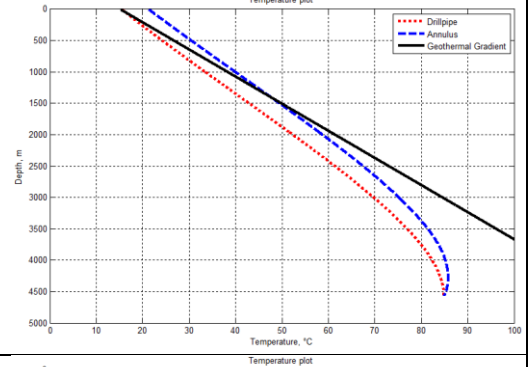
91
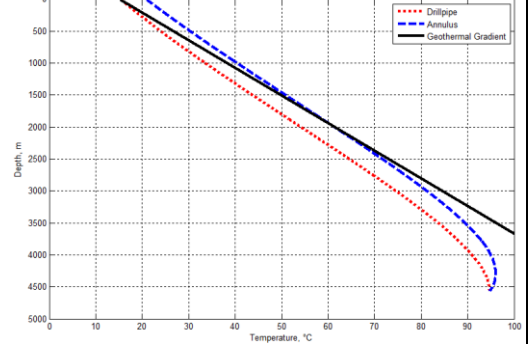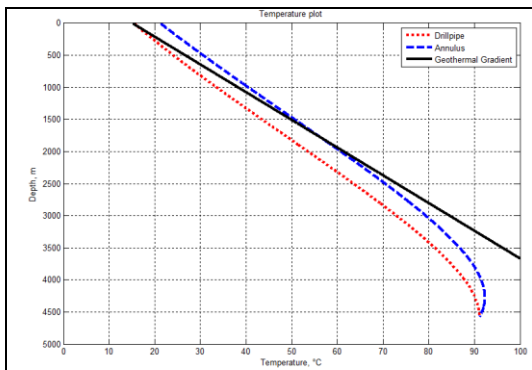
	Heat capacity of earth decreased from 837,4 [J/kgC] to 418,7 [J/kgC]
	Heat capacity of earth increased from 837,4 [J/kgC] to 1256,1 [J/kgC]
	Thermal conductivity drilling fluid decreased from 1,73 to 0,865 [W/m*K]
	Thermal conductivity drilling fluid increased from 1,73 to 2,595 [W/m*K]
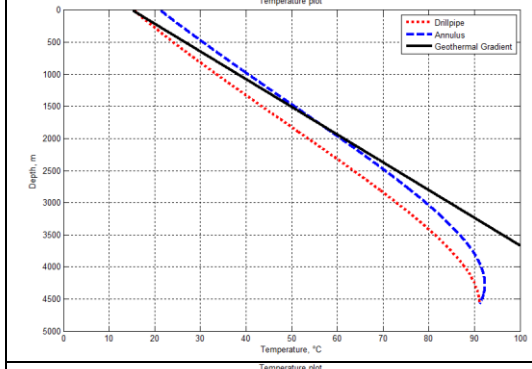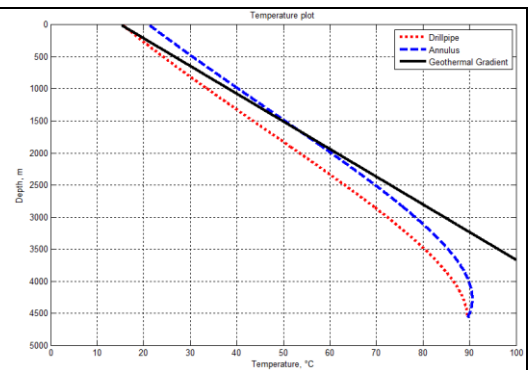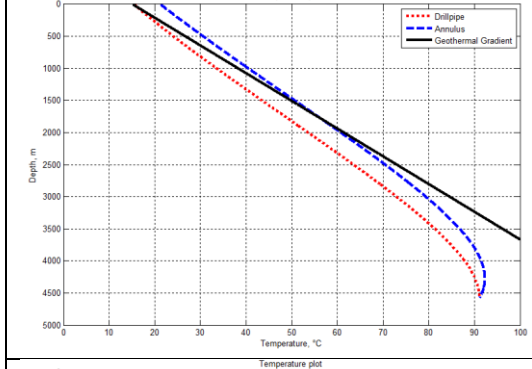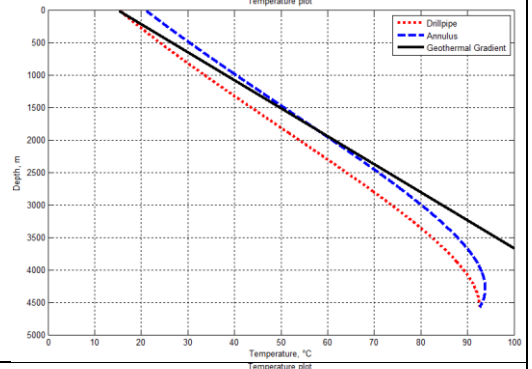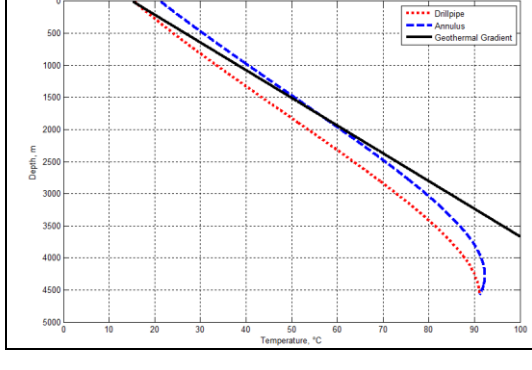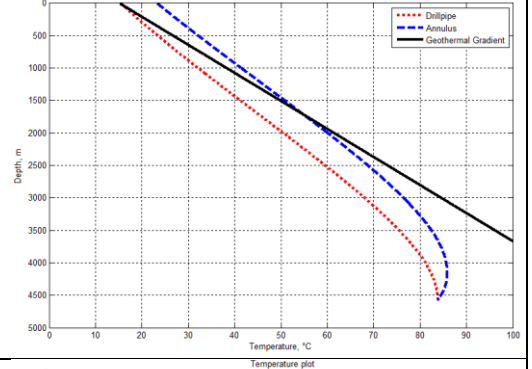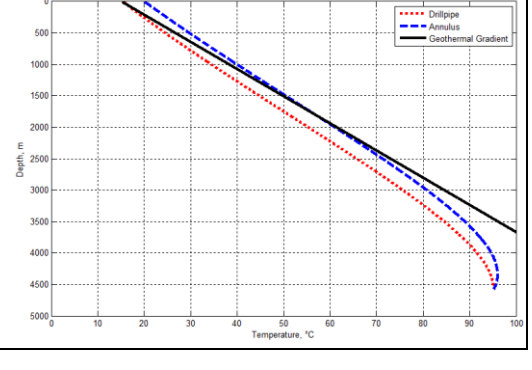
Appendix B – Viscosity experimental results – Viscosity plots

Sample 1

Sample 2

Sample 3

Sample 4

Sample 5

Sample 6

Sample 7

Sample 8

95
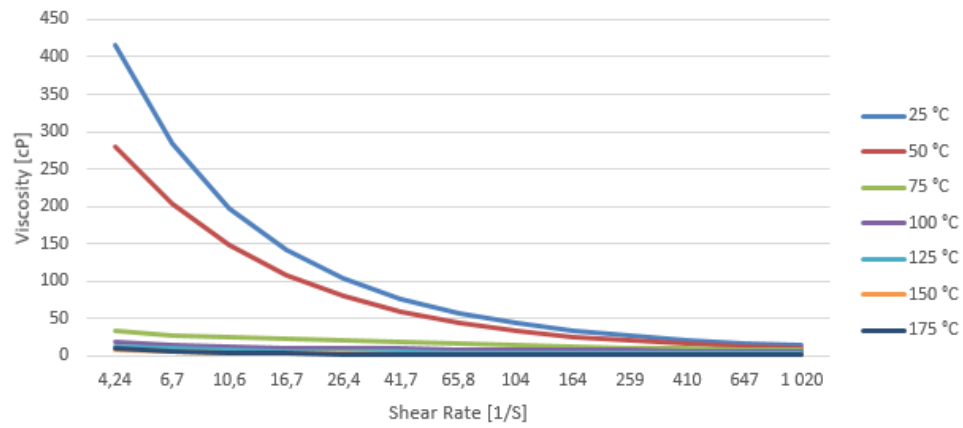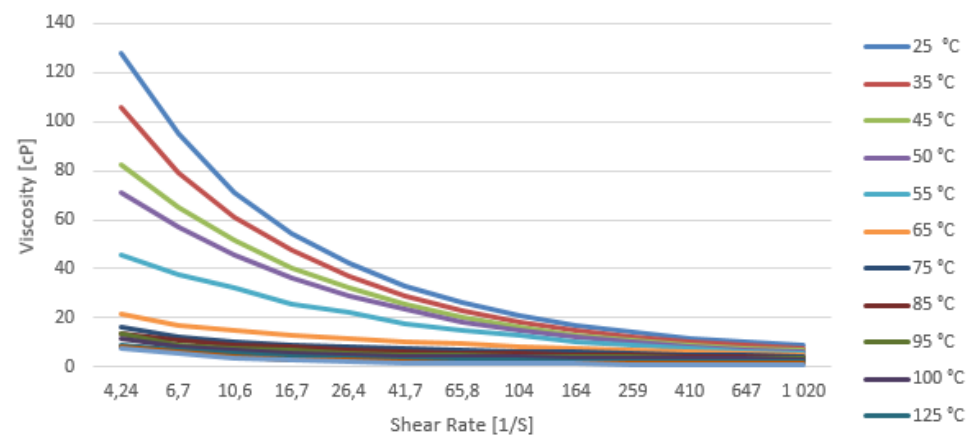
Sample 9

Sample 10

Appendix C – Viscosity experimental results – Shear Stress plots

Sample 1
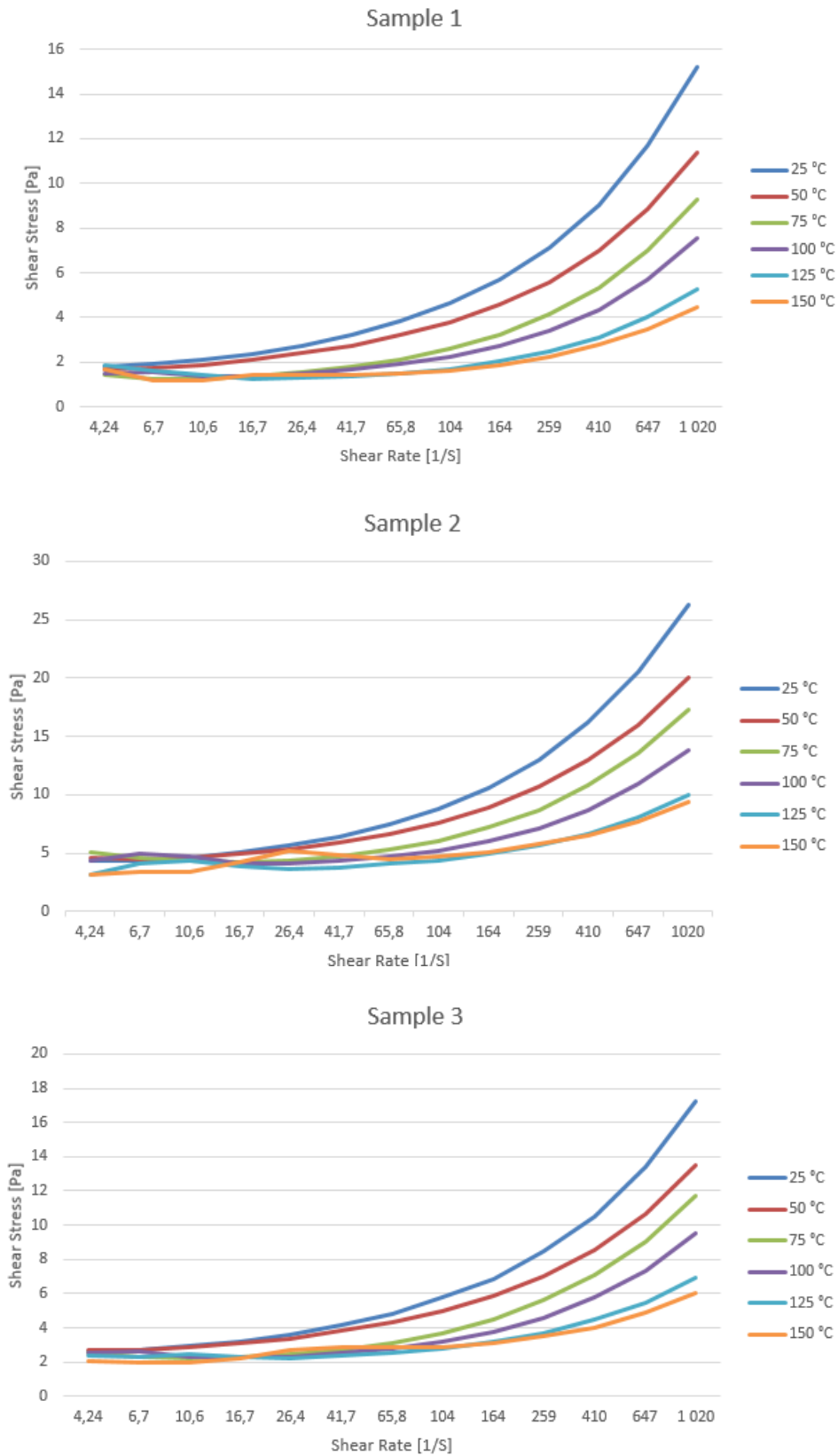
Sample 2
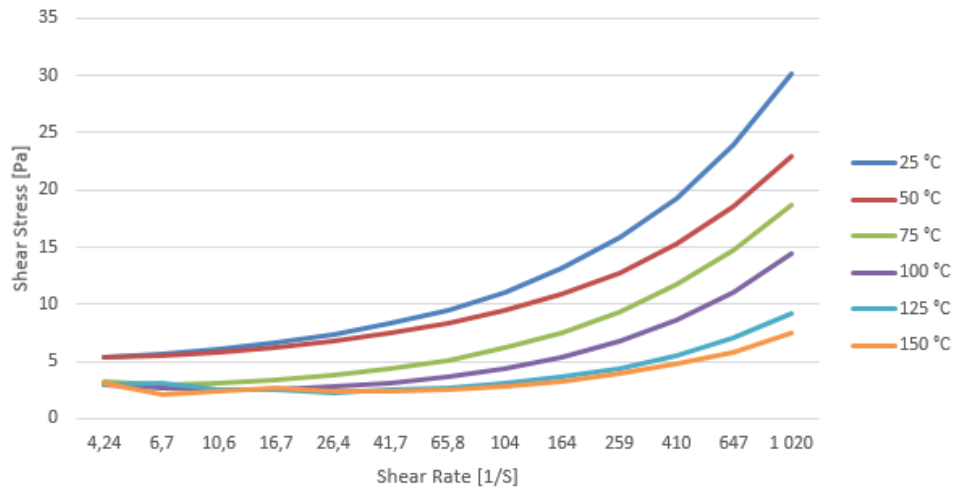
Sample 3
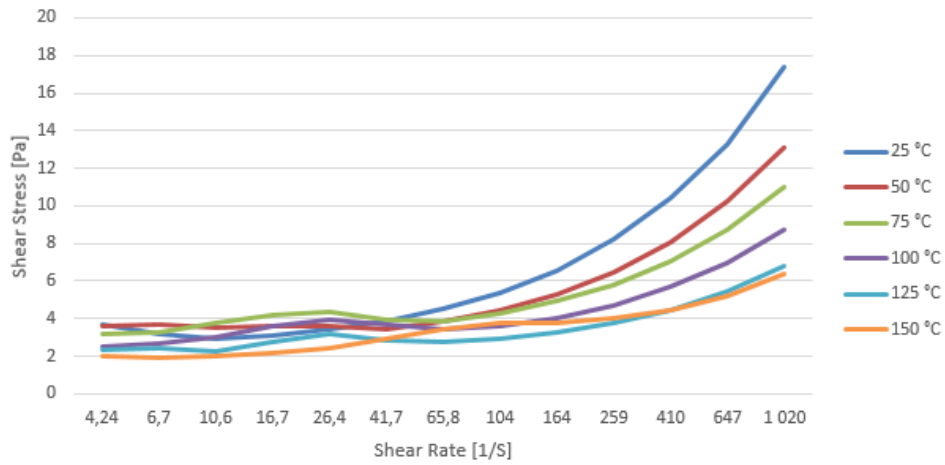
Sample 4
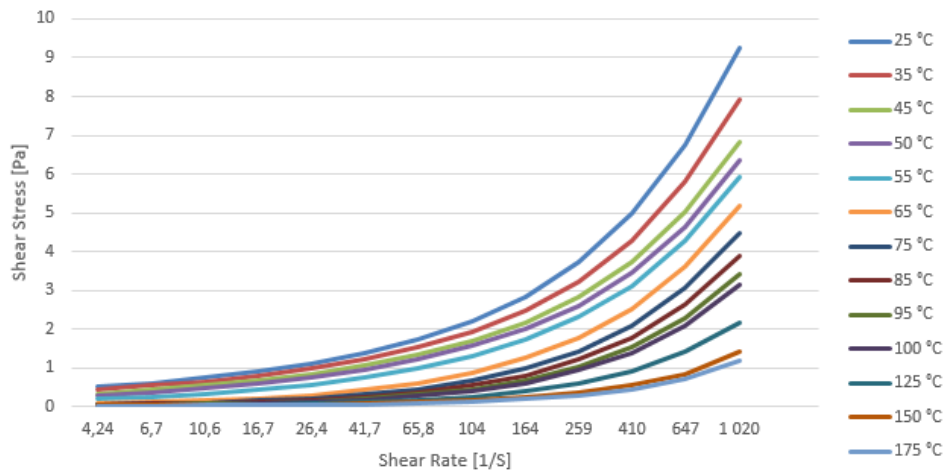
Sample 5

Sample 6

Sample 7

Sample 8

Sample 9

99
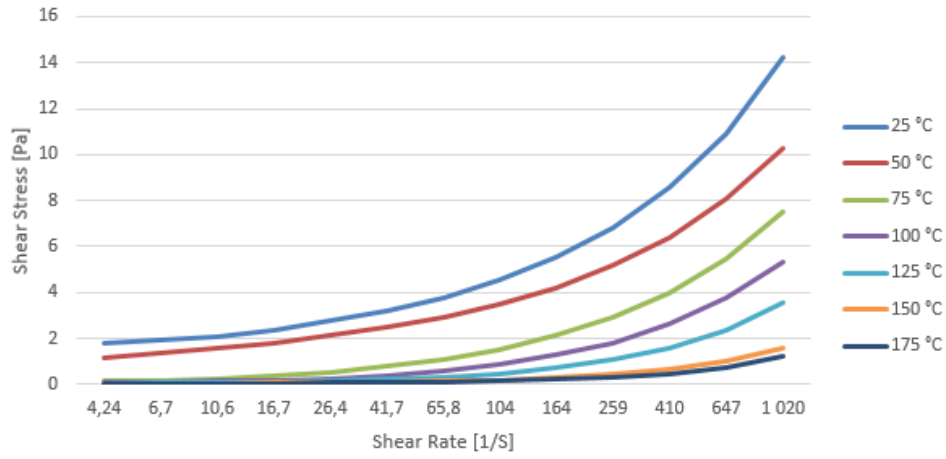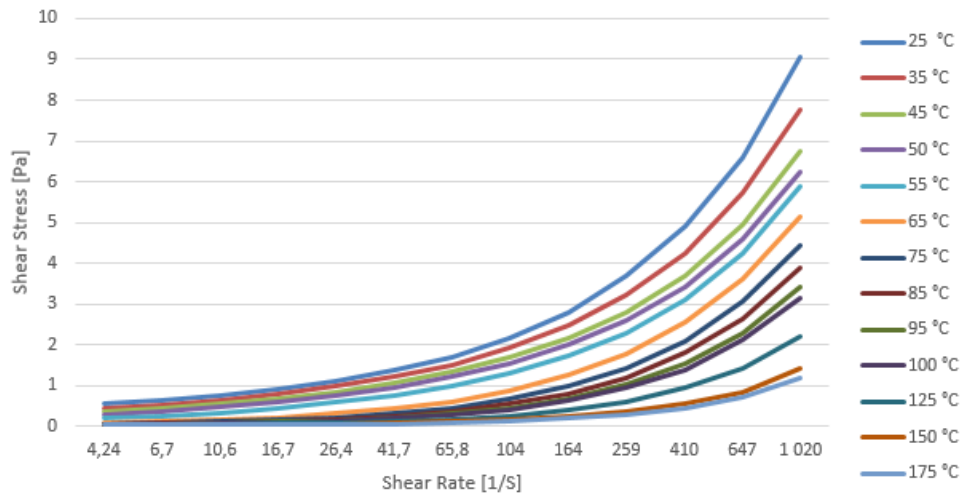
Sample 10
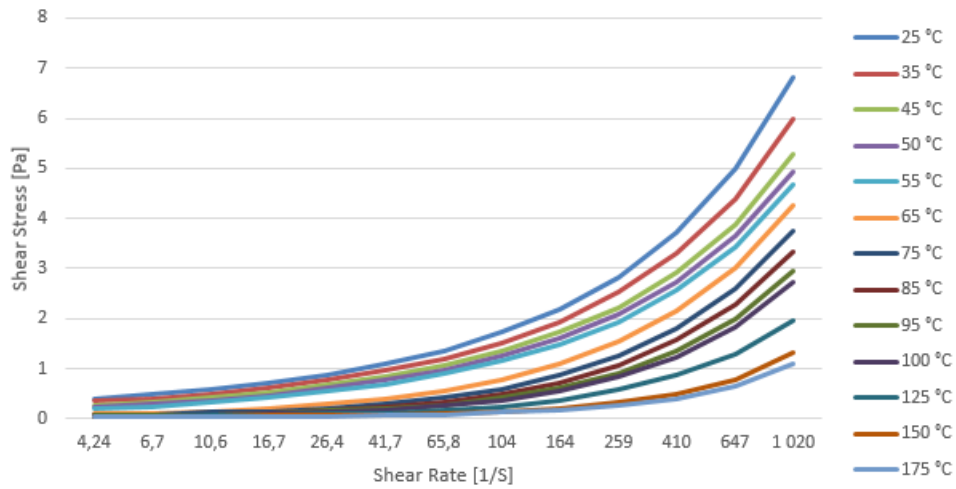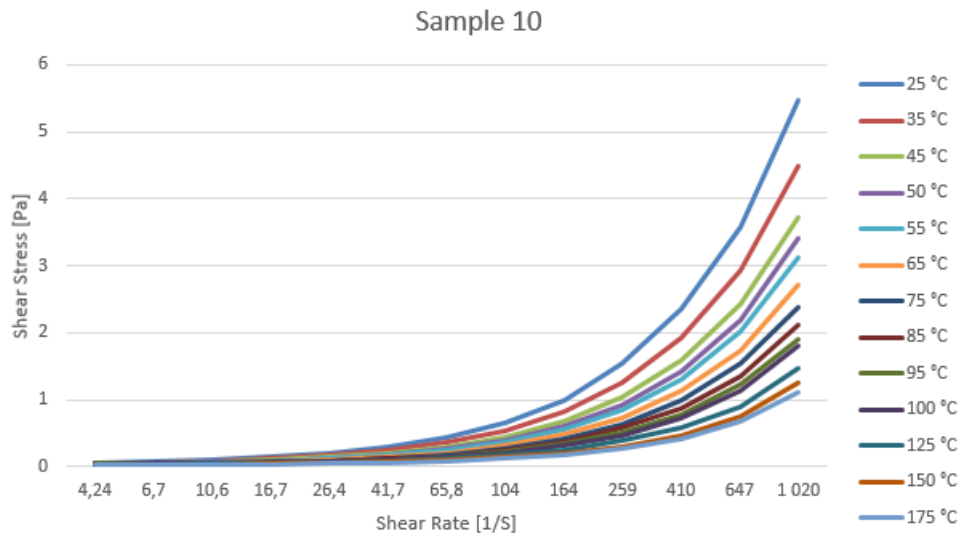
Appendix D – MATLAB codes

These MATLAB codes given in Appendix D, is developed is cooperation by Dan Sui and Martin Tveiterå.

APPENDIX D.1 – TRUE DENSITY AND LINEARIZED DENSITY

```
P_o=1*10^5;              %Initial Pressure;
EI=90;
rou0=1.083*10^3;         %Initial density
 %% Configuration dataII
T_o=20;                  %Initial Temperature
rou_o=rou0;              %Mud density;

Data=[
0     4       20      65      93      154     176
1     1.0925236 1.0831566 1.0585302 1.0492570 1.0180279 0.97110407
4.14  1.0931762 1.0851024 1.0593155 1.0493216 1.0185258 0.98253853
6.89  1.0937453 1.0857900 1.0600174 1.0493027 1.0189743 0.99260761
17.24 1.0941260 1.0867777 1.0614060 1.0501731 1.0201111 1.00638896
34.47 1.0947758 1.0872758 1.0623093 1.0507927 1.0206775 1.00888618
51.71 1.0955276 1.0876101 1.0625414 1.0515112 1.0216129 1.00987491
68.95 1.0959948 1.0879904 1.0628416 1.0519255 1.0222630 1.01084460
103.42 1.0967621 1.0892139 1.0636740 1.0527237 1.0231791 1.01202677
137.9 1.0970778 1.0897271 1.0644723 1.0533395 1.0238443 1.01265758
172.37 1.0976410 1.0901074 1.0654254 1.0537347 1.0249428 1.01382472
344.74 1.1009676 1.0933571 1.0686188 1.0571899 1.0290515 1.01828313
517.11 1.0910518 1.0967704 1.0723135 1.0608352 1.0324336 1.02190098
689.48 1.0933559 1.1000354 1.0755409 1.0641424 1.0364285 1.02643206
1034.21 1.0981804 1.1056306 1.0819649 1.0701723 1.0436734 1.03364231
1378.95 1.1033306 1.1116401 1.0889427 1.0766085 1.0504178 1.04137399]
%% Linear Regression
Data=[
```

```matlab
0     4      20      65      93      154      176
1     1.0925236 1.0831566 1.0585302 1.0492570 1.0180279 0.97110407
4.14  1.0931762 1.0851024 1.0593155 1.0493216 1.0185258 0.98253853
6.89  1.0937453 1.0857900 1.0600174 1.0493027 1.0189743 0.99260761
17.24 1.0941260 1.0867777 1.0614060 1.0501731 1.0201111 1.00638896
34.47 1.0947758 1.0872758 1.0623093 1.0507927 1.0206775 1.00888618
51.71 1.0955276 1.0876101 1.0625414 1.0515112 1.0216129 1.00987491
68.95 1.0959948 1.0879904 1.0628416 1.0519255 1.0222630 1.01084460
103.42 1.0967621 1.0892139 1.0636740 1.0527237 1.0231791 1.01202677
137.9  1.0970778 1.0897271 1.0644723 1.0533395 1.0238443 1.01265758
172.37 1.0976410 1.0901074 1.0654254 1.0537347 1.0249428 1.01382472
344.74 1.1009676 1.0933571 1.0686188 1.0571899 1.0290515 1.01828313
517.11 1.0910518 1.0967704 1.0723135 1.0608352 1.0324336 1.02190098
689.48 1.0933559 1.1000354 1.0755409 1.0641424 1.0364285 1.02643206
1034.21 1.0981804 1.1056306 1.0819649 1.0701723 1.0436734 1.03364231
1378.95 1.1033306 1.1116401 1.0889427 1.0766085 1.0504178 1.04137399]

Data(:,2)=[];
T=[]; P=[]; Rou=[];
for i=2:size(Data,1)

    T=[T,Data(1,2:end)];
    P=[P,Data(i,1)*ones(1,size(Data,2)-1)];
    Rou=[Rou,Data(i,2:end)];
end
P=P*10^5;
Rou=Rou*10^3;
y=(Rou-rou_o)/rou_o;
y=y';
x_1=P-P_o;
x_2=T-T_o;
x=[x_1',x_2'];
co=x\y;

%% Coeffecients
beta_d=1/co(1) % Beta coeffecient
alpha_d=-co(2) % Alpha coeffecient

figure(1)
plot(Data(2:end,1),Data(2:end,2:end)*10^3,'o-','LineWidth',2)
grid
hold on
legend('T=20°C','T=65°C','T=93°C','T=154°C','T=176°C')
xlabel('Pressure(Bar)')
ylabel('Density(kg/m^3)')

T_s=[];
for i=2:6
    T_s=[T_s, rou0+rou0/beta_d*(Data(2:end,1)*10^5-P_o)-rou0*alpha_d*(Data(1,i)-T_o)];
end
figure(2)
plot(Data(2:end,1),Data(2:end,2:end)*10^3,'o',Data(2:end,1),T_s,'-','LineWidth',2)
grid
hold on
legend('T=20°C','T=65°C','T=93°C','T=154°C','T=176°C','Linearizd with T=20°C','Linearizd with T=65°C','Linearizd with T=93°C','Linearizd with T=154°C','Linearizd with T=176°C','Linearizd with T=20°C')
xlabel('Pressure(Bar)')
ylabel('Density(kg/m^3)')
```

APPENDIX D.2 – WELL CONFIGURATION WITH DEPTH, SI UNITS

```matlab
function [d_pi,d_p,w]=wellbore_ai(depth)

for i=1:length(depth)
   if depth(i)<=2087.7;
      d_pi(i)= 0.168275; %Drillpipe 1 OD,meter
      d_p(i)=0.127;      %Drillpipe 1 ID,meter
      w(i)=450;          %Drillpipe 1 Weight,N/m
   elseif (2087.7<depth(i))&&(depth(i)<=3642.6);
      d_pi(i)=0.127;     %Drillpipe 2 OD,meter
      d_p(i)=0.1016;     %Drillpipe 2 ID,meter
      w(i)=290;          %Drillpipe 2 Weight,N/m
   elseif(3642.6<depth(i))&&(depth(i)<=3764.39);
      d_pi(i)=0.127;     %HWDP OD,meter
      d_p(i)=0.0762;     %HWDP ID,meter
      w(i)=620;          %HWDP Weight,N/m
   else(3764.39<depth(i))&(depth(i)<=3941.96);
      d_pi(i)=0.2032;    %Drillcollars OD,meter
      d_p(i)=0.0762;     %Drillcollars IN,meter
      w(i)=2130;         %Drillcollars Weight,N/m
   end
end
```

APPENDIX D.3 – WELL CONFIGURATION WITH REVERSED DEPTH, SI UNITS

```matlab
function [d,d_p,w]=wellbore_td(depth1)

for i=1:length(depth1)
 if depth1(i)<=2087.7;
      d(i) = 0.168275; %Drillpipe 1 OD,meter
      d_p(i)=0.127;    %Drillpipe 1 ID,meter
      w(i)=450;        %Drillpipe 1 Weight,N/m
   elseif (2087.7<depth1(i))&(depth1(i)<=3642.6);
      d(i)=0.127;      %Drillpipe 2 OD,meter
      d_p(i)=0.1016;   %Drillpipe 2 ID,meter
      w(i)=290;        %Drillpipe 2 Weight,N/m
   elseif(3642.6<depth1(i))&(depth1(i)<=3764.39);
      d(i)=0.127;      %HWDP OD,meter
      d_p(i)=0.0762;   %HWDP ID,meter
      w(i)=620;        %HWDP Weight,N/m
   else(3764.39<depth1(i))&(depth1(i)<=3941.96);
      d(i)=0.2032;     %Drillcollars OD,meter
      d_p(i)=0.0762;   %Drillcollars IN,meter
      w(i)=2130;       %Drillcollars Weight,N/m
   end
end
```

APPENDIX D.4 – WELL CONFIGURATION WITH DEPTH, IMPERIAL UNITS

```matlab
function [d_pi,d_p,w]=wellbore(step)

for i=1:length(step)
   if step(i)<=6849.409449;
      d_pi(i) = 0.168275/0.0254; %Drillpipe 1 OD,meter
      d_p(i)=0.127/0.0254;       %Drillpipe 1 ID,meter
      w(i)=450;                  %Drillpipe 1 Weight,N/m
   elseif (6849.409449<step(i))&(step(i)<=11950.7874);
      d_pi(i)=0.127/0.0254;      %Drillpipe 2 OD,meter
      d_p(i)=0.1016/0.0254;      %Drillpipe 2 ID,meter
      w(i)=290;                  %Drillpipe 2 Weight,N/m
   elseif(11950.7875<step(i))&(step(i)<=12350.36089);
      d_pi(i)=0.127/0.0254;      %HWDP OD,meter
      d_p(i)=0.0762/0.0254;      %HWDP ID,meter
      w(i)=620;                  %HWDP Weight,N/m
   else(12350.36089<step(i))&(step(i)<=12932.93963);
```

```
        d_pi(i)=0.2032/0.0254;     %Drillcollars OD,meter
        d_p(i)=0.0762/0.0254;      %Drillcollars ID,meter
        w(i)=2130;                 %Drillcollars Weight,N/m
    end
end
```

APPENDIX D.5 – TEMPERATURE MODEL

```matlab
function [Ta,Td,Tg]=temperature(flow,T_in,T_e,H,depthft)

global r_pi r_ci mu rho_f r_wb c_f k_f r_p k_p k c rho t g_e

bbl = 42;          %convert bbl to gal
flow = flow*bbl;   %gal/hour
%% parameters used in the temperature model
for i=1:length(depthft)

A_p(i) = pi*r_pi(i)^2; %cross-sectional area of drillstring
N_rep(i) = 2*r_pi(i)*flow/A_p(i)/mu*rho_f; %Reynold number for drilling string

A_a(i) = pi*(r_wb^2-r_pi(i)^2); %cross-sectional area of annulus
N_rea(i) = 0.816*2*(r_wb-r_pi(i))*flow*rho_f/(A_a(i)*mu); %Reynold number annulus

N_pr = mu*c_f/k_f; %Prandtl number
h_p(i) = 0.023*N_rep(i)^0.8*N_pr^0.4*k_f/2/r_pi(i); %coefficient of heat transfer of drilling fluid in drillstring
h_a(i) = 0.023*N_rea(i)^0.8*N_pr^0.4*k_f/2/r_wb; %coefficient of heat transfer of drilling fluid in annulus

U_p(i) = (1/h_p(i)+r_p(i)/k_p*log(r_pi(i)/r_p(i))+r_pi(i)/r_p(i)/h_a(i))^-1;%overall coefficient of heat transfer of drilling fluid in
drillstring
U_a(i) = h_a(i);

alpha = k/c/rho; %heat diffusivity of formation
t_D = alpha*t/r_wb^2;
T_D = (0.4063+0.5*log(t_D))*(1+0.6/t_D); %dimensionless temperature

end
%% Model coefficients
for i=1:length(depthft)
A(i) = 2*pi*r_pi(i)*U_p(i)/(rho_f*flow*c_f);
B(i) = 2*pi*r_ci*U_a(i)*k/(rho_f*flow*c_f*(k+r_ci*U_a(i)*T_D));

theta_1(i) = (B(i)+sqrt(B(i)^2+4*A(i)*B(i)))/2;
theta_2(i) = (B(i)-sqrt(B(i)^2+4*A(i)*B(i)))/2;

C_1(i) = (-(T_in-T_e+g_e/A(i))*theta_2(i)*exp(theta_2(i)*H)-g_e)/(theta_1(i)*exp(theta_1(i)*H)-theta_2(i)*exp(theta_2(i)*H));
C_2(i) = ((T_in-T_e+g_e/A(i))*theta_1(i)*exp(theta_1(i)*H)+g_e)/(theta_1(i)*exp(theta_1(i)*H)-theta_2(i)*exp(theta_2(i)*H));
end
Td = []; %Temperature drillpipe
Ta = []; %Temperature annulus
Tg = []; %Geothermal gradient

for i=1:length(depthft)
    Td_t(i) = ((C_1(i)*exp(theta_1(i)*depthft(i))+C_2(i)*exp(theta_2(i)*depthft(i))+g_e*depthft(i)+T_e-g_e/A(i))-32)/1.8;
    Td = [Td; Td_t(i)];
    Ta_t(i) =
(((1+theta_1(i)/A(i))*C_1(i)*exp(theta_1(i)*depthft(i))+(1+theta_2(i)/A(i))*C_2(i)*exp(theta_2(i)*depthft(i))+g_e*depthft(i)+T_e
)-32)/1.8;
    Ta = [Ta; Ta_t(i)];
    t_g(i) = ((depthft(i)*g_e+T_e)-32)/1.8;
    Tg = [Tg; t_g(i)];
end
```

APPENDIX D.6 – VISCOSITY MODEL

```
function [visc_a,visc_d]=viscosity(Ta,Td,Cv_s,Cv_c)

visc_a=(Cv_s*Ta)+Cv_c;%Viscosity in annulus with varying temperature
visc_d=(Cv_s*Td)+Cv_c;%Viscosity in drillpipe with varying temperature
```

APPENDIX D.7 – PRESSURE MODEL

```
function [dp_a,dp_d]=pressure(visc_a,visc_d,depth,distance,flow)

d=distance;
global rho_f d_ci inch feet rough g

unit_d =119.826;
% d_ci = d_ci*inch*feet;
d_ci=0.27305; %casing ID, meter

flow= flow*0.1589873/3600; %Circulation rate

visc_a=visc_a*0.001; %Viscosity annulus
visc_d=visc_d*0.001; %Viscosity drillpipe

[d_pi,d_p]=wellbore_ai(depth); %d_pi-Drillpipe OD;d_p-pipe ID;w-weight

for i=1:length(d_pi)
    A_a(i)=(pi/4)*(d_ci^2-d_pi(i)^2); %Area annulus,m^2
    A_d(i)=(pi/4)*d_p(i)^2;        %Area drillpipe,m^2
    U_a(i)=flow/A_a(i);           %Velocity annulus,m/s
    U_d(i)=flow/A_d(i);           %Velocity drillpipe,m/s
    d_a(i)=d_ci-d_pi(i);          %Diameter annulus,m
end
dens_a=rho_f*unit_d;%Density of fluid annulus[kg/m3],from interpolation
dens_d=rho_f*unit_d;%Density of fluid drillstring[kg/m3],from interpolation

I=0;% Inclinatation,zero because length of depth elements is already in TVD

%% calculation of Re number and friction factor
Re_a=[];
for i=1:length(d_pi)
    Re_a=[Re_a,(dens_a*U_a(i)*d_a(i))/visc_a(i)]; %Rey. nr. annulus
end

for i=1:length(d_pi)
    if (Re_a(1,i)<0.001);
        f_a(i)=0.0; %Friction factor
    elseif (Re_a(1,i)<2000);
        f_a(i)=16/Re_a(1,i); % Fanning friction factor
    else
        if (rough==0) % Smooth pipe
            f_a(i)=0.0056+0.5*Re_a(1,i)^-0.32;%Friction factor
        else
            f_a(i)=1/(-1.8*log((rough/d_a(i)/3.7)^1.11+6.9/Re_a(1,i)))^2; %Friction factor
        end
    end
end

Re_d=[];
for i=1:length(d_pi)
    Re_d=[Re_d,(dens_d*U_d(i)*d_p(i))/visc_d(i)]; %Rey. nr. drillpipe
end

for i=1:length(d_pi)
```

```matlab
        if (Re_d(1,i)<0.001)
            f_d(i)=0.0; %Friction factor
        elseif (Re_d(1,i)<=2000)
            f_d(i)=16/Re_d(1,i); % Fanning friction factor
        else
            if (rough==0) % Smooth pipe
                f_d(i)=0.0056+0.5*Re_d(1,i)^-0.32; %Friction factor
            else
                f_d(i)=1/(-1.8*log((rough/d_pi(i)/3.7)^1.11+6.9/Re_d(1,i)))^2; %Friction factor
            end
        end
    end
end

%% calculation of frictional pressure loss and hydrostatic pressure
% Friction pressure annulus [Bar]:
Dp_fa=[];
for i=1:length(d_pi)
    dp_fa(i)=((2*f_a(i)*dens_a*(U_a(i)).^2*d(i))/d_a(i));
    Dp_fa=[Dp_fa;dp_fa(i)];
end

% Friction pressure drillstring [Bar]:
Dp_fd=[];
for i=1:length(d_pi)
    dp_fd(i)=((2*f_d(i)*dens_d*(U_d(i)).^2*d(i))/d_p(i));
    Dp_fd=[Dp_fd;dp_fd(i)];
end

% Hydrostatic pressure:
for i=1:length(d_pi)
    dp_ha(i)=(dens_a*g*cosd(I)*d(i));%Hydrostatic pressure annulus[Bar]
    dp_hd(i)=(dens_d*g*cosd(I)*d(i));%Hydrostatic pressure drillstring[Bar]
end

%% Calculation of total pressure in the well:
dp_a(1)=10^5; % Annulus

for i=2:length(d_pi)
    dp_a(i)=dp_a(i-1)+(dp_fa(i)+dp_ha(i)); % Annulus
end
dp_d=zeros(1,length(d_pi));
dp_d(end)=dp_a(end); %Bottomhole pressures
for i=length(d_pi)-1:-1:1
    dp_d(i)=dp_d(i+1)-(-dp_fd(i)+dp_hd(i)); % Drillstring
end
```

APPENDIX D.8 – DENSITY MODEL

```matlab
function [DensityA,DensityD]=density(Ta,Td,dp_a,dp_d,P_o,rou0,T_o,alpha,beta)

DensityA=[];
%Density annulus, kg/m^3
for i=1:length(Ta)
    density_a(i)=rou0+(rou0/beta)*(dp_a(i)-P_o)-rou0*alpha*(Ta(i)-T_o);
    DensityA=[DensityA;density_a(i)];
end
DensityD=[];
%Density drillstring,kg/m^3
for i=1:length(Ta)
    density_d(i)=rou0+(rou0/beta)*(dp_d(i)-P_o)-rou0*alpha*(Td(i)-T_o);
    DensityD=[DensityD;density_d(i)];
end
```

APPENDIX D. 9– RECALCULATE PRESSURE MODEL

```matlab
function [dp_anew,dp_dnew]=pressure_update(visc_a,visc_d,depth,distance,flow,density_a,density_d)

d=distance;
global  d_ci inch feet rough g

unit_d =119.826;
% d_ci = d_ci*inch*feet;
d_ci=0.27305;%casing ID,m

flow= flow*0.1589873/3600; %Circulation rate

visc_a=visc_a*0.001; %Viscosity annulus
visc_d=visc_d*0.001; %Viscosity drillpipe
dens_a=density_a;    %Density annulus,kg/m3
dens_d=density_d;    %Density drillpipe,kg/m3


[d_pi,d_p]=wellbore_ai(depth); %d_pi-Drillpipe OD;d_p-string ID;w-weight

for i=1:length(d_pi)
  A_a(i)=(pi/4)*(d_ci^2-d_pi(i)^2); %Area annulus,m^2
  A_d(i)=(pi/4)*d_p(i)^2;        %Area drillpipe,m^2
  U_a(i)=flow/A_a(i);           %Velocity annulus,m/s
  U_d(i)=flow/A_d(i);           %Velocsity drillpipe,m/s
  d_a(i)=d_ci-d_pi(i);          %Diameter annulus,m
end

I=0; %Inclinatation,zero because length of depth elements is already in TVD

%% calculation of Re number and friction factor
Re_a=[];
for i=1:length(d_pi)
  Re_a=[Re_a,(dens_a(i)*U_a(i)*d_a(i))/visc_a(i)]; % Rey. nr. annulus
end

for i=1:length(d_pi)
  if (Re_a(1,i)<0.001);
    f_a(i)=0.0; %Friction factor
  elseif (Re_a(1,i)<2000);
    f_a(i)=16/Re_a(1,i); %Fanning friction factor
  else
    if (rough==0) % Smooth pipe
      f_a(i)=0.0056+0.5*Re_a(1,i)^-0.32;
    else
      f_a(i)=1/(-1.8*log((rough/d_a(i)/3.7)^1.11+6.9/Re_a(1,i)))^2;
    end
  end
end

Re_d=[];
for i=1:length(d_pi)
  Re_d=[Re_d,(dens_d(i)*U_d(i)*d_p(i))/visc_d(i)]; %Rey. nr. annulus
end

for i=1:length(d_pi)
  if (Re_d(1,i)<0.001)
    f_d(i)=0.0; %Friction factor
  elseif (Re_d(1,i)<=2000)
    f_d(i)=16/Re_d(1,i); %Fanning friction factor
  else
    if (rough==0) % Smooth pipe
```

```
            f_d(i)=0.0056+0.5*Re_d(1,i)^-0.32;
        else
            f_d(i)=1/(-1.8*log((rough/d_pi(i)/3.7)^1.11+6.9/Re_d(1,i)))^2;
        end
    end
end


%% calculation of frictional pressure loss and hydrostatic pressure
% Friction pressure annulus [Bar]:
Dp_fa=[];
for i=1:length(d_pi)
    dp_fa(i)=((2*f_a(i)*dens_a(i)*(U_a(i)).^2*d(i))/d_a(i));
    Dp_fa=[Dp_fa;dp_fa(i)];
end

% Friction pressure drillstring [Bar]:
Dp_fd=[];
for i=1:length(d_pi)
    dp_fd(i)=((2*f_d(i)*dens_d(i)*(U_d(i)).^2*d(i))/d_p(i));
    Dp_fd=[Dp_fd;dp_fd(i)];
end

% Hydrostatic pressure:
for i=1:length(d_pi)
    dp_ha(i)=(dens_a(i)*g*cosd(I)*d(i));%Hydrostatic press.annulus[Bar]
    dp_hd(i)=(dens_d(i)*g*cosd(I)*d(i));%Hydrostatic press.drillstring[Bar]
end

%% calculation of total pressure in the well:

dp_anew(1)=10^5; %Annulus

for i=2:length(d_pi)
    dp_anew(i)=dp_anew(i-1)+(dp_fa(i)+dp_ha(i)); %Annulus
end
dp_dnew=zeros(1,length(d_pi));
dp_dnew(end)=dp_anew(end); %Bottomhole pressure
for i=length(d_pi)-1:-1:1
    dp_dnew(i)=dp_dnew(i+1)-(-dp_fd(i)+dp_hd(i)); %Drillstring
end
```

APPENDIX D.10– RECALCULATE DENSITY MODEL

```
function [density_anew,density_dnew]=density_update(Ta,Td,dp_anew,dp_dnew,P_o,rou0,T_o, alpha,beta);

DensityAnew=[];
%Density annulus,kg/m^3
for i=1:length(Ta)
    density_anew(i)=rou0+(rou0/beta)*(dp_anew(i)-P_o)-rou0*alpha*(Ta(i)-T_o);
    DensityAnew=[DensityAnew;density_anew(i)];
end
DensityDnew=[];
%Density drillstring,kg/m^3
for i=1:length(Ta)
    density_dnew(i)=rou0+(rou0/beta)*(dp_dnew(i)-P_o)-rou0*alpha*(Td(i)-T_o);
    DensityDnew=[DensityDnew;density_dnew(i)];
end
```

APPENDIX D.11– TORQUE AND DRAG MODEL

```
function
[d,D,h,r,angle,Fs,F_L,F_H,F_Lc,F_Hc,flag,TL,TH,TS,TLc,THc,F_Lb,F_Hb,F_Lcb,F_Hcb,TLb,THb,TSb,TLcb,THcb,Fsb]=TandD(Buoyanc
y,MD,DL,I,Azi,depth,depth1,DL1,V_h,N_r,b,dMD,L, fric)

% global d_ci
d_ci=0.27305;
D = d_ci;
Buoyancy=flipud(Buoyancy); %Varying buoyancy factor
[d,d_p,w]=wellbore_td(depth1);

for i=1:length(d_p)
    r(i)=d(i)/2;
    angle(i)=atand((60*V_h)/(2*pi*N_r*r(i))); %angle of friction vector
end

H=[]; %DLS filter
for i=2:length(DL1)-1
    R_past=dMD/DL1(i-1);  %Radius,i-1
    R_pres=dMD/DL1(i);    %Radius,i
    R_fut=dMD/DL1(i+1);   %Radius,i+1

    x_past=R_past*(1-cos(DL1(i-1)/2));
    x_pres=R_pres*(1-cos(DL1(i)/2));
    x_fut=R_fut*(1-cos(DL1(i+1)/2));

    h(i)=0.5*(x_past+x_fut)+x_pres; %Height
    H=[H;h(i-1)];
end

% Static load with varying buoyancy factor
Fsb(1)=0;
for i=2:length(DL1)-1
    Fsb(i)=Fsb(i-1)+(w(i)*L*cosd(I(i))*Buoyancy(i));
end

% Static load with constant buoyancy factor
Fs(1)=0;
for i=2:length(DL1)-1
    Fs(i)=Fs(i-1)+(w(i)*L*cosd(I(i))*b);
end
%Drag force calculation, constant buoyancy factor
F_L(1)=0; % Drag force,F1=0 because at bottom of well
F_H(1)=0; % Drag force,F1=0 because at bottom of well
F_Lc(1)=0;% Drag force,F1=0 because at bottom of well
F_Hc(1)=0;% Drag force,F1=0 because at bottom of well
flag=[0];

for i=2:length(DL1)-1

    if h(i)<(D-d); % Straight inclined,constant buoyancy factor
        F_L(i)=F_L(i-1)+(b*L*w(i)*(cosd(I(i))-(fric*sind(I(i))))); %Drag Force straight-Lowering
        F_H(i)=F_H(i-1)+(b*L*w(i)*(cosd(I(i))+(fric*sind(I(i))))); %Drag Force straight-Hoisting
        F_Lc(i)=F_Lc(i-1)+b*L*w(i)*(cosd(I(i))-fric*sind(I(i))*sind(angle(i)));%Drag force-lowering combined motion
        F_Hc(i)=F_Hc(i-1)+b*L*w(i)*(cosd(I(i))+fric*sind(I(i))*sind(angle(i)));%Drag force-hoisting combined motion
        flag=[flag;0];

    else % Curved,constant buoyancy factor
        if I(i)==I(i-1)
```

```matlab
        F_L(i)=F_L(i-1)*exp(-fric*abs(DL1(i)-DL1(i-1))); %Drag Force curved-Lowering
        F_H(i)=F_H(i-1)*exp(+fric*abs(DL1(i)-DL1(i-1))); %Drag Force curved-Hoisting
        F_Lc(i)=F_Lc(i-1)+(F_L(i-1)*(exp(-fric*abs(DL1(i)-DL1(i-1)))-1)*sind(angle(i)));%Drag force-lowering combined motion
        F_Hc(i)=F_Hc(i-1)+(F_H(i-1)*(exp(+fric*abs(DL1(i)-DL1(i-1)))-1)*sind(angle(i)));%Drag force-hoisting combined motion
        flag=[flag;1];
    else
        F_L(i)=F_L(i-1)*exp(-fric*abs(DL1(i)-DL1(i-1)))+b*L*w(i)*(sind(I(i))-sind(I(i-1)))/((I(i)-I(i-1))*pi/180);% Drag Force curved -
Lowering
        F_H(i)=F_H(i-1)*exp(+fric*abs(DL1(i)-DL1(i-1)))+b*L*w(i)*(sind(I(i))-sind(I(i-1)))/((I(i)-I(i-1))*pi/180);% Drag Force curved -
Hoisting
        F_Lc(i)=F_Lc(i-1)+(((F_L(i-1)*(exp(-fric*abs(DL1(i)-DL1(i-1)))-1)*sind(angle(i))))+(b*L*w(i)*((sind(I(i))-sind(I(i-1)))/((I(i)-I(i-
1))*pi/180))));% Drag Force curved - Lowering
        F_Hc(i)=F_Hc(i-1)+(((F_H(i-1)*(exp(+fric*abs(DL1(i)-DL1(i-1)))-1)*sind(angle(i))))+(b*L*w(i)*((sind(I(i))-sind(I(i-1)))/((I(i)-
I(i-1))*pi/180))));% Drag Force curved - Hoisting
        flag=[flag;1];
    end
  end
end
%Torque calculation,constant buoyancy factor
TL(1)=fric*r(1)*b*L*w(1)*sind(I(1)); %Torque lowering
TH(1)=fric*r(1)*b*L*w(1)*sind(I(1)); %Torque hoisting
TS(1)=fric*r(1)*b*L*w(1)*sind(I(1)); %Torque static
TLc(1)=TL(1)*cosd(angle(1));        %Torque lowering combined motion
THc(1)=TH(1)*cosd(angle(1));        %Torque hoisting combined motion

for i=2:length(DL1)-1
  if h(i)<(D-d); % Straight,constant buoyancy factor
    TL(i)=TL(i-1)+(fric*r(i)*b*L*w(i)*sind(I(i))); %Torque lowering
    TH(i)=TH(i-1)+(fric*r(i)*b*L*w(i)*sind(I(i))); %Torque hoisting
    TS(i)=TS(i-1)+(fric*r(i)*b*L*w(i)*sind(I(i))); %Torque static
    TLc(i)=TL(i)*cosd(angle(i)); %Torque straight lowering combined motion
    THc(i)=TH(i)*cosd(angle(i)); %Torque straight hoisting combined motion
  else % Curved,constant buoyancy
    TL(i)=TL(i-1)+(fric*r(i)*F_L(i-1)*abs(DL1(i)-DL1(i-1))); %Torque lowering
    TH(i)=TH(i-1)+(fric*r(i)*F_H(i-1)*abs(DL1(i)-DL1(i-1))); %Torque hoisting
    TS(i)=TS(i-1)+(fric*r(i)*Fs(i-1)*abs(DL1(i)-DL1(i-1)));  %Torque static
    TLc(i)=TL(i)*cosd(angle(i)); %Torque curved lowering combined motion
    THc(i)=TH(i)*cosd(angle(i)); %Torque curved hoisting combined motion
  end

end

%Drag force calculation, varying buoyancy factor
F_Lb(1)=0;% Drag force,F1=0 because at bottom of well
F_Hb(1)=0; % Drag force,F1=0 because at bottom of well
F_Lcb(1)=0;% Drag force,F1=0 because at bottom of well
F_Hcb(1)=0;% Drag force,F1=0 because at bottom of well

for i=2:length(DL1)-1

  if h(i)<(D-d); % Straight,varying buoyancy factor
    F_Lb(i)=F_Lb(i-1)+(Buoyancy(i)*L*w(i)*(cosd(I(i))-(fric*sind(I(i))))); %Drag Force straight - Lowering
    F_Hb(i)=F_Hb(i-1)+(Buoyancy(i)*L*w(i)*(cosd(I(i))+(fric*sind(I(i))))); %Drag Force straight - Hoisting
    F_Lcb(i)=F_Lcb(i-1)+Buoyancy(i)*L*w(i)*(cosd(I(i))-fric*sind(I(i))*sind(angle(i)));%Drag Force straight - Lowering combined
motion
    F_Hcb(i)=F_Hcb(i-1)+Buoyancy(i)*L*w(i)*(cosd(I(i))+fric*sind(I(i))*sind(angle(i)));%Drag Force straight - Hoisting combined
motion
  else % Curved,varying buoyancy factor
    if I(i)==I(i-1)
      F_Lb(i)=F_Lb(i-1)*exp(-fric*abs(DL1(i)-DL1(i-1))); %Drag force curved - Lowering
      F_Hb(i)=F_Hb(i-1)*exp(+fric*abs(DL1(i)-DL1(i-1))); %Drag force curved - Hoisting
      F_Lcb(i)=F_Lcb(i-1)+(F_Lb(i-1)*(exp(-fric*abs(DL1(i)-DL1(i-1)))-1)*sind(angle(i))); %Drag force curved lowering combined
motion
      F_Hcb(i)=F_Hcb(i-1)+(F_Hb(i-1)*(exp(+fric*abs(DL1(i)-DL1(i-1)))-1)*sind(angle(i))); %Drag force curec hoisting combined
motion
    else
```

```matlab
        F_Lb(i)=F_Lb(i-1)*exp(-fric*abs(DL1(i)-DL1(i-1)))+Buoyancy(i)*L*w(i)*(sind(I(i))-sind(I(i-1)))/((I(i)-I(i-1))*pi/180);% Drag
Force curved - Lowering
        F_Hb(i)=F_Hb(i-1)*exp(+fric*abs(DL1(i)-DL1(i-1)))+Buoyancy(i)*L*w(i)*(sind(I(i))-sind(I(i-1)))/((I(i)-I(i-1))*pi/180);% Drag
Force curved - Hoisting
        F_Lcb(i)=F_Lcb(i-1)+(((F_Lb(i-1)*(exp(-fric*abs(DL1(i)-DL1(i-1)))-1)*sind(angle(i))))+(Buoyancy(i)*L*w(i)*((sind(I(i))-
sind(I(i-1)))/((I(i)-I(i-1))*pi/180))));% Drag Force curved - Lowering
        F_Hcb(i)=F_Hcb(i-1)+(((F_Hb(i-1)*(exp(+fric*abs(DL1(i)-DL1(i-1)))-1)*sind(angle(i))))+(Buoyancy(i)*L*w(i)*((sind(I(i))-
sind(I(i-1)))/((I(i)-I(i-1))*pi/180))));% Drag Force curved - Hoisting
    end
  end

end

%Torque calculation, varying buoyancy factor
TLb(1)=fric*r(1)*Buoyancy(1)*L*w(1)*sind(I(1)); %Torque lowering
THb(1)=fric*r(1)*Buoyancy(1)*L*w(1)*sind(I(1)); %Torque hoisting
TSb(1)=fric*r(1)*Buoyancy(1)*L*w(1)*sind(I(1)); %Torque static
TLcb(1)=TLb(1)*cosd(angle(1)); %Torque lowering combined motion
THcb(1)=THb(1)*cosd(angle(1)); %Torque hoisting combined motion


for i=2:length(DL1)-1
  if h(i)<(D-d); % Straight,varying buoyancy factor
    TLb(i)=TLb(i-1)+(fric*r(i)*Buoyancy(i)*L*w(i)*sind(I(i))); %Torque lowering
    THb(i)=THb(i-1)+(fric*r(i)*Buoyancy(i)*L*w(i)*sind(I(i))); %Torque hoisting
    TSb(i)=TSb(i-1)+(fric*r(i)*Buoyancy(i)*L*w(i)*sind(I(i))); %Torque static
    TLcb(i)=TLb(i)*cosd(angle(i)); %Torque straight combined motion lowering
    THcb(i)=THb(i)*cosd(angle(i)); %Torque straight combined motion lowering
  else % Curved,varying buoyancy factor
    TLb(i)=TLb(i-1)+(fric*r(i)*F_Lb(i-1)*abs(DL1(i)-DL1(i-1))); %Torque lowering
    THb(i)=THb(i-1)+(fric*r(i)*F_Hb(i-1)*abs(DL1(i)-DL1(i-1))); %Torque hoisting
    TSb(i)=TSb(i-1)+(fric*r(i)*Fsb(i-1)*abs(DL1(i)-DL1(i-1))); %Torque static
    TLcb(i)=TLb(i)*cosd(angle(i)); %Torque curved combined motion lowering
    THcb(i)=THb(i)*cosd(angle(i)); %Torque curced combined motion hoisting
  end
end
```

APPENDIX D.12–MODEL

```matlab
clear all;
clc;
close all

global r_pi r_ci mu rho_f r_wb c_f k_f r_p k_p k c rho t g_e
global feet inch d_ci rough g


%% Loaded excel well data
filename='data11.xlsx';                  %Excel data input
step=xlsread(filename,'Q2:Q139', [], 'basic');   %TVD segments,ft
distance=xlsread(filename,'O2:O139', [], 'basic'); %Delta TVD,m
depth=xlsread(filename,'I2:I139', [], 'basic');   %TVD segments,m
MD=xlsread(filename,'F2:F139', [], 'basic');      %MD segmetns,m
DL=xlsread(filename,'J2:J1139', [], 'basic');     %Dogleg values,degrees
DL_r=xlsread(filename,'N2:N140', [], 'basic');    %One extra row needs to be included from excel file, because DLS-filter
"removes" the last value from the measurements
I=xlsread(filename,'G2:G139', [], 'basic');       %Inclination,degrees
Azi=xlsread(filename,'H2:H139', [], 'basic');     %Azimuth,degrees

% Values are flipped in order to calcualte the torque and drag from bottom
% of the well upwards.
MD1=flipud(MD);      %Flipped MD segmetns,m
DL1=flipud(DL_r);    %Flipped dogleg values
I=flipud(I);         %Flipped inclination,degrees
Azi=flipud(Azi);     %Flipped azimuth,degrees
depth1=flipud(depth);%Flipped TVD segments,m
```

110

```matlab
%%  unit conversion
inch = 0.08333;      %convert inch to foot
bbl = 42;            %convert bbl to gal
feet =0.3048;        %convert feet to meter

%% Wellbore architecture and feeding input data
H = depth(end)/feet; %well depth, feet,
d_bit = 8.375;       %drill bit size, inch
d_ci = 10.75;        %casing ID, inch, for the case study
% d_ci = 8.625;      %casing ID, inch, for the demostration well
flow = 200;          %circulation rate, bbl/hour, for the case study
% flow=300;          %circulation rate, bbl/hour, for the demostration well
T_in = 77;           %inlet drilling fluid temperature,F (25 degrees C)
mu = 77;             %drilling fluid viscosity, lb/(ft-hr)(31.7 mPaS)
k_f = 2.6;           %drilling fluid thermal conductivity,Btu/(ft-F-hr),case study
% k_f = 1;           %drilling fluid thermal conductivity,Btu/(ft-F-hr),demostration well
k_p = 20;            %drillstring thermal conductivity, Btu/(ft-F-hr)
c_f = 0.4;           %drilling fluid specific heat, Btu/(lb-F)
rho_f =9.016547;     %drilling fluid density,lb/gal,1,080420365 s.g. from density interpolation
k = 2.9;             %formation thermal conductivity,Btu/(ft-F-hr)1,3,case study
% k = 1.3;           %formation thermal conductivity,Btu/(ft-F-hr)1,3,demostration well
c = 0.2;             %formation specific heat, Btu/(lb-F)
rho = 165;           %formation density, lb/ft^3
T_e = 59.5;          %surface earth temperature,F
g_e = 0.025;         %geothermal gradient,F/ft,case study  (0,0455 C/m)
% g_e = 0.0127;      %geothermal gradient,F/ft,temperature study part (0,0231 C/m)
t = 44;              %circulation hours
rough=1.55*10^-4;    %Roughness
g=9.81;              %Acceleration of gravity
depthft = step;      %TVD segments, ft
fric=0.2;            %Friction coefficient
Cv_s=-0.160116;      %viscosity linear model--slope
Cv_c=33.76;          %viscosity linear model--intercept

%***************** indirect values from dataset and configuration data
[d_pi,d_p,w]=wellbore(step);  %d_pi-Drillpipe OD;d_p-Drillpipe ID; w-weight
for i=1:138
r_pi(i) = d_pi(i)*inch/2;
r_p(i) = d_p(i)*inch/2;
end
r_wb = d_ci*inch/2;
r_ci = d_ci*inch/2;

%% Simulation of temperature model
[Ta,Td,Tg]=temperature(flow,T_in,T_e,H,depthft);
%output,degree,Ta--temperature profile,annulus;Td--temperature profile,pipe
%Tg--formation temperature

%% Simulation of viscosity model
[visc_a,visc_d]=viscosity(Ta,Td,Cv_s,Cv_c);
%visc_a--viscosity of fluids in annulus

%% Simulation of pressure profile
[dp_a,dp_d]=pressure(visc_a,visc_d,depth,distance,flow);
%pressure distribution

%% Simulation of density profile
P_o=1*10^5;              %Initial Pressure;
rou0=1080.4203653;       %Initial density,from interpolation
T_o=25;                  %Initial Temperature
alpha=4.5429e-04;        %Alpha coefficient
beta=4.4983e+09;         %Beta coefficient

[density_a,density_d]=density(Ta,Td,dp_a,dp_d,P_o,rou0,T_o, alpha,beta);

%% Simulation of pressure profile, recalcualted pressure distribution
```

```matlab
[dp_anew,dp_dnew]=pressure_update(visc_a,visc_d,depth,distance,flow,density_a,density_d);

%% Simulation of density profile
P_o=1*10^5;              %Initial Pressure;
rou0=1080.4203653;       %Initial density, from interpolation
T_o=25;                  %Initial Temperature
alpha=4.5429e-04;        %Alpha coefficient
beta=4.4983e+09;         %Beta coefficient

[density_anew,density_dnew]=density_update(Ta,Td,dp_anew,dp_dnew,P_o,rou0,T_o, alpha,beta);
%% Simulation of Buoyancyfactor profile
density_pipe=7850; %Density of pipe, kg/m3
% Buoyancy=buo(density_a,density_d,depth,density_pipe);
Buoyancy=buo(density_anew,density_dnew,depth,density_pipe);%Buoyancy factor

%% Simulation of Torque and drag profile
V_h = 0.25;          %hoisting/lowering speed(m/s)
N_r = 120;           %RPM
b=1-(1080.5/7850);   %0,86235,constant buoyancy factor
dMD=30;              %Depth between measurements
fric=0.2;            %Friction Coeffecient
L=30;                %Length in meters between inclination measurements
[d,D,h,r,angle,Fs,F_L,F_H,F_Lc,F_Hc,flag,TL,TH,TS,TLc,THc,F_Lb,F_Hb,F_Lcb,F_Hcb,TLb,THb,TSb,TLcb,THcb,Fsb]=TandD(Buoyancy,MD,DL,I,Azi,depth,depth1,DL1,V_h,N_r,b,dMD,L, fric);

%% plotting the figures
figure(1) % Temperature plot
plot(Td,depthft*0.3048,':r',Ta,depthft*0.3048,'--b',Tg,depthft*0.3048,'k','LineWidth',3)
set(gca,'YDir','Reverse')
hold on
grid on
xlabel('Temperature, °C')
ylabel('Depth, m')
legend ('Drillpipe' , 'Annulus','Geothermal Gradient')
title ('Temperature plot')
% axis ([0,100,0,2600])

figure(2) % Viscosity plot
plot(visc_d,depthft*0.3048,':y',visc_a,depthft*0.3048,'--g','LineWidth',3)
set(gca,'YDir','Reverse')
hold on
grid on
xlabel('Viscosity, mPaS')
ylabel('Depth, m')
legend ('Drillpipe Fluid Viscosity' , 'Annulus Fluid Viscosity')
title ('Viscosity Plot')
% axis ([0,40,0,4000])

figure(3) % Pressure plot
plot(dp_d*10^-5,depth,'r',dp_a*10^-5,depth,'--b','LineWidth',2);
set(gca,'YDir','Reverse')
hold on
grid on
xlabel('Pressure, [Bar]')
ylabel('Depth, m')
legend ('Drillpipe' , 'Annulus')
title ('Pressure plot')
axis ([0,430,0,4000])

figure(4) % Density plot
plot(density_d,depth,'r',density_a,depth,'--b','LineWidth',2);
set(gca,'YDir','Reverse')
hold on
grid on
xlabel('Density, [Kg/m^3]')
ylabel('Depth, m')
```

112

```matlab
legend ('Drillpipe' , 'Annulus')
title ('Density plot')

figure(5) % Pressure plot, recalculated pressure
plot(dp_dnew*10^-5,depth,'r',dp_anew*10^-5,depth,'--b','LineWidth',2);
set(gca,'YDir','Reverse')
hold on
grid on
xlabel('Pressure, [Bar]')
ylabel('Depth, m')
legend ('Drillpipe' , 'Annulus')
title ('Recalculated Pressure plot')
axis ([0,430,0,4000])

figure(6) % Density plot, recalculated
plot(density_dnew,depth,'r',density_anew,depth,'--b','LineWidth',2);
set(gca,'YDir','Reverse')
hold on
grid on
xlabel('Density, [Kg/m^3]')
ylabel('Depth, m')
legend ('Drillpipe' , 'Annulus')
title ('Recalculated Density plot')


figure(7) % Buoyancy factor plot
plot(Buoyancy,depth,'--b','LineWidth',2);
set(gca,'YDir','Reverse')
hold on
grid on
xlabel('Buoyancy')
ylabel('Depth, m')
legend ('Buoyancy Factor')
title ('Buoyancy Plot')

figure(8) % Drag force, all operational modes, with constant and varying buoyancy factor
plot(0.001*F_L,depth1,'r',0.001*F_H,depth1,':k',0.001*F_Lb,depth1,'g',0.001*F_Hb,depth1,'y',0.001*Fsb,depth1,'b',0.001*Fs,d
epth1,':r',0.001*F_Lc,depth1,'',0.001*F_Hc,depth1,'c',0.001*F_Lcb,depth1,'k',0.001*F_Hcb,depth1,'m',flag*-
100,depth1,'ko','LineWidth',2)
set(gca, 'XAxisLocation', 'top')
hold on
grid on
xlabel('Drag Force, kN')
ylabel('Depth, m')
legend ('Drag - Lowering - Constant Buoyancy Factor' , 'Drag - Hoisting - Constant Buoyancy Factor','Drag - Lowering - Varying
Buoyancy Factor' , 'Drag - Hoisting - Varying Buoyancy Factor','Static load - Varying Buoyancy Factor','Static load - Constant
Buoyancy Factor','Drag Lowering Combined Motion - Constant Buoyancy Factor','Drag Hoisting Combined Motion - Constant
Buoyancy Factor','Drag Lowering Combined Motion - Varying Buoyancy Factor','Drag Hoisting Combined Motion - Varying
Buoyancy Factor')
title ('Drag Force')
axis ([-250,1700,0,4000])
set(gca,'YDir','Reverse')

figure(9) % Torque lowering
plot(TL*10^-3,depth1,'y',TLc*10^-3,depth1,'g',TLb*10^-3,depth1,'r',TLcb*10^-3,depth1,'b',flag*-2,depth1,'Ko','LineWidth',2)
set(gca, 'XAxisLocation', 'top')
hold on
grid on
xlabel('Torque, KNm')
ylabel('Depth, m')
legend ('Torque Lowering - Constant Buoyancy Factor','Torque Lowering Combined motion - Constant Buoyancy Factor','Torque
Lowering - Varying Buoyancy Factor','Torque Lowering Combined motion - Varying Buoyancy Factor')
title ('Torque - Lowering')
set(gca,'YDir','Reverse')
axis ([-3,10,0,4000])
```

```
figure(10) % Torwue hoisting
plot(TH*10^-3,depth1,'y',THc*10^-3,depth1,'k',THb*10^-3,depth1,'c',THcb*10^-3,depth1,'b',flag*-2,depth1,'Ko','LineWidth',2)
set(gca, 'XAxisLocation', 'top')
hold on
grid on
xlabel('Torque, KNm')
ylabel('Depth, m')
legend ('Torque Hoisting - Constant Buoyancy Factor','Torque Hoisting Combined motion - Constant Buoyancy Factor','Torque
Hoisting - Varying Buoyancy Factor','Torque Hoisting Combined motion - Varying Buoyancy Factor')
title ('Torque - Hoisting')
set(gca,'YDir','Reverse')
axis ([-3,10,0,4000])

figure(11) % Torque static
plot(TS*10^-3,depth1,'k',TSb*10^-3,depth1,'c',flag*-2,depth1,'Ko','LineWidth',2)
set(gca, 'XAxisLocation', 'top')
hold on
grid on
xlabel('Torque, KNm')
ylabel('Depth, m')
legend ('Torque Static - Constant Buoyancy Factor','Torque Static - Varying Buoyancy Factor')
title ('Torque - Static')
set(gca,'YDir','Reverse')
axis ([-3,10,0,4000])

figure(12) % Drag force, with and without combined motion
plot(0.001*F_L,depth1,'r',0.001*F_H,depth1,'k',0.001*Fs,depth1,'b',0.001*F_Lc,depth1,'y',0.001*F_Hc,depth1,'g',flag*-
100,depth1,'ko','LineWidth',2)
set(gca, 'XAxisLocation', 'top')
hold on
grid on
xlabel('Drag Force, kN')
ylabel('Depth, m')
legend ('Drag - Lowering - Constant Buoyancy Factor' , 'Drag - Hoisting - Constant Buoyancy Factor','Static load - Constant
Buoyancy Factor','Drag - Lowering Combined Motion - Constant Buoyancy Factor','Drag - Hoisting Combined Motion - Constant
Buoyancy Factor')
title ('Drag Force Constant Buoyancy Factor')
axis ([-250,1700,0,4000])
set(gca,'YDir','Reverse')

figure(13) % Drag force
plot(0.001*F_Lb,depth1,'g',0.001*F_Hb,depth1,'y',0.001*Fsb,depth1,'b',0.001*F_Lcb,depth1,'k',0.001*F_Hcb,depth1,'m',flag*-
100,depth1,'ko','LineWidth',2)
set(gca, 'XAxisLocation', 'top')
hold on
grid on
xlabel('Drag Force, kN')
ylabel('Depth, m')
legend ('Drag - Lowering - Varying Buoyancy Factor' , 'Drag - Hoisting - Varying Buoyancy Factor','Static load - Varying Buoyancy
Factor','Drag - Lowering Combined Motion - Varying Buoyancy Factor','Drag - Hoisting Combined Motion - Varying Buoyancy
Factor')
title ('Drag Force Varying Buoyancy Factor With Depth')
axis ([-250,1700,0,4000])
set(gca,'YDir','Reverse')

% figure(14)
% plot(TL*10^-3,depth1,'y',TH*10^-3,depth1,'r',TS*10^-3,depth1,'g',TLc*10^-3,depth1,'b',THc*10^-3,depth1,'k',flag*-
10,depth1,'Ko','LineWidth',2)
% set(gca, 'XAxisLocation', 'top')
% hold on
% grid on
% xlabel('Torque, KNm')
% ylabel('Depth, m')
% legend('Torque Lowering - Constant Buoyancy','Torque Hoisting - Constant Buoyancy','Torque Static - Constant Buoyancy
Factor','Torque Lowering Combined motion - Constant Buoyancy Factor','Torque Hoisting Combined motion - Constant
Buoyancy Factor')
```

```
% title ('Torque ')
% set(gca,'YDir','Reverse')
% % axis ([-500,4000,0,2600])

figure(15) % Striaght inclined or curved
plot(TS*10^-3,depth1,'w',flag*-2,depth1,'Ko','LineWidth',2)
set(gca, 'XAxisLocation', 'top')
hold on
grid on
ylabel('Depth, m')
title ('Straight inclined or curved')
set(gca,'YDir','Reverse')
axis ([-3,3,0,4000])

figure(16) % Torque with constant buoyancy and varying buoyancy
plot(TL*10^-3,depth1,'y',TH*10^-3,depth1,'r',TS*10^-3,depth1,'g',TLb*10^-3,depth1,'b',THb*10^-3,depth1,'k',TSb*10^-
3,depth1,'m',flag*-2,depth1,'Ko','LineWidth',2)
set(gca, 'XAxisLocation', 'top')
hold on
grid on
xlabel('Torque, kNm')
ylabel('Depth, m')
legend('Torque Lowering - Constant Buoyancy Factor','Torque Hoisting - Constant Buoyancy Factor','Torque Static - Constant
Buoyancy Factor','Torque Lowering - Varying Buoyancy Factor','Torque Hoisting - Varying Buoyancy Factor','Torque Static -
Varying Buoyancy Factor')
title ('Torque - Buoyancy Effect ')
set(gca,'YDir','Reverse')
axis ([-3,10,0,4000])

figure(17) % Torque - effect of combined motion
plot(TL*10^-3,depth1,'y',TH*10^-3,depth1,'r',TS*10^-3,depth1,'g',TLc*10^-3,depth1,'b',THc*10^-3,depth1,'k',flag*-
2,depth1,'Ko','LineWidth',2)
set(gca, 'XAxisLocation', 'top')
hold on
grid on
xlabel('Torque, kNm')
ylabel('Depth, m')
legend('Torque Lowering - Constant Buoyancy','Torque Hoisting - Constant Buoyancy','Torque Static - Constant Buoyancy
Factor','Torque Lowering Combined motion - Constant Buoyancy Factor','Torque Hoisting Combined motion - Constant
Buoyancy Factor')
title ('Torque ')
set(gca,'YDir','Reverse')
axis ([-3,10,0,4000])

figure(18) % Drag force - effect of varying buoyancy factor
plot(F_L*0.001,depth1,'y',F_H*0.001,depth1,'r',Fs*0.001,depth1,'g',F_Lb*0.001,depth1,'b',F_Hb*0.001,depth1,'k',Fsb*0.001,de
pth1,'m',flag*-100,depth1,'Ko','LineWidth',2)
set(gca, 'XAxisLocation', 'top')
hold on
grid on
xlabel('Drag Force, kN')
ylabel('Depth, m')
legend('Drag Force Lowering - Constant Buoyancy Factor','Drag Force Hoisting - Constant Buoyancy Factor','Static Load -
Constant Buoyancy Factor','Drag Force Lowering - Varying Buoyancy Factor','Drag Force Hoisting - Varying Buoyancy
Factor','Static Load - Varying Buoyancy Factor')
title ('Drag Force - Buoyancy Effect ')
set(gca,'YDir','Reverse')
axis ([-250,1700,0,4000])

figure(19) % Drag force - effect of combined motion and buoyancy factor
plot(F_Lc*0.001,depth1,'y',F_Hc*0.001,depth1,'r',Fs*0.001,depth1,'g',F_Lcb*0.001,depth1,'b',F_Hcb*0.001,depth1,'k',Fsb*0.00
1,depth1,'m',flag*-100,depth1,'Ko','LineWidth',2)
set(gca, 'XAxisLocation', 'top')
hold on
grid on
xlabel('Drag Force, kN')
```

```
ylabel('Depth, m')
legend('Drag Force Lowering Combined motion - Constant Buoyancy Factor','Drag Force Hoisting Combined motion - Constant
Buoyancy Factor','Static Load - Constant Buoyancy Factor','Drag Force Lowering Combined motion - Varying Buoyancy
Factor','Drag Force Hoisting Combined motion - Varying Buoyancy Factor','Static Load - Varying Buoyancy Factor')
title ('Drag Force - Buoyancy Effect - Combined Motion Included ')
set(gca,'YDir','Reverse')
axis ([-250,1700,0,4000])
```